ISSN 2074-272X

науково-практичний журнал 2017/1

Електротехніка і Електромеханіка

Electrical Engineering & Electromechanics

За 2015р. журнал отримав індекс 83.98 від міжнародної наукометричної бази Index Copernicus

«ELECTRICAL ENGINEERING & ELECTROMECHANICS»

SCIENTIFIC & PRACTICAL JOURNAL

Journal was founded in 2002 by

National Technical University «Kharkiv Polytechnic Institute»

Co-Founder – State Institution «Institute of Technical Problems of Magnetism of the NAS of Ukraine»

ISSUE 1/2017

TABLE OF CONTENTS

Editorial office address: Dept. of Electrical Apparatus, NTU «KhPI», Kyrpychova Str., 21, Kharkiv, 61002, Ukraine
phones: +380 57 7076281, +380 67 3594696, **e-mail:** a.m.grechko@gmail.com (**Grechko O.M.)**

ISSN (print) 2074-272X
ISSN (online) 2309-3404

Printed 24.02.2017. Format 60 x 90 ⅛. Paper – offset. Laser printing. Edition 200 copies. Order no.66/172-01-2017.

Printed by Printing house «Madrid Ltd» (11, Maksymilianivska Str., Kharkiv, 61024, Ukraine)

UDC 621.3: 537.8: 910.4 **doi: 10.20998/2074-272X.2017.1.01**

M.I. Baranov

AN ANTHOLOGY OF THE DISTINGUISHED ACHIEVEMENTS IN SCIENCE AND TECHNIQUE. PART 36: NOBEL PRIZE LAUREATES IN PHYSICS FOR 1995-1999

Purpose. Implementation of brief analytical review of the distinguished scientific achievements of the world scientists-physicists, awarded the Nobel Prize in physics for period 1995-1999. Methodology. Scientific methods of collection, analysis and analytical treatment of scientific and technical information of world level in area of modern theoretical and experimental physics. Results. The brief analytical review of the scientific openings and distinguished achievements of scientists-physicists is resulted in area of modern physical and technical problems which were marked the Nobel bonuses on physics for period 1995-1999. Originality. Systematization is executed with exposition in the short concentrated form of the known scientific and technical materials, devoted opening of tau-lepton, experimental discovery of electronic neutrino, opening of superfluidity of liquid helium-3, creation of methods of cooling and «capture» of atoms by a laser ray, opening of new form of quantum liquid with excitations of fractional electric charge and clearing up of quantum structure of electroweak interactions of elementary particles scientists-physicists. Practical value. Popularization and deepening of scientific and technical knowledges for students, engineer and technical specialists and research workers in area of modern theoretical and experimental physics, extending their scientific range of interests and further development of scientific and technical progress in human society. References 25, figures 13.

Key words: **modern physics, achievements, tau-lepton, electronic neutrino, superfluidity of liquid helium-3, cooling and «capture» of atoms, quantum liquid with excitations of fractional electric charge, quantum structure of electroweak interactions of elementary particles, review**.

Приведен краткий аналитический обзор выдающихся научных достижений ученых мира, отмеченных Нобелевской премией по физике за период 1995-1999 гг. В число таких достижений вошли открытие тау-лептона, экспериментальное обнаружение электронного нейтрино, открытие сверхтекучести жидкого гелия-3, создание методов охлаждения и «пленения» атомов с помощью лазерного света, открытие новой формы квантовой жидкости с возбуждениями дробного электрического заряда и прояснение квантовой структуры электрослабых взаимодействий элементарных частиц. Библ. 25, рис. 13.

Ключевые слова: **современная физика, достижения, тау-лептон, электронное нейтрино, сверхтекучесть жидкого гелия-3, охлаждение и «пленение» атомов, квантовая жидкость с возбуждениями дробного электрического заряда, квантовая структура электрослабых взаимодействий элементарных частиц, обзор.**

Introduction. The Nobel Prize has been more than a century is one of the most prestigious international awards in the world. It is awarded by the Nobel Committee of the Royal Swedish Academy of Sciences for outstanding scientific research, revolutionary invention, a major contribution to culture and the development of human society [1]. Nobel Prize in physics, chemistry, physiology, medicine, literature and peace were established in accordance with the will-known Swedish engineer and inventor of dynamite Alfred Nobel (1833-1896) according to which for these purposes, and the financial support of Nobel laureates was created fund Nobel. They are handed to 1901 in the capital of Sweden – Stockholm (except for the Nobel Peace Prize award ceremony which takes place in the capital of Norway – Oslo). Traditionally, the annual awards ceremony for the winners of this prestigious award is held on the day of the death of A. Nobel – December 10th. Note that in 1968 by the Bank of Sweden Prize in Economics in memory of A. Nobel (Nobel Prize in Economics) was established [1]. The size of remuneration of the Nobel Prize, for example, in 2012, amounted to 8 million SEK (1.2 millon USD). Until 2012, this amount was considered the award of 10 million SEK. The Board of Directors of the Nobel Foundation in the summer of 2012 was forced to take a decision on the «cuts» monetary reward laureates for 20 % due to the need to «*preserve the fund's capital in the long term*» [1].

1. The discovery of the tau-lepton. According to the classification adopted in the physics of elementary particles tau-leptons are the third generation of microparticles [1, 2]. American experimental physicist Martin Lewis Perl (Fig. 1) working at Stanford heavy duty linear electron accelerator at energies up to 21 GeV with the length of the accelerator «tube» in 3200 m (USA) [3] in 1975 opened a new elementary particle tau-lepton (in other words, a «heavy» electron) [4]. This is an important discovery in high-energy physics and elementary particles confirmed the theory of «Big Bang» in the creation of the Universe [1, 5].

Fig. 1. Prominent American experimental physicist Martin Lewis Perl (1927-2014), Nobel Prize Laureate in physics for 1995

For this fundamental scientific result M. Pearl in 1995 was awarded the Nobel Prize in Physics [4, 5]. This award he shared with other prominent American physicist Frederick Reines (Fig. 2) who discovered the neutrino [4, 6].

Fig. 2. Prominent American experimental physicist Frederick Reines (1918-1998), Nobel Prize Laureate in physics for 1995

2. The discovery of the neutrino. In 1930, an outstanding Austrian theoretical physicist Wolfgang Pauli (1900-1958) advanced the hypothesis of the existence of such «light» of elementary particles like the electron neutrino v_e according to the relevant [2] to the absolutely stable particles with no charge and rest mass [4 6]. Working in creative tandem with the renowned American experimental physicist at Los Alamos National Laboratory (New Mexico, United States) Clyde Cowan (1919-1974), F. Reines in 1956 to reverse the radioactive beta decay of atomic nuclei (β^+ − decay) on the experimental nuclear reactor found in the decay products of the electron neutrino v_e [6]. By the time of the award of F. Reines said Prize for 1995 K. Cowan was no longer alive. Therefore his name was not on the list of Nobel Prize winners (according to the current position of this award is only awarded to applicants living this prestigious award).

3. The discovery of superfluidity of liquid helium-3. In 1972, American physicist David Morris Lee (Fig. 3), working in the US as Professor at Cornell University, in collaboration with another Professor of this University Robert Coleman Richardson (Fig. 4) and graduate student Douglas Dean Osheroff (Fig. 5) have published research results opening at a temperature of about 0.001 K of superfluidity in the isotope helium $_2{}^3He$ − liquid helium-3 [7-9]. Recall that in 1937 the outstanding Soviet experimental physicist Peter Kapitsa (1894-1984), Head of the Institute for Physical Problems (IPhP) of the Academy of Sciences of the USSR (Moscow), with the absolute temperatures below 2.19 K was discovered a unique physical effect in the material – the phenomenon of superfluidity in the isotope helium $_2{}^4He$ − liquid helium-II [10]. For the «*basic inventions and discoveries in the field of low-temperature*» Academician of the Academy of Sciences of the USSR P.L. Kapitsa was awarded the Nobel Prize in physics for 1978 [4, 10]. Taking into account the fundamental nature of obtained by D.M. Li, R.C. Richardson, and D.D. Osheroff scientific results, in 1996 they were awarded the Nobel Prize in physics [4, 7-9]. The discovery of superfluidity of liquid helium-3 promoted promising fundamental and applied research in many fields of physics [4, 7].

Fig. 3. Prominent American experimental physicist David Morris Lee, born in 1931, Nobel Prize Laureate in physics for 1996

Fig. 4. Prominent American physicist Robert Coleman Richardson, (1937-2013), Nobel Prize Laureate in physics for 1996

Fig. 5. Prominent American experimental physicist Douglas Dean Osheroff, born in 1945, Nobel Prize Laureate in physics for 1996

4. Creation of methods to cool and «capture» of matter atoms. American Research Center of Bell Laboratories in the number of Nobel Prize winners take on today's leading position in the world [11]. In this well-known scientific centers in 1983 as head of the Department of quantum electronics future Nobel Laureate Steven Chu worked (Fig. 6). While addressing the supercooling and the «capture» of atoms using laser technology, in 1985. S. Chu and his colleagues William Daniel Phillips (Fig. 7), and Claude Cohen-Tannoudji (Fig. 8) achieved great success [11-15].

Fig. 6. Prominent American experimental physicist Steven Chu, born in 1948, Nobel Prize Laureate in physics for 1997

Fig. 7. Prominent American physicist William Daniel Phillips, born in 1948, Nobel Prize Laureate in physics for 1997

Fig. 8. Prominent French physicist Claude Cohen-Tannoudji, born in 1933, Nobel Prize Laureate in physics for 1997

It is well known that in the microcosm of the atom of matter the temperature measure (molecules) or particles their kinetic energy [2, 11]. A great contribution to this energy and, respectively, in the temperature gives the translational velocity of said microscopic objects. A smaller contribution of this indicator makes the frequency of natural oscillations [2, 11]. Therefore, the faster moving and more micro-object vary, so it will be «hot». By physicists it was found that at «minus» 270 °C (about 3 K) translational velocity substance atom is about 100 m/s [11]. T the ambient temperature («plus» 20 °C) atoms, this velocity value is close to 1000 m/s [2, 10, 16]. If we reduce the speed of 0.01 m/s, then the atom is

virtually «frozen». This can be done by various physical methods. Studies conducted in the United States by S. Chu, W. Phillips, and C. Cohen-Tannoudji showed that the most convenient for this method is the method of laser cooling of atoms [11-15]. This group of physicists in the study using a laser beam of atomic processes have achieved the absolute temperature of the substance of the neutral atoms of the order of 10^{-6} K [11]. It is for this phenomenal achievement S. Chu, W.D. Phillips and C. Cohen-Tannoudji were awarded the Nobel Prize in physics for 1997 [4, 11-15]. Developed laser method of supercooling and the «capture» of the atoms in this way is currently used in the design of high-precision atomic clocks, as well as precise positioning and satellite navigation [13]. An important fact characterizing S. Chu like an unusual and talented person, is that S. Chu during the 2004-2008 biennium was the director of the world-famous Ernest Lawrence National Laboratory Lawrence (if the state is 4 thousand employees and an annual budget of 650 million US dollars) and is actively involved in alternative sources of energy (in particular biofuels, artificial photosynthesis and methods of generating electricity from solar radiation), and in the period 2009-2013 – Minister of Energy of the United States [12, 13].

5. Discovery of a new form of quantum fluid with fractional excitations of electric charge. The physical concept of «quantum fluid» was introduced in the period 1937-1941 by outstanding Soviet theoretical physicist Lev Davidovich Landau (1908-1968) is being developed at that time in the IPhP of the Academy of Sciences of the USSR (at the Academician of the Academy of Sciences of the USSR P.L. Kapitsa then worked fruitfully in the field of low-temperature physics and discovered experimentally in 1937 the phenomenon of superfluidity of liquid helium-II) the quantum theory of superfluidity of liquid helium-II [10, 17]. For a quantum fluid characteristic it is that it decisive role in the behavior of its microcomponent (constituent elements) are beginning to play the quantum effects. In this liquid, quantum uncertainty traces its origin (e.g., atoms) according to the Heisenberg uncertainty relation [2, 17] are starting to significantly exceed the current mutual distances between them. Therefore, the physical properties of these liquids will be determined solely by stochastic laws of quantum physics. In the period 1981-1982 research groups of Horst Ludwig Störmer (Fig. 9) and Daniel C. Tsui (Fig. 10) who studied «*the integer quantum Hall effect*» opened in 1980 by Klaus von Klitzing (born in 1943) at «helium» temperatures (till 1 K) and strong static magnetic fields (at magnetic flux density till 30 T) in the silicon field effect transistor and the award of the Nobel Prize in physics for 1985 [4, 18], using a two-dimensional ultra-pure gallium arsenide films at lower temperatures (below 1 K) and stronger permanent magnetic fields (for the magnetic flux density over 30 T) opened new «*fractional quantum Hall effect*» [18-20].

Fig. 9. Prominent German experimental physicist Horst Ludwig Störmer, born in 1949, Nobel Prize Laureate in physics for 1998

Fig. 10. Prominent American experimental physicist Daniel C. Tsui, born in 1939, Nobel Prize Laureate in physics for 1998.

For a better understanding of a difficult material should be noted that even in 1879 young American physicist Edwin Herbert Hall (1855-1938) exploring the flow of direct current strength along the I_H thin gold plate placed perpendicular to the lines of induction B_H external constant magnetic field discovered the phenomenon arises between the «free» edges of the plate electric potential difference or voltage U_H («*Hall effect*») [16]. As is known the cause of the rejection of U_H is drifting plates of electrons from the main direction of their drift to its «free» edges of the corresponding action on them in a magnetic field Lorentz force [2]. The value of U_H was directly proportional to the current I_H and B_H induction. In addition, the «Hall» R_H resistance equal to the ratio U_H/I_H

described by the relation of the form [18]: $R_H=B_H/(n_e e_0)$, where n_e is the average density of free electrons with the electric unit charge $e_0=1.602\cdot10^{-19}$ C in the material of the flat-plate conductor. That is why the Hall effect could be used for measuring the magnetic field, and determining the concentration of charge carriers (positive «holes») in conductors and semiconductors. E.H. Hall performed his experiments at room temperature (about 293 K) and the levels of magnetic induction B_H less than 1 T [18]. In the early 1980s by K. von Klitzing at the above-mentioned extreme conditions it was found that the «Hall» conductor resistance R_H (semiconductor) with increasing levels of exposure to it the magnetic induction B_H does not change continuously, but jumps, taking discrete (quantized) values $R_{Hi}=h/(ie_0^2)$, where i=1,2,3,.. are the integer quantum numbers i; h=6,626·10^{-34} J·s is the Planck constant [2]. Note that in this case the value of h/e_0^2 is approximately 26 Ω. According to the eminent German physicist Carl von Klitzing turned out that the «Hall» R_H resistance, regardless of the type of material under the action it ultralow temperatures and strong magnetic field is quantized. The experimentally discovered by K. von Klitzing «*integer quantum Hall effect*» was explained sequential filling of Landau levels (discrete energy levels of electrons in a magnetic field) with increasing magnetic induction level. In these experiments by H.L. Störmer and D.C. Tsui scientists have discovered new quantum leaps for the «Hall» resistance $R_{Hk}=h/(ke_0^2)$ which is three times higher than the largest R_{Hi} in earlier experiments by K. von Klitzing. The fundamental difference in this case was the fact that the value of k is the fractional value (1/3, etc.). In 1983, the American theoretical physicist Robert Betts Laughlin (Fig. 11) proposed a theoretical justification of this effect.

Fig. 11. Prominent American theoretical physicist Robert Betts Laughlin, born in 1950, Nobel Prize Laureate in physics for 1998

According to the theoretical substantiation by R.B. Laughlin of the open empirically by H.L. Störmer and D.C. Tsui «*fractional quantum Hall effect*» at the sufficiently low temperature and very strong magnetic field, a two-dimensional «electron gas» conductor (semiconductor) of the Fermi liquid becomes a kind of a new type of quantum fluid [18, 21]. Electrons with half-integer values of their spin are part of this «Laughlin» quantum fluid, and occurring in her excitement starting to behave like quasi-particles with integer spin (as bosons) [18-21]. «Laughlin» quantum liquid became a Bose liquid, for which it is possible Bose condensation, and hence the phenomenon of superfluidity and superconductivity. The latter phenomenon was made possible when driving in this particular quantum fluid is electrically charged. R.B. Laughlin in the proposed theory suggests that these quasi-particles in the quantum liquid are collective entities whose existence is ensured by long-range interaction between electrons and a strong magnetic field. According to R.B. Laughlin a composite quasi-particle (boson) in the «Laughlin» quantum liquid is a combination of an electron and three magnetic flux quanta [18, 21]. New «Laughlin» quantum liquid characterized by unusual physical properties added to it the electron is so energetically unfavorable for it, that it be born excitation with a fractional electric charge $e_0/3$ [18]. R.B. Laughlin first theoretically demonstrated that quasiparticles in condensed state of matter can have fractional electric charges. This theoretical approach by R.B. Laughlin allows individuals to explain the «*fractional quantum Hall effect*» previously set by H.L. Störmer and D.C. Tsui. For the fundamentality and «*discovery of a new form of quantum fluid with fractional electric charge excitations*» H.L. Störmer, D.C. Tsui, and R.B. Laughlin was awarded Nobel Prize in physics for 1998 [4, 18-21]. It should be noted that despite the fact that fractional electric charge quasiparticles participating in the course of events «*the fractional quantum Hall effect*» in a kind of Bose condensate set and measured now, thanks to the outstanding achievements in electronics and metrology reliably talk about the direct supervision of the microparticles with charge is premature. However, the research results of the new Nobel Laureates allow us to state that there was an important event in the scientific world, which forces scientists to reconsider many of the provisions in our current understanding of the world around us.

6. Clarification of the quantum structure of electroweak interactions of elementary particles. In the 1960s, by prominent American Sheldon Lee Glashow (born 1932), Steven Weinberg (1933-1996) and Pakistani Abdus Salam (1926-1996) theoretical physicists, quantum theory of weak and electromagnetic interactions in microcosm has been developed using the principle of gauge invariance [22]. This theory was based on the fact that in the microcosm the weak and electromagnetic interactions are manifestations of a single electroweak interaction. The practical application of this theory to calculate the physical properties of elementary particles which it should predict had no good results [23]. In the 1970s to address the problem in the field of elementary particle physics actively involved physicists of the University of Utrecht (Netherlands), Martinus Veltman (Fig. 12) and Gerard Hooft (Fig. 13). They do a mathematical formulation of gauge theories and

renormalization theory of so-called non-Abelian gauge theories which are the foundation of all modern physics of elementary particles [24]. Developed by these theoretical physicists mathematical apparatus and, based on a computer program showed that many of the most problematic aspects of a non-Abelian gauge theories – the theory of electroweak interactions in the process of mathematical calculations are compensated [22-24]. This program became the foundation for the difficult work of scientists to verify the different approaches to the renormalization theory, which would allow to obtain a reasonable prediction of particle physics.

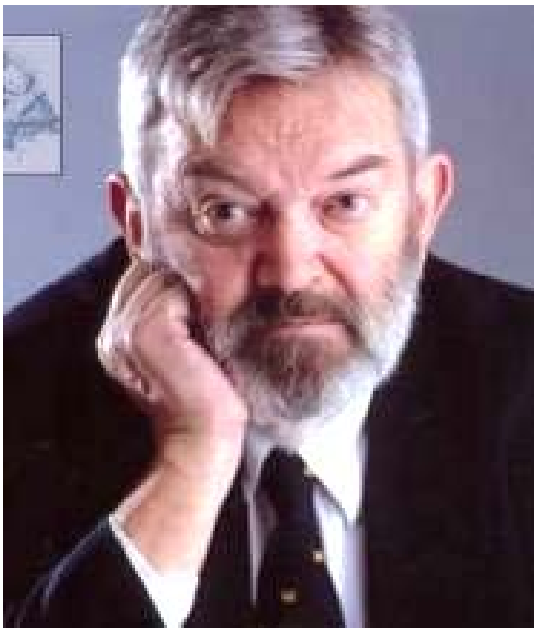

Fig. 12. Prominent Dutch theoretical physicist
Martinus Veltman, born in 1931,
Nobel Prize Laureate in physics for 1999

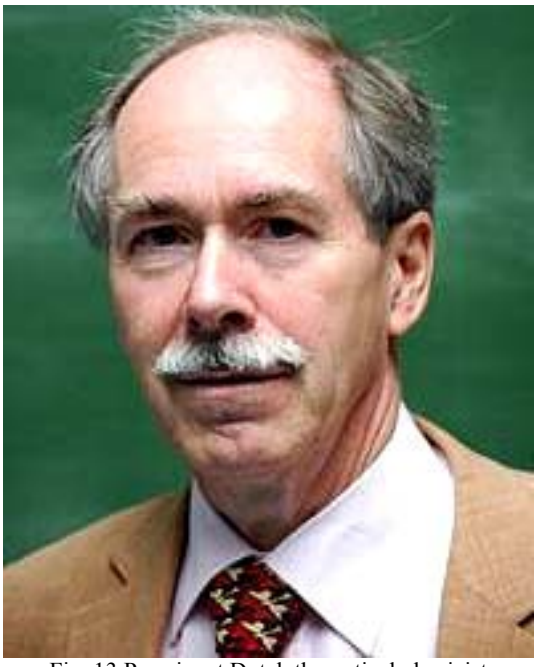

Fig. 13 Prominent Dutch theoretical physicist
Gerard Hooft, born in 1946,
Nobel Prize Laureate in physics for 1999

Developed by G. Hooft and M. Veltman new mathematical methods of renormalization of Yang-Mills fields as massless, and the weight was due to spontaneous symmetry violation in the microcosm of the laws, allowed to predict some effects of electroweak interactions of elementary particles [22-24]. So, in 1977, it based on these methods and theoretical approaches failed to predict the mass of the top quark, experimentally discovered in 1995 at the Enrico Fermi National Laboratory of Nuclear Research (USA) [22]. In addition, by using the proposed by G. Hooft and M. Veltman quantum theory of electroweak interactions were predicted mass of the intermediate vector bosons $W^{\pm}$ and Z^0 – two new elementary particles discovered thereafter experimentally at the Large Hadron Collider [3] at the European Center for Nuclear Research (CERN, Switzerland) [22, 24]. One of the Nobel Prize Laureates in physics in 1979, Sh.L. Glashow (the Prize «*for his fundamental contribution to the theory unifying weak and electromagnetic interactions*» in the field of elementary particle physics, he shared with his fellow physicists and collaborators S. Weinberg and A. Salam [4, 25]) on the scientific achievementsof M. Veltman and G. Hooft said the following [24]: «*... the theory of electroweak interactions cannot be engaged in earnest without computing innovations introduced by Veltman and Hooft*». In 1999 «*for clearing the quantum structure of electroweak interactions*» M. Veltman and G. Hooft were awarded [4, 22-25] Nobel Prize in physics. In subsequent years, M. Veltman and G. Hooft in the field of elementary particle theory fruitfully engaged in so-called «Higgs» problem associated with superheavy Higgs boson H^* which field is, according to physicists, generates mass of all existing in the microcosm particles [24].

REFERENCES

1. Available at: http://news.21.by/other-news/2012/10/09/635932.html (accessed 09 October 2012).

2. Kuz'michev V.E. *Zakony i formuly fiziki* [Laws and formulas of physics]. Kiev, Naukova Dumka Publ., 1989. 864 p. (Rus).

3. Baranov M.I. *Antologiia vydaiushchikhsia dostizhenii v nauke i tekhnike: Monografiia v 2-kh tomakh. Tom 1.* [An anthology of outstanding achievements in science and technology: Monographs in 2 vols. Vol.1]. Kharkov, NTMT Publ., 2011. 311 p. (Rus).

4. Khramov Yu.A. *Istoriia fiziki* [History of Physics]. Kiev, Feniks Publ., 2006. 1176 p. (Rus).

5. Available at: http://www.peoples.ru/science/physics/martin_lewis_perl (accessed 11 April 2012). (Rus).

6. Available at: https://en.wikipedia.org/wiki/Frederick_Reines (accessed 15 August 2012).

7. Available at: https://en.wikipedia.org/wiki/David_Lee_(physicist) (accessed 25 September 2013).

8. Available at: https://en.wikipedia.org/wiki/Robert_Coleman_Richardson (accessed 22 May 2012).

9. Available at: https://en.wikipedia.org/wiki/Douglas_Osheroff (accessed 21 February 2012).

10. Baranov M.I. *Izbrannye voprosy elektrofiziki: Monografija v 2-h tomah. Tom 1: Elektrofizika i vydajushhiesja fiziki mira* [Selected topics electrophysics: Monographs in 2 vols. Vol.1:

Electrophysics and outstanding physics of the world]. Kharkov, NTU «KhPI» Publ., 2008. 252 p. (Rus).
11. Available at: http://www.nkj.ru/archive/articles/10172 (accessed 05 May 2011).
12. Available at: http://lenta.ru/lib/14194434 (accessed 19 April 2012).
13. Available at: https://en.wikipedia.org/wiki/Steven_Chu (accessed 10 July 2011).
14. Available at: https://en.wikipedia.org/wiki/William_Daniel_Phillips (accessed 23 March 2012).
15. Available at: https://en.wikipedia.org/wiki/Claude_Cohen-Tannoudji (accessed 03 May 2012).
16. Kuhling H. *Spravochnik po fizike. Per. s nem*. [Dictonary on Physics. Translated from German]. Moscow, Mir Publ., 1982. 520 p. (Rus).
17. Baranov M.I. An anthology of the distinguished achievements in science and technique. Part 34: Discovery and study of quantum-wave nature of microscopic world of matter. *Electrical engineering & electromechanics*, 2016, no.5, pp. 3-15. (Rus). **doi: 10.20998/2074-272X.2016.5.01.**
18. Available at: http://vivovoco.astronet.ru/VV/NEWS/PRIRODA/1999/NB_PHYS.HTM (accessed 10 April 2014). (Rus).
19. Available at: https://en.wikipedia.org/wiki/Horst_Ludwig_St%C3%B6rmer (accessed 12 May 2011).
20. Available at: http://www.nkj.ru/archive/articles/8176 (accessed 23 July 2013). (Rus).
21. Available at: https://en.wikipedia.org/wiki/Robert_B._Laughlin (accessed 06 December 2013).
22. Available at: http://gruzdoff.ru/wiki/'т_Хоофт,_Герард (accessed 21 May 2012). (Rus).
23. Available at: http://velchel.ru/index.php?cnt=9&nbio=704&nubsub=0&sub=0 (accessed 11 April 2013). (Rus).
24. Available at: http://encyclopaedia.biga.ru/enc/science_and_technology/VELTMAN_MARTIN.html (accessed 18 September 2013). (Rus).
25. Available at: http://nobelprize.org/nobel_prizes/physics (accessed 02 June 2015).

Received 29.12.2015

M.I. Baranov, Doctor of Technical Science, Chief Researcher,
Scientific-&-Research Planning-&-Design Institute «Molniya»
National Technical University «Kharkiv Polytechnic Institute»,
47, Shevchenko Str., Kharkiv, 61013, Ukraine,
phone +38 057 7076841, e-mail: eft@kpi.kharkov.ua

How to cite this article:
Baranov M.I. An anthology of the distinguished achievements in science and technique. Part 36: Nobel Prize Laureates in Physics for 1995-1999. *Electrical engineering & electromechanics*, 2017, no.1, pp. 3-9. **doi: 10.20998/2074-272X.2017.1.01.**

UDC 621.3.04: 621.316 **doi: 10.20998/2074-272X.2017.1.02**

E.I. Baida, B.V. Klymenko

INVESTIGATION OF MECHANICAL STRESSES IN THE DRIVE SHAFT OF MV VACUUM CIRCUIT BREAKER

Introduction. In the last 10-15 years a dominant position in the market of medium voltage circuit breakers, vacuum circuit breakers have taken in which as an actuator mono- or bistable actuators with permanent magnets are used. Such circuit breakers are characterized by simplicity of design, high reliability, require preventive maintenance for many years. Development, research and improvement of vacuum circuit breakers are carried out at the Department for Electrical Apparatus, National Technical University «Kharkiv Polytechnic Institute». While working on the circuit breakers, developers have to deal with two related objectives – electrical and mechanical. This paper considers the solution of one of these problems – calculation of mechanical forces in the drive shaft of the vacuum circuit breaker in static and dynamic modes. This work was preceded by the failure of the results of measurements of the prototype circuit breakers' contacts. Measurements have shown that these values do not match the expected values (there were less than the value of 0.8 to 1 mm). The assumption about the reasons for this discrepancy needed to be detailed checked. The results of the work done are presented in this paper. Purpose. Investigation of static and dynamic mechanical stresses and strains in the drive shaft of the vacuum circuit breaker mechanism to determine its characteristics and material selection. Methods. The investigation of mechanical processes is performed by the finite element method in the COMSOL software package. Results. We obtain the static and dynamic characteristics of the circuit breaker drive shaft: deformations, reaction forces, stresses. These characteristics made it possible to determine the actual course of the contacts, select shaft material and calculate the forces acting on the bearings. Conclusions. It is shown that the contact velocity and contact pressure are different from the theoretical value due to the deformation of the shaft. The forces acting on the thrust bearings dynamically are by 16-39% higher than the static ones. It is assumed that further refinement of the mathematical model takes into account the traction insulators and housing, as well as dynamics of the circuit breaker. References 19, figures 12.
Key words: **vacuum circuit breakers, mechanical calculations, shaft deformation.**

В статье исследуются процессы, которые определяют механические напряжения в приводном вале вакуумного выключателя в статическом и динамическом режимах работы. Показано, что механическая деформация вала вызывает уменьшение провала контактов на величину до 30% и сил контактного нажатия на (10-11)%, эти значения не критичны и мало влияют на работу выключателя. Получены значения сил, действующих на опоры вала. Показано, что динамические усилия в опорах на (19-38)% больше статических. Полученные значения усилий позволяют выбрать материал вала и подшипники. Библ. 19, рис. 12.
Ключевые слова: **вакуумные выключатели, механические напряжения, деформация вала.**

Introduction. In the past 10-15 years a dominant position on the market of medium voltage (MV) circuit breakers, vacuum circuit breakers have taken in which as a drive bistable electromagnetic actuators with high-coercive permanent magnets are used. The leader in this area is the concern ABB, the first provided such a circuit breaker (VM1) in 1990 [1]. In Ukraine, these circuit breakers are manufactured by CJSC «High Voltage Union» and «AVM AMPERE» [2]. In the circuit breakers BB-TEL («Tavrida Electric» [3]) the electromagnetic actuators with low-coercive permanent magnets are used. Vacuum circuit breakers with electromagnetic actuators are characterized by simplicity of design, high reliability and they do not require preventive maintenance for many years.

At the Department for Electrical Apparatus, NTU «KhPI» for more than 10 years works are underway related to research, improvement and development of new configurations of vacuum circuit breakers and MV contactors [4-7]. One of the directions of such works is investigation of mechanical processes in circuit breakers with vertical (relative to the drive module) poles with vacuum interrupters. The design of these circuit breakers provides transfer of motion from the actuator to the movable contacts through the drive shaft (Fig. 1) the actuator through the axis 3 rotates the shaft which axes 4 are connected to the movable contacts through traction insulators.

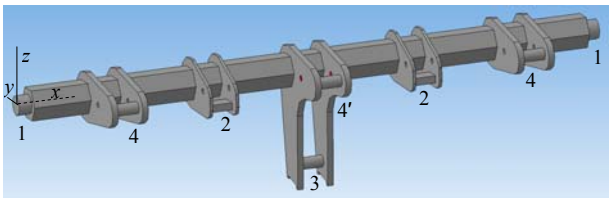

Fig. 1. Circuit breaker's drive shaft, where 1 – shaft mount axes in bearings; 2 – planes of force application of OFF springs; 3 – electromagnetic actuator's rod mounting axis; 4, 4′ – moving contacts' rod mounting axes in the end and medium poles; *x*, *y*, *z* – coordinate system axes

Problem definition. During investigation of the circuit breaker drive operation on research prototypes the following have been founded:

– on the shaft which is mounted in two bearings without intermediate supports, significant load are applied so the shaft is deformed, and the failure of contacts and forces of their preload decrease (relative forces calculated for a absolutely rigid shaft);

– shaft deformation has complex nature (bending and twisting) and as a result in bearings there are not only radial but also axial forces;

– shaft torsional vibrations arising in dynamic modes affect the course and contacts preload.

In this regard, it has been defined range of questions, the answers to which lead to an understanding of

directions of design of such devices, namely: 1) whether the critical is reduction of the forces of contact pressure due to deformation of the shaft? 2) whether the contact bounces at vibrations of the shaft are possible? 3) how critical are axial forces in the bearings? 4) how the course and preload of the contacts at they wear do change?

The aims and goal. The aim of the work is to create a mathematical model to calculate the forces and deformations of the drive shaft in static and dynamic modes, in order to determine the effect of these parameters on the operation of the vacuum circuit breaker of the configuration under consideration, which could serve as the basis for making recommendations for the design of devices of this type.

Despite the fact that in the literature the shafts calculation is widely presented ([8-11] show the most basic research), the problem is that the calculations of shafts ***of such a design*** under such conditions of mounting (Fig. 1) are absent. As shown in [12], calculations of complex structures can be carried out only by numerical methods, so all calculations in this paper were carried out in the COMSOL package by the finite element method.

The 3D model of the shaft (Fig. 1) has been created in the AutoCAD environment, and then exported to the COMSOL environment.

The calculation of the circuit breaker shaft of the accepted model. As an example, here is an example of calculation of the shaft of the experimental MV vacuum circuit breaker. Initial data: steel shaft length – 574 mm; sectional shape – hexagon with inscribed circle diameter of 32 mm; the ratio of actuator axis stroke and traction insulators axes – 1.5; total force of OFF springs (acting on the surface 2 of Fig. 1) – 1000 N; the total force of the initial compression of the contact springs (applied to the axes 4 of Fig. 1) – 6600 N (2200 N per pole); move of the axis 3 (Fig. 1) of the actuator after the contacts touch – 6 mm; theoretical course of traction insulators axes after touching the contacts (failure of contacts at absolutely rigid shaft, the axes 4 of Fig. 1) – 3.92 mm, by the far point of the axes diameter – 4.3 mm; contact spring stiffness – 280 kN / m; the total reaction force of the contact springs at the absolutely rigid shaft (applied to the axes 4 of Fig. 1) in the final position of the shaft – 9900 N (3300 N per pole).

The assumptions adopted in the calculation: mounting of the shaft supports are rigid; shaft ends rest on the non-deformable bearings; OFF springs stiffness is not taken into account (by order of magnitude less than the rigidity of the contact springs). The boundary conditions: displacement of the axis 3 in the direction minus y (Fig. 1) in the range 0 mm ... 6 mm is given; on planes 2 (Fig. 1) specific values of OFF spring forces are given; on the axes 4 specific values of the forces of contact springs with regard to their preload are given; on the surfaces 1 and the ends of the shaft conditions $\vec{\Delta} \cdot \vec{n} = 0$ are given(where $\vec{\Delta}$ is the displacement vector, $\vec{n}$ – is the normal to the surface). The last condition ensures rotation of the shaft about its longitudinal axis x without friction and without axial movement.

The calculation results in statics. Due to the deformation of the shaft (Fig. 2) the values of stroke of contacts rods and forces of contact pressure as compared with the calculation results at absolutely rigid shaft change. Appropriate calculated dependences are shown in Fig. 3.

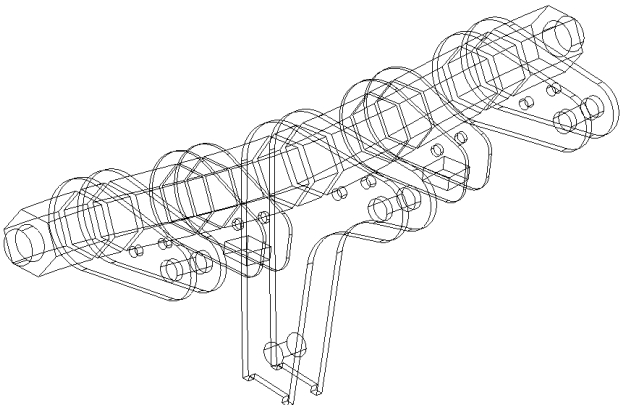

Fig. 2. Shaft deformation at 20 times magnification

As it follows from Fig. 3,*a*, in the final position of the travel distance is less than at the absolutely rigid shaft at 1.05 mm for medium pole and at 1.3 mm for the outer poles. This reduction in travel causes the reduction in contact pressure forces (Fig. 3,*b*). In particular, the initial pressing is reduced compared with pressing for the non-deformable shaft to 140 N, final for the extreme pole – to 340 N for the medium – to 280 N which is 10% ... 11% of the contact pressure and has little effect on the circuit breaker operation.

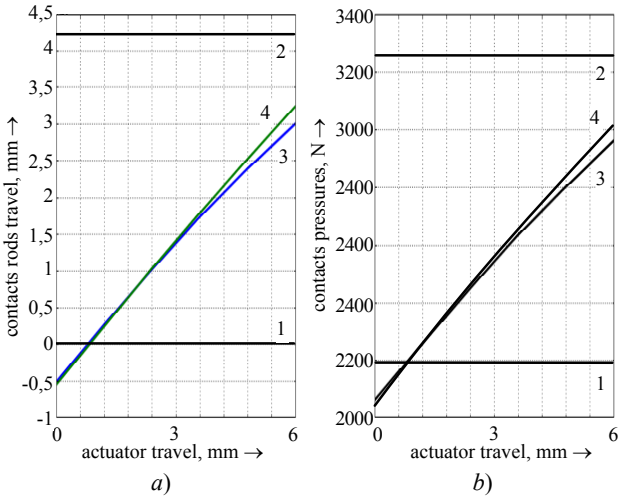

Fig. 3. Dependencies of contacts rods travel (*a*) and contact pressure (*b*) as a function of the actuator travel: 1 – the initial value for the rigid shaft (contact touch); 2 – the final value at the absolutely rigid shaft; 3 – the calculated value in the end pole; 4 – the estimated value in the medium pole

One of the important calculated parameters are the values of the forces acting on the shaft from the circuit breaker housing or forces acting on the bearings (final values are presented at the maximum travel). As a result of calculations, the values of forces by the coordinates are obtained (Fig. 1): $R_x = 3428$ N, $R_y = 5275$ N, $R_z = 4969$ N.

Longitudinal force R_x arises from the shaft ends stop to the bearings and bending of the shaft. This radial force will be equal to:

$$F_r = \sqrt{R_z^2 + R_y^2} = 7245 \text{ N}. \quad (1)$$

Obtained values make it possible to evaluate the operating conditions of bearings and choose their sizes. Design load corresponds, for example, 6304-2RSH-SKF bearing (Sweden) with dimensions 20×52×15 with acceptable loads: dynamic – 15.9 kN and static – 7.8 kN. It is supposed that the permissible axial force reaches 70 % of the radial load unused. Consequently, the permissible axial load is (15900 – 7245) · 0.7 = 8655 N. Thus, both radial and axial loads are less than the allowable value found.

The calculation results in dynamics. Static analysis does not provide complete information about the stresses, displacements and acting operating forces. This is associated with considerable force, speed and the moving masses in the process of the circuit breaker operation. Therefore, it is necessary to take into account the dynamics of the circuit breaker operation.

Accounting of traction insulators masses. The masses of moving traction insulators attached to axes 4 (Fig. 1) are taken into account by the increase in the density of the axes materials according to the formula:

$$m = \rho \cdot V, \quad (2)$$

where m is the known mass of the traction insulator equal to 0.725 kg; ρ is the unknown material density; V is the known volume of the one axis 4.

In the considered example, the density value was found to be $2.56 \cdot 10^5$ kg/m^3.

Determination of the damping coefficients. In transient analysis it is necessary to take into account the damping parameters that determine the power losses in the system (damping of vibrations of the system).

Damping by Rayleigh [13] suggests a method of accounting damping parameters depending on the mass of moving bodies and the rigidity of the system and includes the definition of the parameters of the diagonal matrix of stiffness or damping:

$$C_i = \alpha(M) + \beta(K) \cdot \omega_i^2, \quad (3)$$

where C_i is the stiffness matrix; $\alpha(M)$ is the attenuation coefficient depending on the mass M of the body; $\beta(K)$ is the attenuation coefficient depending on the system rigidity K; $\omega_i = 2 \cdot \pi f_i$ is the angular frequency of the i-th mode; f_i is the corresponding frequency of the i-th mode.

Rigidity of the i-th mode can be represented as

$$C_i = 2 \cdot \xi_i \cdot \omega_i, \quad (4)$$

there ξ_i is the viscous damping coefficient.

If damping coefficients for the i-th and j-th modes are known, the coefficients $\alpha(M)$ and $\beta(K)$ are determined by the expression:

$$\frac{1}{2} \cdot \begin{vmatrix} \frac{1}{\omega_i} & \omega_i \\ \frac{1}{\omega_j} & \omega_j \end{vmatrix} \cdot \begin{vmatrix} \alpha(M) \\ \beta(K) \end{vmatrix} = \begin{vmatrix} \xi_i \\ \xi_j \end{vmatrix}. \quad (5)$$

For steel the losses factor η = 0.2 is known [14]. Then, assuming that $\xi_i = \xi_j$ and taking into account that $\xi = \eta / 2$, we obtain

$$\xi_i = \xi_j = 0.1,$$

and corresponding values of $\alpha(M)$ and $\beta(K)$.

Natural oscillation frequencies calculations were carried out in a special mode of the COMSOL software. Fig. 4 shows the shaft shapes for the first and the second modes (enlarged).

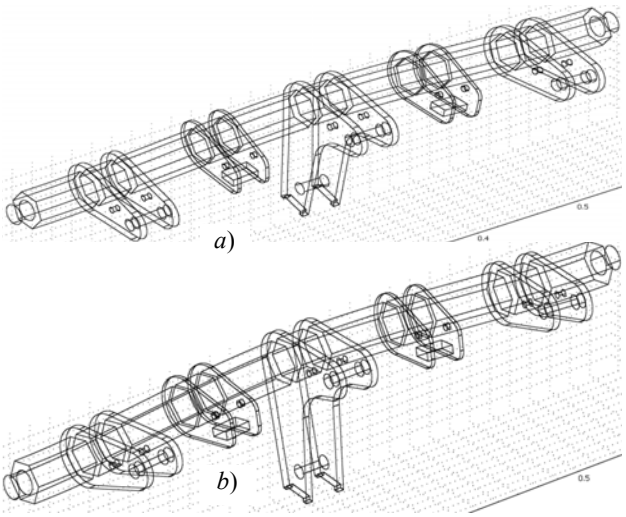

Fig. 4. Shapes of the first (*a*) and the second (*b*) modes of the shaft oscillations

As a result of calculations the following frequency values were obtained: f_1 = 242.8 Hz, f_1 = 338.0 Hz.

Based on the frequencies found, by means of (5) the coefficients of damping of the shaft oscillations were found:

$$\alpha = 177.6 \text{ s}^{-1}, \quad \beta = 5.5 \cdot 10^{-5} \text{ s}.$$

Formation of the equations of motion of the electromagnet rod and initial conditions. To calculate the dynamics it is necessary to set the temporal dependence of the movement of the actuator rod within the failure of contacts. Such calculations have been carried out previously on the basis of the coupled solution of the electromagnetic field equations, the electric circuit equations and the equation of motion [15-19]. Taking into account the location of the coordinate system, approximating temporal dependence of the actuator travel will be as follows:

$$S_y(t) = \begin{cases} -6 \cdot 10^{-3} \cdot \sin(500 \cdot t)[m], & if \ t < \pi / 1000 \\ -6 \cdot 10^{-3}[m], & if \ \pi / 1000 \end{cases}. \quad (6)$$

As the origin the circuit breaker contacts closure time after which the actuator «takes» the failure of contacts is assumed.

Initial velocity of the actuator's rod axes (item 3, Fig. 1):

$$V_0 = \frac{dS_y(0)}{dt} = -3 \text{ m/s}. \quad (7)$$

Initial velocity of the shaft points:

$$v_{0i} = \vec{\omega} \times \vec{r}_i. \quad (8)$$

In (8) we noted:

$$\vec{\omega} = \vec{e}_x \cdot \frac{V_0}{l}, \quad \vec{r}_i = \vec{e}_y \cdot y + \vec{e}_z \cdot z \,, \tag{9}$$

where l is the distance from the shaft axis of rotation to the actuator's rod mounting axis 3 (Fig. 1); $\vec{r}_i$ is the distance from points belonging to the shaft to its longitudinal axis x.

The calculation results at the initial values of the force and travel of pressure of contacts. Diagrams of temporal dependencies of contacts rods axes travel (item 4, Fig. 1) are shown in Fig. 5.

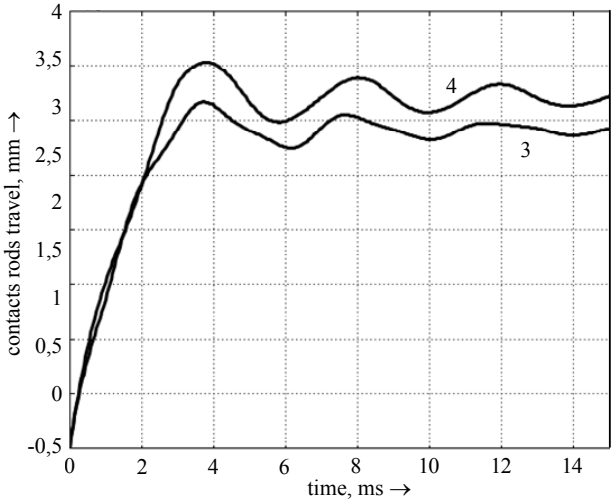

Fig. 5. Temporal dependencies of contacts rod axes travel:
3 – travel calculated value in the end pole;
4 – travel calculated value in the medium pole

From Fig. 5 it is seen that the movement of the axes of contact rods is oscillatory in nature, however, these oscillations are not critical, as their scope is relatively small (the largest value is approximately 0.25 mm which is much less of the pressure travel – about 4 mm) and does not result in the opening of contacts. Obviously, the same oscillations and forces contact pressure will be exposed (Fig. 6).

From Fig. 6 it follows that the final values of the forces tend to their values in statics – 2961 N and 3016 N, and the force of the initial pressing (in contrast to the situation in statics) at the moment of contact closure does not reduce due to the inertia of the shaft and other connected design elements.

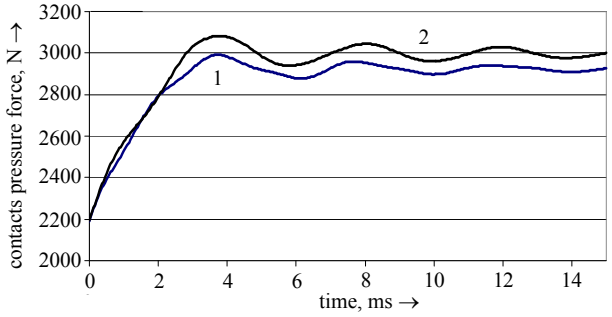

Fig. 6. Oscillation of the contact pressure force at the end (1) and medium (2) poles

Fig. 7 shows the total force of contact pressure as a function of time.

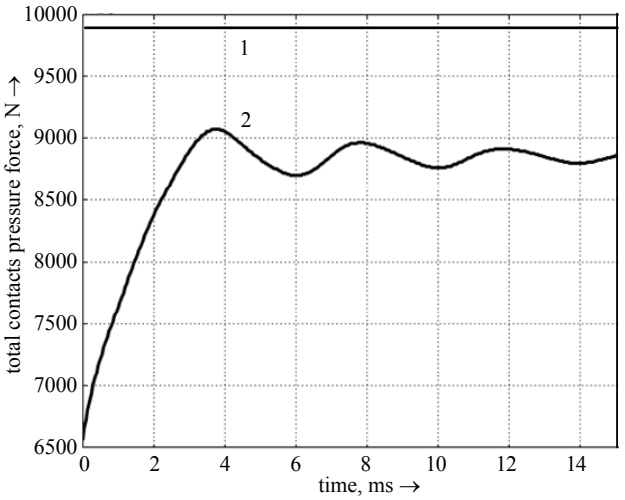

Fig. 7. Total force of contact pressure at absolutely rigid shaft (1) and calculated force (2)

In the final position after the end of the transient, the difference between the pressure at the absolutely rigid shaft and the calculated values is $9893 - 8927 = 966$ N which is of the order of 10 % of the theoretical and is not critical.

Dynamic values of bearing reactions are of some interest (Fig. 8).

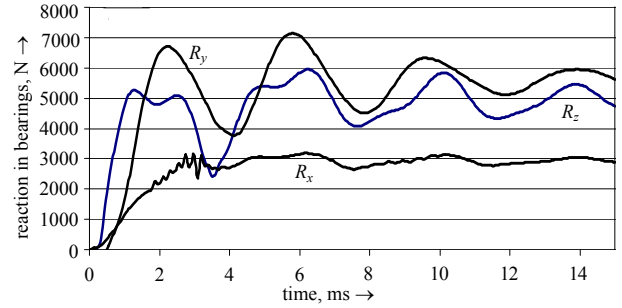

Fig. 8. Dynamic reactions of forces in bearings by coordinate axes

As follows from the Figure, the maximum dynamic responses over the static reaction on the axes: x – 1.38 times; y – 1.35 times; z – 1.19 times. Fig. 9 shows the graph of the radial dynamic force.

Calculations show that the value of the axial force does not exceed the permissible value. Fig. 10 shows the permissible axle force on the axle and axial force of the bearing. The Figure shows that the dynamic axial force does not exceed the permissible value.

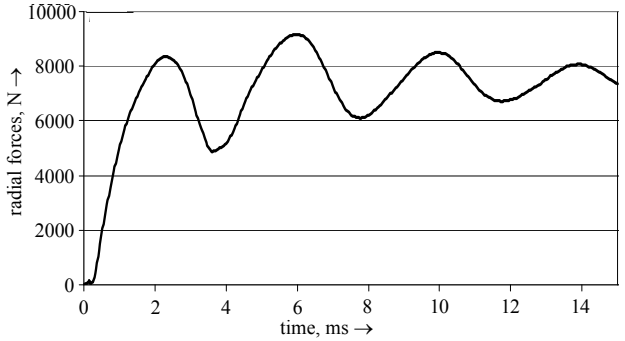

Fig. 9. Radial forces in the bearing

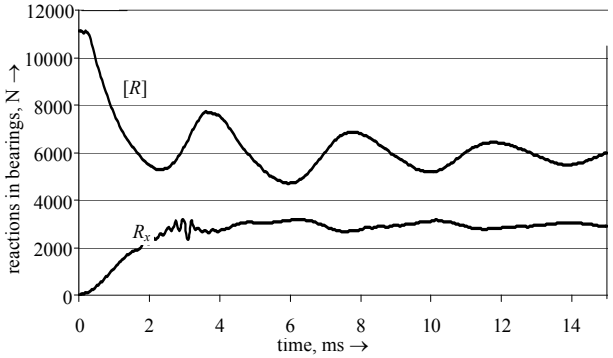

Fig. 10. Temporal dependencies of the axial R_x and permissible axial [R] forces on the bearing

The calculation results in the case of halving compression travel of the contacts at their wear (maximum contact wear during operation). In the process of operation of the circuit breaker as a result of the contact wear value of the failure of contacts reduces which affects the operation of the circuit breaker. Calculation results with decreasing contact failure twice (maximum contact wear) are presented below.

The final value of the contact pressure force decreases: on the end poles from 2961 N to 2545 N; on the medium pole – from 3016 N to 2550 N as compared with the values for new contacts. Bearings reaction here also changes: R_x –from 2428 N to 782 N; R_y – from 5275 N to 3164 N; R_z – from 4969 N to 4320 N.

Fig. 11 shows graphs of temporal dependencies of contacts rods axes travel (item 4 in Fig. 1) at reduced course of the compression.

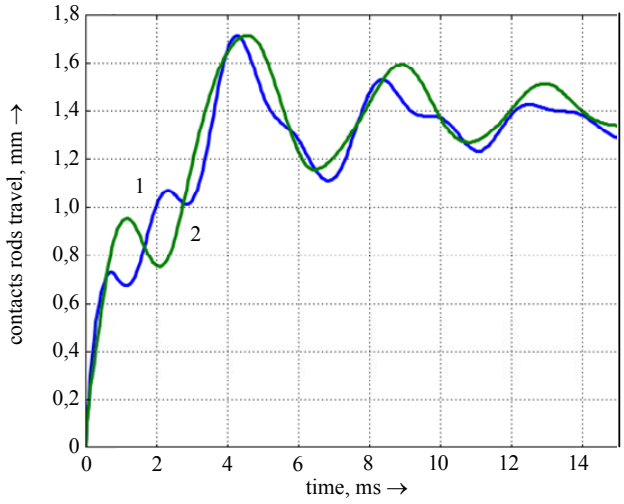

Fig. 11. Contacts rods axes travel in time:
1 – calculation value of the travel in the end pole;
2 – calculation value of the travel in the medium pole

The graphs shown in Fig. 11 demonstrate that the contact wear leads to a certain increase in the swing of oscillations of the contacts rods axes stroke – the maximum amplitude value increases to 0.3 mm which is far less even halved pressure stroke – to 2 mm, so here the contact opening does not occur.

Fig. 12 shows the calculated graph of the changes in the dynamics of the forces of contact pressure only at the end poles of the circuit breaker (as at the medium pole the pushing force is more) at reduced pressure stroke. As we can see, the force of contact pressure does not drop below the critical value – 2000 N.

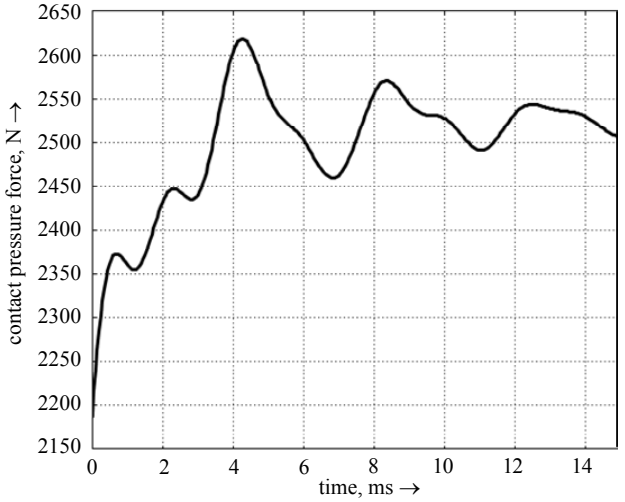

Fig. 12. Oscillations of the contact pressure force at the end poles at halving pressure stroke

In order to verify the adopted calculation assumption of the stiffness of the circuit breaker housing, calculation of its deformation in the stationary mode taking into account the effect on it of respective stationary forces R_x, R_y, R_z provided rigidly fixing of the lower surface is carried out. Because of the symmetry of the structure, calculation of the half of the housing was carried out with the corresponding boundary condition on the plane of symmetry. The calculation results show that the maximum deformation of the housing is observed in the plane of symmetry (middle) in its upper part and is equal to $7.2 \cdot 10^{-5}$ m which is much less that shaft deformation.

Conclusions.

1. During the operation the shaft is exposed essential deformations due to which because of the reduction of the pressure stroke, contact force decreases by 10% ... 11% in comparison with the calculated values provided undeformable shaft. Such a reduction is not critical and slightly affects the operation of the circuit breaker.
2. Oscillations of contacts rods axes and contact pressure forces, taking into account the shaft deformations in dynamics, do not lead to contacts bouncing at ON operation.
3. Complicated shaft deformation leads to the appearance of the axial forces.
4. Dynamic forces in the bearings are by 19% ... 38% more than static ones, which should be considered at selecting bearings.
5. At the contact wear the contacts rods travel and contact pressure reduce: at double decreasing the pressure stroke – for 466 N in the medium pole and for 416 N in the end poles. However, the reduced force (about 2550 N per pole) ensures normal operation of the circuit breaker.
6. In the case of the maximum contact wear (reduction in pressure stroke twice), the dynamic vibrations of the system do not lead to bouncing (vibration) of contacts.
7. To reduce the shaft deformations it is necessary that end shaft surfaces should stop on the bearings, and the

bearings must be mounted rigidly in the housing which increases the rigidity of the entire system.

8. On the basis of the calculations as the material of the shaft we can recommend steel 30 hardened with $\sigma_в = 11 \cdot 10^8$ N/m^2 or another steel with similar characteristics.

REFERENCES

1. VM1. Medium voltage vacuum circuit-breaker with magnetic actuator Available at: https://library.e.abb.com/public/5800cc5773e0b321c12575d0004d7342/LE_VM1(EN)B_1VCP000185-0904x.pdf (accessed 03 October 2016).

2. *Modernizirovannyi vakuumnyi vykliuchatel' s elektromagnitnym aktuatorom* (Modernized vacuum pole breaker with magnetic actuator). Available at: http://www.nbuv.gov.ua/old_jrn/Natural/eie/2011_3/22.pdf/ (accessed 11 December 2014). (Rus).

3. *Vakuumnye vykliuchateli 6-20 kV* (Vacuum circuit-breakers 6-20 kV). Available at: http://www.tavrida.com/ter/solutions/VCB/ (accessed 09 October 2016). (Rus).

4. Klymenko B.V., Bugaychuk V.M., Grechko A.M. Electromagnetic actuators for MV vacuum circuit-breakers. *Bulletin of NTU «KhPI»* , 2004, no.42, pp. 73-80. (Rus).

5. Klymenko B.V., Grechko A.M., Bugaychuk V.M. Prototype two-position solenoid actuator for MV vacuum circuit-breaker. *Electrical engineering & electromechanics*, 2005, no.2, pp. 23-28. (Rus). **doi: 10.20998/2074-272X.2005.2.06.**

6. Klymenko B.V., Grechko A.M., Bugaychuk V.M., Vyrovets S.V. A fast electromagnetic drive for an average-voltage vacuum switch with ousting of magnetic field. *Electrical engineering & electromechanics*, 2006, no.4, pp. 22-26. (Rus). **doi: 10.20998/2074-272X.2006.4.03.**

7. Klymenko B.V., Grechko A.M., Eres'ko A.V. An electromagnetic drive with a twoposition magnetic catch for medium-voltage vacuum circuit breakers. *Electrical engineering & electromechanics*, 2007, no.6, pp. 40-43. (Rus). **doi: 10.20998/2074-272X.2007.6.08.**

8. Birger I.A. *Raschet na prochnost' detalei mashin* [Calculation of the strength of machine parts]. Moscow. Mashinostroenie Publ., 1993. 639 p. (Rus).

9. Maslov G.S. *Raschety kolebanii valov: spravochnik* [Calculations shaft vibrations: Handbook] Moscow. Mashinostroenie Publ., 1980. 151 p. (Rus).

10. Ponomarev S.D. *Raschety na prochnost' v mashinostroenii. T.3* [Calculations of strength in mechanical engineering. Vol.3]. Moscow, Mashgiz Publ., 1959. 1118 p. (Rus).

11. Groman M.B., Kogaev V.P., Shneiderovich R.M. *Valy i osi. Konstruirovanie i raschet* [Shafts and axis. Design and calculation]. Moscow, Mashinostroenie Publ., 1970. 320 p. (Rus).

12. Zenkevich O. *Metod konechnykh elementov v tekhnike* [FEM in the techniques]. Moscow, Mir Publ., 1975. 541 p. (Rus).

13. Available at: http://help.solidworks.com/2013/russian/solidworks/cworks/c_rayleigh_damping.htm (accessed 05 November 2016).

14. Available at: https://syont.files.wordpress.com/2007/05/damping-properties-of-materials.pdf (accessed 02 November 2016).

15. Baida E.I. Electromagnetic equations based calculation of transients in an electromechanical mechanism. *Electrical engineering & electromechanics*, 2008, no.5, pp. 39-43. (Rus). **doi: 10.20998/2074-272X.2008.5.09.**

16. Baida E.I. Modeling of dynamic characteristics of DC electromagnetic mechanisms with a magnetic latch. *Electrical engineering & electromechanics*, 2010, no.2, pp. 3-5. (Rus). **doi: 10.20998/2074-272X.2010.2.01.**

17. Baida E.I. Calculation of dynamics twoposition electromagnet of direct-current with magnetic catch. *Electrical engineering & electromechanics*, 2010, no.4, pp. 10-12. (Rus). **doi: 10.20998/2074-272X.2010.4.02.**

18. Baida E.I. Influence of additional resistance on pre-start time of two-position electromagnetic drive with magnetic latch for MV vacuum circuit-breaker. *Electrical engineering & electromechanics*, 2011, no.4, pp. 13-15. (Rus). **doi: 10.20998/2074-272X.2011.4.03.**

19. Baida E.I. A mathematical model for calculating the dynamics of two-position electromagnetic actuator vacuum circuit breakers medium voltage. *Journal of scientific publications graduate and doctoral students*, 2013, no.1, pp. 136-141. (Rus).

Received 30.11.2016

E.I. Baida[1]*, Candidate of Technical Science, Associate Professor,*

B.V. Klymenko[1]*, Doctor of Technical Science, Professor,*

[1] National Technical University «Kharkiv Polytechnic Institute», 2, Kyrpychova Str., Kharkiv, 61002, Ukraine,

phone +38 096 1877707, +38 050 6534982,

e-mail: baida.kpi@gmail.com, b.v.klymenko@gmail.com

How to cite this article:

Baida E.I., Klymenko B.V. Investigation of mechanical stresses in the drive shaft of MV vacuum circuit breaker. *Electrical engineering & electromechanics*, 2017, no.1, pp. 10-15. **doi: 10.20998/2074-272X.2017.1.02.**

UDC 621.3.01 **doi: 10.20998/2074-272X.2017.1.03**

B.I. Kuznetsov, T.B. Nikitina, A.V. Voloshko, I.V. Bovdyj, E.V. Vinichenko, B.B. Kobilyanskiy

EXPERIMENTAL RESEARCH OF MAGNETIC FIELD SENSORS SPATIAL ARRANGEMENT INFLUENCE ON EFFICIENCY OF CLOSED LOOP OF ACTIVE SCREENING SYSTEM OF MAGNETIC FIELD OF POWER LINE

Purpose. ***Experimental research of magnetic field sensors spatial arrangement influence on efficiency of closed loop active screening system by magnetic field of high voltage power lines developed a three-phase single-circuit high voltage power lines, creating a rotating magnetic field with the most complex space-time structure.*** ***Methodology.*** ***Optimal spatial arrangement of the magnetic field sensors is determined by solving the active magnetic field screening system synthesis problems with which the system provides the greatest efficiency of the active magnetic field shielding. Synthesis of active screening system is reduced to the problem of multi-criteria nonlinear programming with constraints in which calculation of the objective functions and constraints are carried out on the basis of Biot-Savart-Laplace law. The problem is solved by a stochastic multi-agent optimization by multiswarm of particles which can significantly reduce the time to solve it. Calculated arrangement of magnetic field sensors in a given space defined by the points at which the values of the corresponding components of the vector of magnetic induction take minimal values.*** ***Results.*** ***For the first time experimentally that changes in the position of the magnetic field sensors relative to their calculated position reduces the effectiveness of screening. The optimum position of the magnetic field sensors are the points at which the levels of the magnetic induction vector of projections orthogonal to the planes of the compensating coils are minimum values.*** ***Originality.*** ***For the first time invited to place sensors closed loop active screening system by magnetic field of high voltage power lines at the points where the calculated levels of corresponding projections of the magnetic induction vector orthogonal planes compensating windings are minimum values.*** ***Practical value.*** ***Practical recommendations for evidence-based selection of the spatial arrangement of the magnetic field sensors in a given area to ensure maximum efficiency of the active magnetic field screening system.*** References 14. figures 6.

Key words: **power frequency magnetic field, high voltage power lines model, active screening system model, experimental research.**

Проведено экспериментальное исследование влияния пространственного расположения датчиков магнитного поля на эффективность замкнутой системы активного экранирования магнитного поля линий электропередачи на разработанном макете трехфазной одноцепной воздушной линии электропередачи, создающей вращающееся поле с наиболее сложной пространственно-временной структурой. Экспериментально показано, что наибольшую эффективность имеет замкнутая система активного экранирования магнитного поля, у которой датчики магнитного поля пространственно расположены в расчетных точках, полученных при синтезе системы, в которых значения соответствующих компонент вектора магнитной индукции принимают минимальное значение. Библ. 14, рис. 6.

Ключевые слова: **магнитное поле промышленной частоты, макет воздушной линии электропередачи, макет системы активного экранирования, экспериментальные исследования.**

Introduction. Ministry of Fuel and Energy of Ukraine [1] in 2014 introduced regulatory levels of the magnetic field (MF) with a frequency of 50 Hz. Many residential buildings and structures are located in the vicinity of overhead power lines so that the level of the magnetic field inside them exceeds these standards. The use of active screening systems can reduce the levels of magnetic fields to standard values and continue the operation of such buildings.

Analysis of existing active screening systems. In the systems of active screening of man-made magnetic field of industrial frequency [2-10] as the executive body they use special winding – active cables, the number of which is determined by the specifics of the problem being solved. Active screening system can include one, two, three, six, twenty-four or more windings. To control these coils they use a different number of magnetic field meters – magnetometers: one, two, three, six, twenty-four or more. Number of magnetometers usually equals to the number of controlled winding or number of windings pairs. In particular, with six coils type magnetometer three Helmholtz coils may be used, located in the center of the magnetic field shielding region [10] or six magnetometers disposed in respective planes and orthogonally oriented with respect to the control windings.

In the synthesis of closed systems of active shielding magnetic field, power transmission lines an important issue is to determine the position of the magnetic field sensors, in which the efficiency of the system has the greatest value. Typically, a closed system is configured in such a way that with the help of the given magnetic windings of the executive bodies to minimize the level of the magnetic field at the points of the installation of the magnetic field sensors. One approach to the definition of the position of the magnetic field sensors based on the solution of the active screening system synthesis problem of the magnetic field by providing the maximum efficiency of the system of active screening of the magnetic field. Synthesis of active screening system is reduced to the problem of multi-criteria linear programming with restrictions, in which calculation of the objective functions and constraints are carried out on the basis of the of Biot-Savart-Laplace low [11, 12]. The problem is solved by a stochastic multi-agent optimization by multiswarm of particles [13, 14] which can significantly reduce the time to solve it. Calculated arrangement of magnetic field sensors in a given space defined by the points at which the values of the corresponding components of the vector of magnetic induction take minimal values.

The goal of the work is the experimental study of the influence of the spatial arrangement of the magnetic field sensors on the efficiency of the closed system of the active screening of the magnetic field of power lines on the layout developed a three-phase single-circuit overhead transmission line, creating a rotating field with the most complex space-time structure.

The sketch of the transmission line layout, control windings, as well as the region of space in which the magnetic field must be shielded are shown in Fig. 1. Active screening system comprises two compensating winding forming the compensating magnetic field when current flows through it, generated by the control system (CS) in the magnetic field feedback signal function, that formed by the magnetic field sensors (FS) installed in the protected space. The CS receives power from the secondary power source.

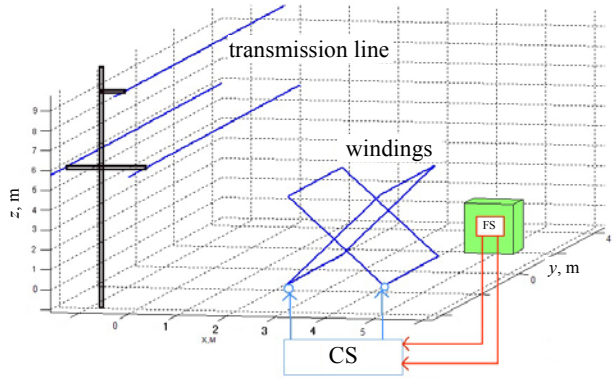

Fig. 1. Sketch of the active screening system layout

The coordinates of the spatial location and geometric dimensions of the compensation coils, as well as the parameters of the active screening system regulators determined on the basis developed in [11] the active screening system MF synthesis method in the course of solving multiobjective optimization problem. Fig. 2 shows the lines of equal levels of magnetic flux density with enabled active screening system.

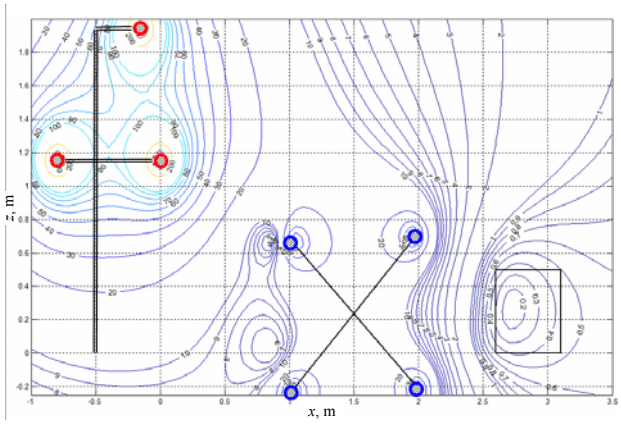

Fig. 2. Lines of equal levels of magnetic flux density with enabled active screening system

Note that the need to use two compensating windings due to the fact that the three-phase single-circuit transmission line creates an almost circular magnetic field. Fig. 3,*a* shows an exemplary travel time curve formed by the initial induction vector of the magnetic field generated by this power line. Therefore, to compensate for this source of magnetic field must have at least two compensation coil to generate a circular magnetic field.

Fig. 3,*b* shows a locus formed by the vector of the magnetic field generated by the two compensating windings. As can be seen from this figure, by means of compensating windings creates a magnetic field that is close enough to the original to the magnetic field generated by power lines.

Fig. 3,*c* shown in the hodograph formed induction vector of the total magnetic field generated by power lines and compensating windings when the active screening system. As can be seen from this figure, the hodograph formed induction vector remaining after the screening of the active magnetic field system has an order of magnitude smaller unit compared to the initial magnetic field.

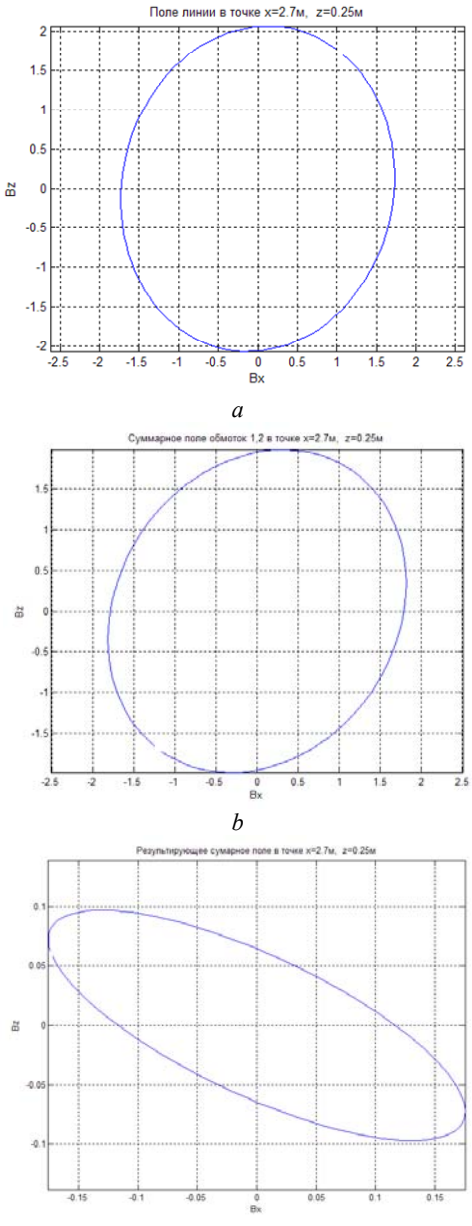

Fig. 3. Hodographs of vectors of magnetic flux density: *a*) the original, created by power lines; *b*) compensation windings; *c*) the total generated by the power lines and the system enabled

Layout of the transmission line and active screening system. For experimental studies the layout of power transmission lines and active screening system is developed. Fig. 4,*a* shows the external view of transmission line layout, and Fig. 4,*b* shows the external view of the compensation system layout. This Figure shows the compensation coils and magnetic field sensors.

a

b

Fig. 4. External view of the layout:
a) transmission line; *b*) compensation system

These mock-ups were carried out pre-experimental studies to verify the adequacy of the mathematical models of the magnetic field on the basis of the Biot-Savar-Laplace law [11, 12] the real processes occurring in models of transmission lines and compensating windings active screening system. As shown by experimental studies of models of transmission lines and compensating windings at different currents and different modes of operation, the deviation of the experimental values of the magnetic induction generated by power lines layout and compensating windings of calculated made by the method of [11] do not exceed 7 %.

The results of experimental investigations. Let us now consider the experimental study of the active screening system. The system has two independent magnetic field sensors in which the channels are closed current control compensation windings. First, we consider the experimental study of the active screening system when magnetic field sensors are arranged in the reference points of the space in which it is necessary to shield the magnetic field. These calculated points correspond to points at which the values of the corresponding components of the vector of magnetic induction take a minimum value. To determine these points first solved the problem of synthesis of active screening system. The initial parameters for the synthesis of the system are the parameters of power line – operating current, the geometry and the number of wires, the location of the transmission line with respect to the protected space, as well as the size of the protected area and the characteristic value of the magnetic field, which should be achieved as a result of screening. The result of the synthesis system is the number, shape, spatial arrangement, wiring diagram, currents compensation coils, as well as the resulting value of the magnetic field at the points of the protected area, as well as the parameters of the control system controls. Based on the resultant distribution system during the synthesis of the resultant magnetic field in this area are the points at which the values of the corresponding components of the vector of magnetic induction take minimal values.

Fig. 5,*a* shows the surface distribution of the original magnetic field power transmission line in the middle section of the space and the surface magnetic field distribution-enabled system, and Fig. 5,*b* shows the surface level of the compensation magnetic field induction system such baseline magnetic field of the power line.

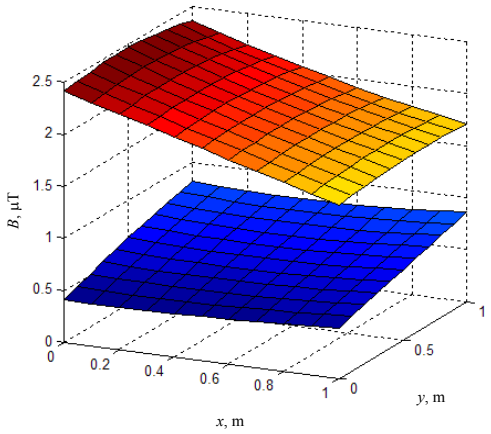

a

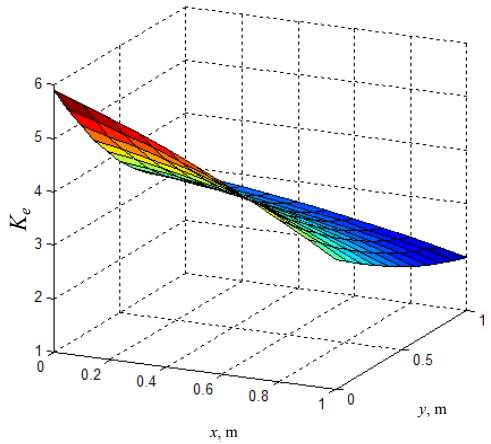

b

Fig 5. Surfaces of distribution: *a*) the magnetic flux density of the initial magnetic field and the magnetic field of power line with enabled system; *b*) the level of compensation of the magnetic flux density using the system

Thus, when the system level active shielding of magnetic flux density in the considered region remains practically constant and is not greater than 0.5 μT, and the level of compensation of the magnetic field is more than 5 μT.

Note that the deviation of the experimental values of the magnetic flux density layout enabled active screening system from the calculated obtained in [11] does not exceed 10 %. Moreover, these variations are mainly due to inexact installation of the magnetometer, and the error operation controls open and closed control channels.

Fig. 6 shows the same distribution surface, as in Fig. 5 when placed in a magnetic field sensors central area shielding. With this arrangement, the sensor system has the greatest shielding effectiveness in the central part of the screening space – precisely where the magnetic field sensors are arranged. However, with this arrangement, the sensor system is active shielding has a higher level of residual magnetic induction in virtually all areas where it is necessary to shield the magnetic field.

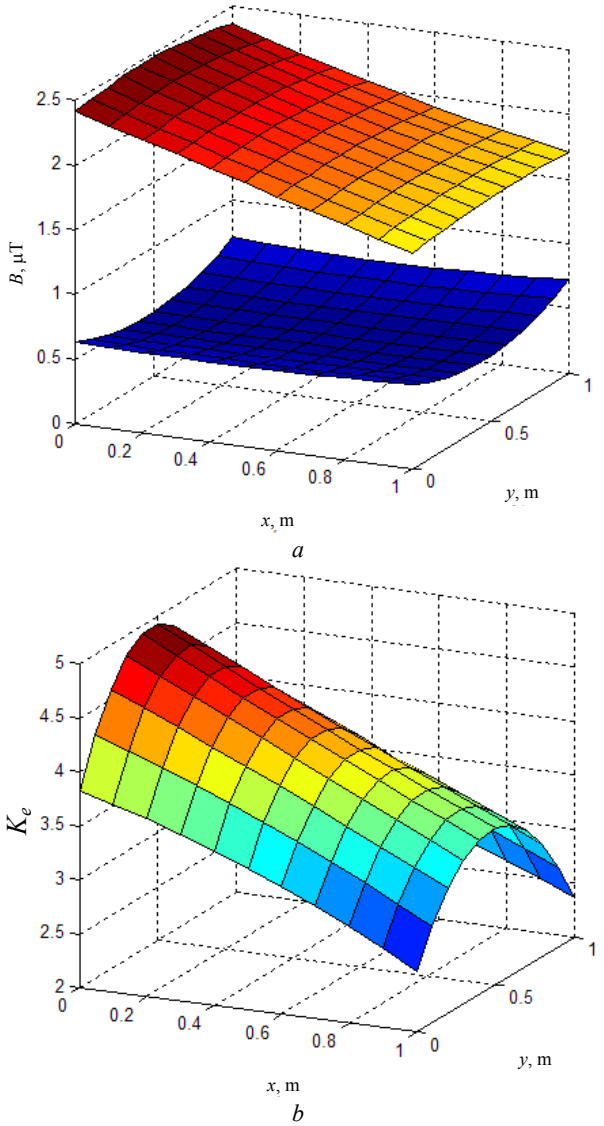

Fig. 6. Surfaces of distribution: *a*) the magnetic flux density of the initial magnetic field and the magnetic field of power line with enabled system; *b*) the level of compensation of the magnetic flux density by the system when placing field sensors in the central area of the screening

Conclusions.

Thus, it is experimentally found that the change of the position of magnetic field sensors relative to their calculated position reduces the efficiency of the screening system. The optimum position of the magnetic field sensors is the points at which the levels of projections of the magnetic flux density vector orthogonal to the planes of the compensating coils have minimum values.

REFERENCES

1. *Pravila ulashtuvannya electroustanovok. Vyd. 3, pererob. i dop* [Electrical Installation Regulations. 3rd edition, revised and enlarged]. Kyiv, Minpalyvenergo of Ukraine Publ., 2010. 736 p. (Ukr).

2. Active Magnetic Shielding (Field Cancellation). Available at: http://www.emfservices.com/afcs.html (accessed 10 September 2012).

3. Beltran H., Fuster V., García M. Magnetic field reduction screening system for a magnetic field source used in industrial applications. *9 Congreso Hispano Luso de Ingeniería Eléctrica (9 CHLIE)*, Marbella (Málaga, Spain), 2005, pp. 84-99.

4. Celozzi S., Garzia F. Active shielding for power-frequency magnetic field reduction using genetic algorithms optimization. *IEE Proceedings – Science, Measurement and Technology*, 2004, Vol.151, no.1, pp. 2-7. **doi: 10.1049/ip-smt:20040002**.

5. Ter Brake H.J.M., Wieringa H.J., Rogalla H. Improvement of the performance of a mu -metal magnetically shielded room by means of active compensation (biomagnetic applications). *Measurement Science and Technology*, 1991, Vol.2(7), pp. 596-601. **doi: 10.1088/0957-0233/2/7/004.**

6. Yamazaki K., Kato K., Kobayashi K. MCG Measurement in the environment of active magnetic shield. *Neurology and Clinical Neurophysiology*, 2004, Vol. 40, pp. 1-4.

7. Celozzi S. Active compensation and partial shields for the power-frequency magnetic field reduction. *Conference Paper of IEEE International Symposium on Electromagnetic Compatibility*. Minneapolis (USA), 2002, Vol.1, pp. 222-226. **doi: 10.1109/isemc.2002.1032478.**

8. Shenkman A., Sonkin N., Kamensky V. Active protection from electromagnetic field hazards of a high voltage power line. *HAIT Journal of Science and Engineering. Series B: Applied Sciences and Engineering*, Vol. 2, Issues 1-2, pp. 254-265.

9. Ter Brake H.J.M., Huonker R., Rogalla H. New results in active noise compensation for magnetically shielded rooms. *Measurement Science and Technology*, 1993, Vol. 4, Issue 12, pp. 1370-1375. **doi: 10.1088/0957-0233/4/12/010.**

10. Kazuo Kato, Keita Yamazaki, Tomoya Sato, Akira Haga, Takashi Okitsu, Kazuhiro Muramatsu, Tomoaki Ueda, Masahito Yoshizawa. Shielding effect of panel type active magnetic compensation. *IEEJ Transactions on Fundamentals and Materials*, 2005, Vol. 125, Issue 2, pp. 99-106. **doi: 10.1541/ieejfms.125.99.**

11. Rozov V.Yu., Reutskyi S.Yu. Pyliugina O.Yu. The method of calculation of the magnetic field of three-phase power lines. *Tekhnichna elektrodynamika*, 2014, no.5, pp. 11-13. (Rus).

12. Nikolova N.K., Bakr M.H. *Electromagnetics I. Matlab Experiments Manual for EE2FH3*. Department of Electrical and Computer Engineering McMaster University, 2012. 96 p.
13. Clerc M. *Particle Swarm Optimization*. London, ISTE Ltd., 2006. 244 p. **doi: 10.1002/9780470612163.**
14. Gazi V., Passino K.M. *Swarm Stability and Optimization*. Springer, 2011. 318 p. **doi: 10.1007/978-3-642-18041-5.**

Received 15.09.2016

B.I. Kuznetsov[1], *Doctor of Technical Science, Professor,*
T.B. Nikitina[2], *Doctor of Technical Science, Professor,*
A.V. Voloshko[1], *Candidate of Technical Science,*
I.V. Bovdyj[1], *Candidate of Technical Science,*
E.V. Vinichenko[1], *Candidate of Technical Science,*
B.B. Kobilyanskiy[1], *Candidate of Technical Science, Associate Professor,*
[1] State Institution «Institute of Technical Problems of Magnetism of the NAS of Ukraine»,
19, Industrialna Str., Kharkiv, 61106, Ukraine,
phone +38 050 5766900, e-mail: bikuznetsov@mail.ru
[2] Kharkov National Automobile and Highway University,
25, Petrovskogo Str., Kharkov, 61002, Ukraine,
e-mail: tatjana55555@gmail.com

How to cite this article:
Kuznetsov B.I., Nikitina T.B., Voloshko A.V., Bovdyj I.V., Vinichenko E.V., Kobilyanskiy B.B. Experimental research of magnetic field sensors spatial arrangement influence on efficiency of closed loop of active screening system of magnetic field of power line. *Electrical engineering & electromechanics*, 2017, no.1, pp. 16-20. **doi: 10.20998/2074-272X.2017.1.03.**

UDC 681.5 **doi: 10.20998/2074-272X.2017.1.04**

N.J. Khlopenko, I.N. Khlopenko

STRUCTURAL SYNTHESIS OF A STABILIZING ROBUST CONTROLLER OF THE ROTOR FLUX LINKAGE

Purpose. *The aim is to structural synthesis of robust stabilizing control of the rotor flux vector control system of induction motor.* ***Methodology.*** *Synthesis controller structure was carried out in two stages. The first stage constructed a mathematical model of the channel of the rotor flux with parametric uncertainty and calculated transfer function of H_∞-suboptimal controller by method of the mixed sensitivity. The second stage was carried out the expansion of the transfer function of the continued fraction for the Euclidean algorithm. This fraction was used to construct the controller structural scheme.* ***Results.*** *Computer modeling of the transfer function of H_∞-suboptimal controller. Achieved decomposition found the transfer function of the continued fraction. The flow diagram of suboptimal H_∞-controller with a proportional and integrating links and a few summers. The curves of transient rotor flux linkage in packages Robust Control Toolbox and Simulink. They coincide in the steady state, but differ among themselves in the transition.* ***Originality.*** *We developed the method of structural synthesis of robust stabilizing controller of the flux linkage rotor, H_∞-suboptimal structural scheme of which is presented in the form of simple compounds integrating and proportional elements of the same order as the controller with the strictly correct transfer function, and takes into account the parametric uncertainty of control object.* ***The results of the simulation of transient processes in a variety of packages MATLAB applications confirms the adequacy and small sensitivity of the system to parametric perturbation.*** *The practical value. The resulting structure of the controller makes it possible to carry out the modernization of electric control systems, in use, with minimal financial costs.* References 10, figures 6.

Key words: **electric drive, vector control, flux linkage channel, structure of H_∞-optimal controller.**

Цель. *Целью работы является структурный синтез стабилизирующего робастного регулятора потокосцепления ротора системы векторного управления асинхронного электропривода.* ***Методология.*** *Синтез структуры регулятора проводился в два этапа. На первом этапе строилась математическая модель канала потокосцепления ротора с параметрической неопределенностью и рассчитывалась передаточная функция H_∞-субоптимального регулятора по методу смешанной чувствительности. На втором этапе выполнялось разложение найденной передаточной функции в цепную дробь по алгоритму Евклида. Эта дробь использовалась для построения структурной схемы регулятора.* ***Результаты.*** *Проведено компьютерное моделирование передаточной функции H_∞-субоптимального регулятора. Выполнено разложение найденной передаточной функции в цепную дробь. Построена структурная схема H_∞-субоптимального регулятора с интегрирующих и пропорциональных звеньев и нескольких сумматоров. Получены кривые переходных процессов потокосцепления ротора в пакетах Robust Control Toolbox и Simulink. Они совпадают на установившемся режиме, а на переходном несколько отличаются между собой.* ***Новизна.*** *Построена математическая модель канала потокосцепления ротора с параметрической неопределенностью. Разработана методика структурного синтеза робастного регулятора системы управления потокосцеплением, которая обеспечивает нахождение оптимальной передаточной функции регулятора с параметрической неопределенностью в виде структуры, содержащей интегрирующие и пропорциональные звенья и сумматоры.* ***Практическое значение.*** *Полученная структура регулятора дает возможность проводить модернизацию систем управления электроприводов, находящихся в эксплуатации, с минимальными финансовыми затратами.* Библ. 10, рис. 6.

Ключевые слова: **электропривод, векторное управление, канал потокосцепления, структура H_∞-оптимального регулятора.**

Introduction. Stricter quality requirements for the functioning of the vector control of induction electric drives in conditions of uncertainty leads to the need to stabilize the rotor flux. This is essential problem of structural synthesis of robust stabilizing controller. However, such a regulator is usually of higher order which makes it difficult to use the vector control system. Decomposition of robust regulator on the elementary units allows you to get rid of this shortcoming. Its essence is to control the representation of a structure consisting of standard units. To create a regulator of such links element base exists. Realization of control on the basis of this framework permits to stabilize the rotor flux linkage, as well as to modernize the control systems in use, with little financial cost.

The issues of stabilization of the parameters of vector control systems with uncertainties involved many researchers [1-6]. They built mathematical models and synthesized robust controls for many kinds of systems.

The goal of the work is structural synthesis of robust stabilizing control of the rotor flux vector control system of induction electric drive.

The theoretical basis for the structural synthesis of robust control knob served H_∞-theory [7] and the theory of continued fractions [8]. Calculations were carried out with the assistance of MATLAB-7 expansion packs [9]. The studies were discussed at the VII International Scientific and Technical conference «Innovations in Shipbuilding and Ocean Engineering» (Ukraine, Nikolaev, 2016).

Methods and results of investigations. Fig. 1 is a block diagram of the channel of the rotor flux linkage in the space of signals «input-output» [10], which includes

the transfer functions of the frequency converter and the stator windings 1 and rotor windings 2 of induction motor with squirrel-cage rotor.

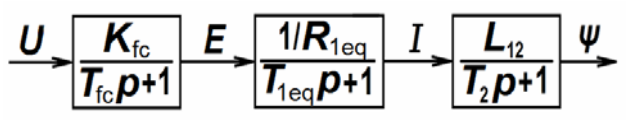

Fig. 1. A block diagram of the rotor flux linkage channel

In this scheme, the uncertainty of the parameters that are most sensitive to changes in the object model, the gain of the frequency converter have been chosen K_{fc}, equivalent active resistances R_{1eq} and R_2, inductances L_1, L_2 and mutual inductance L_{12} of stator winding 1 and rotor winding 2, and $R_{1eq} = R_1+(k_2)^2R_2$ (R_1 is the active resistance); $k_2 = L_{12}/L_2$.

We proceed from the block diagram of the equations of state in the normal form of the operator:

$$\begin{aligned} pE &= -\frac{1}{T_{fc}}E + \frac{K_{fc}}{T_{fc}}U; \\ pI &= -\frac{1}{T_{1eq}}I + \frac{1}{R_{1eq}T_{1eq}}E; \\ p\Psi &= -\frac{1}{T_2}\Psi + \frac{L_{12}}{T_2}I, \end{aligned} \tag{1}$$

where p is the Laplace operator; E is the EMF of the frequency converter; U is the control action (the projection of the stator voltage vector in the direction of the vector of the rotor flux linkage); I is the current in the channel of the rotor flux linkage; T_{fc} is the time constant of the frequency converter; $T_{1eq} = L_{1eq}/R_{1eq}$ is the electromagnetic stator winding time constant; $L_{1eq} = \sigma L_1$ is its equivalent inductance; Ψ is the magnitude of the rotor flux linkage; $T_2 = L_2/R_2$ is the rotor winding electromagnetic time constant; $\sigma = 1 - (L_{12})^2/(L_1L_2)$ is the scattering coefficient of the magnetic field.

Coefficients k_2 and σ are assumed constant. We introduce the dimensionless quantities

$$x_1 = \frac{\Psi}{\Psi_n},\quad x_2 = \frac{I}{I_n},\quad x_3 = \frac{E}{E_n},\quad u = \frac{U}{U_n}, \tag{2}$$

where n is the index of nominal quantities.

We proceed in the equations (1) to dimensionless quantities (2):

$$\begin{aligned} px_1 &= -\frac{1}{T_2}x_1 + \frac{L_{12}I_n}{T_2\Psi_n}x_2; \\ px_2 &= -\frac{1}{T_{1eq}}x_2 + \frac{E_n}{R_{1eq}T_{1eq}I_n}x_3; \\ px_3 &= -\frac{1}{T_{fc}}x_3 + \frac{K_{fc}U_n}{T_{fc}E_n}u. \end{aligned} \tag{3}$$

Using equations (3), we construct a structural diagram of a system in the state space (Fig. 2).

We assume that undetermined system parameters K_{fc}, R_{1eq}, R_2, L_1, L_2 and L_{12} change in intervals

$$\begin{aligned} K_{fc} &= K_{fc\,n}(1 + p_{K_{fc}}\delta_{K_{fc}}); \\ R_{1eq} &= R_{1eq\,n}(1 + p_{R_{1eq}}\delta_{R_{1eq}}); \\ R_2 &= R_{2n}(1 + p_{R_2}\delta_{R_2}); \\ L_{1eq} &= L_{1eq\,n}(1 + p_{L_{1eq}}\delta_{L_{1eq}}); \\ L_2 &= L_{2n}(1 + p_{L_2}\delta_{L_2}); \\ L_{12} &= L_{12n}(1 + p_{L_{12}}\delta_{L_{12}}), \end{aligned} \tag{4}$$

where $p_{K_{fc}}$, $p_{R_{1eq}}$, p_{R_2}, $p_{L_{1eq}}$, p_{L_2}, $p_{L_{12}}$ are the relative values of the coefficients of variance of undetermined parameters $\delta_{K_{fc}}$, $\delta_{R_{1eq}}$, δ_{R_2}, $\delta_{L_{1eq}}$, δ_{L_2} and $\delta_{L_{12}}$.

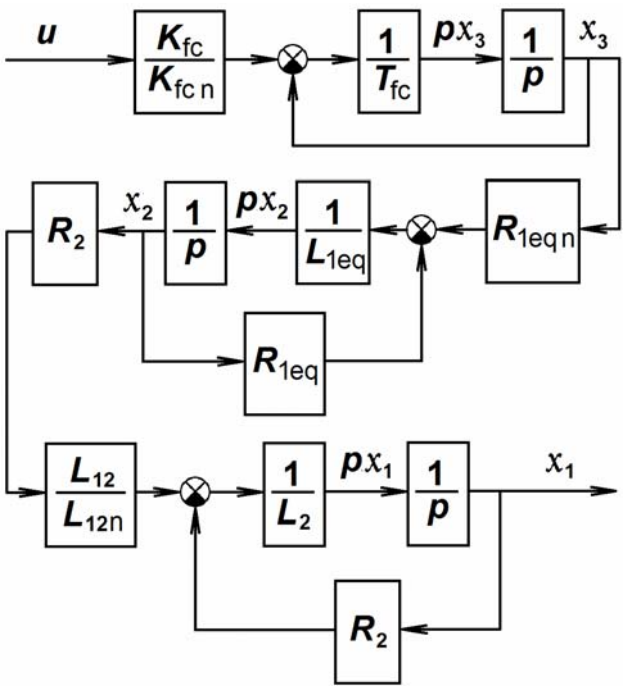

Fig. 2. A block diagram of the rotor flux linkage channel in the state space

We replace each of the parameters (4) shown in Fig. 2 a block diagram. The result is a structural diagram of a system with parametric uncertainty shown in Fig. 3.

We proceed from this block diagram to the vector equations of state in the operator form:

$$\begin{aligned} px &= Ax + B_1w + B_2u; \\ z &= C_1x + D_{11}w + D_{12}u; \\ y &= C_2x + D_{21}w + D_{22}u, \end{aligned} \tag{5}$$

where

$$A = \begin{bmatrix} -\frac{R_{2n}}{L_{2n}} & \frac{R_{2n}}{L_{2n}} & 0 \\ 0 & -\frac{R_{1eq\,n}}{L_{1eq\,n}} & \frac{R_{1eq\,n}}{L_{1eq\,n}} \\ 0 & 0 & -\frac{1}{T_{fc}} \end{bmatrix};$$

$$B_1=\begin{bmatrix} 0 & 0 & 0 & \frac{p_{R_2}}{L_{2n}} & \frac{p_{L_{12}}}{L_{2n}} & 0 & -\frac{p_{R_2}}{L_{2n}} \\ 0 & -p_{L_{1eq}} & -\frac{p_{R_{1eq}}}{L_{1eqn}} & 0 & 0 & 0 & 0 \\ \frac{p_{K_{fc}}}{T_{fc}} & 0 & 0 & 0 & 0 & 0 & 0 \end{bmatrix};$$

$$C_1=\begin{bmatrix} 0 & 0 & 0 \\ 0 & -\frac{R_{1eqn}}{L_{1eqn}} & \frac{R_{1eqn}}{L_{1eqn}} \\ 0 & R_{1eqn} & 0 \\ 0 & R_{2n} & 0 \\ 0 & R_{2n} & 0 \\ -\frac{R_{2n}}{L_{2n}} & \frac{R_{2n}}{L_{2n}} & 0 \\ R_{2n} & 0 & 0 \end{bmatrix}; C_2=\begin{bmatrix}1 & 0 & 0\end{bmatrix};$$

$$D_{11}=\begin{bmatrix} 0 & 0 & 0 & 0 & 0 & 0 & 0 \\ 0 & -p_{L_{1eq}} & -\frac{p_{R_{1eq}}}{L_{1eqn}} & 0 & 0 & 0 & 0 \\ 0 & 0 & 0 & 0 & 0 & 0 & 0 \\ 0 & 0 & 0 & 0 & 0 & 0 & 0 \\ 0 & 0 & 0 & p_{R_2} & 0 & 0 & 0 \\ 0 & 0 & 0 & \frac{p_{R_2}}{L_{2n}} & \frac{p_{L_{12}}}{L_{2n}} & 0 & -\frac{p_{R_2}}{L_{2n}} \\ 0 & 0 & 0 & 0 & 0 & 0 & 0 \end{bmatrix};$$

$$B_2^T=\begin{bmatrix} 0 & 0 & \frac{1}{T_{fc}} \end{bmatrix}; \; D_{12}^T=\begin{bmatrix}1 & 0 & 0 & 0 & 0 & 0 & 0\end{bmatrix};$$

$$D_{21}=\begin{bmatrix}0 & 0 & 0 & 0 & 0 & 0 & 0\end{bmatrix}; \; D_{22}=\begin{bmatrix}0\end{bmatrix};$$

$x = (x_1, x_2, x_3)^T$ is the phase vector; y is the 1D output vector by which closes feedback ; $z=(z_1, z_2,\ldots, z_7)^T$, $w=(w_1, w_2,\ldots, w_7)^T$ are the respectively the input and output vectors of uncertainty shown in Fig. 3.

The obtained equation (5) corresponds to the transfer function matrix $P(p)$, which is the standard form has the form (6):

$$P(p)=\begin{bmatrix} A & B_1 & B_2 \\ C_1 & D_{11} & D_{12} \\ C_2 & D_{21} & D_{22} \end{bmatrix}. \qquad (6)$$

It contains known and does not contain elements of uncertainty.

The matrix transfer function containing the uncertainty of the form (7):

$$\Delta(p)=\begin{bmatrix} \delta_{K_{fc}} & 0 & 0 & 0 & 0 & 0 & 0 \\ 0 & \delta_{L_{1eq}} & 0 & 0 & 0 & 0 & 0 \\ 0 & 0 & \delta_{R_{1eq}} & 0 & 0 & 0 & 0 \\ 0 & 0 & 0 & \delta_{R_2} & 0 & 0 & 0 \\ 0 & 0 & 0 & 0 & \delta_{L_{12}} & 0 & 0 \\ 0 & 0 & 0 & 0 & 0 & \delta_{L_2} & 0 \\ 0 & 0 & 0 & 0 & 0 & 0 & \delta_{R_2} \end{bmatrix}. \qquad (7)$$

It defines the relationship of the vector $w(p)$ with the vector $z(p)$.This relationship is described by the expression of matrix $w(p)=\Delta(p)\cdot z(p)$ which displays the system of equations (8):

$$w_1=\delta_{K_{fc}} z_1; \; w_2=\delta_{L_{1eq}} z_2;$$
$$w_3=\delta_{R_{1eq}} z_3; \; w_4=\delta_{R_2} z_4; \qquad (8)$$
$$w_5=\delta_{L_{12}} z_5; \; w_6=\delta_{L_2} z_6; \; w_7=\delta_{R_2} z_7.$$

This system of equations is obtained by Fig. 3.

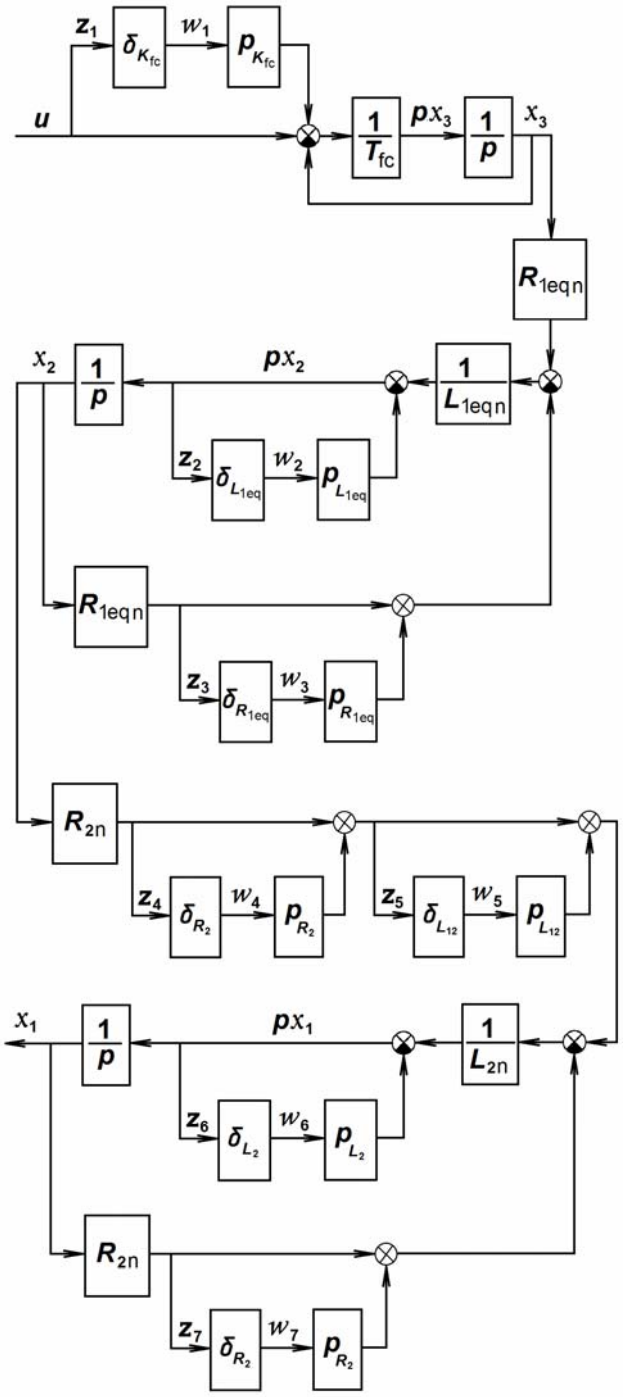

Fig. 3. A block diagram of the rotor flux linkage channel with undetermined parameters

Thus, a mathematical model of the channel of the rotor flux linkage in the space of states with parametric uncertainty is built.

Synthesis of optimal stabilizing $K(p)$ control was conducted by a mixed sensitivity for the object $P(p)$ the uncertainty $\Delta(p)$.

The block diagram of the object $P(p)$ with uncertainty $\Delta(p)$ and the controller $K(p)$ is presented in Fig. 4.

The numerical solution was carried out at the following values of the original data with T_{fc}=0.001 s; R_{1n}=2.65 Ω; R_{2n}=2.0 Ω; L_{1n}=0.186 H; L_{2n}=0.189 H; L_{12n}=0.179 H; σ=0.0996 corresponding to the induction electric drive with motor MDXMA100-32.

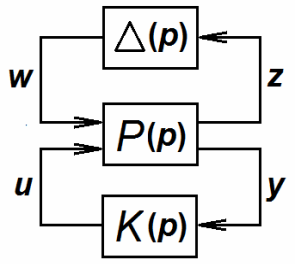

Fig. 4. The block diagram of the object $P(p)$ with uncertainty $\Delta(p)$ and the controller $K(p)$

Quality controlled system by means of three weighting functions [9] attached to the object $P(p)$. In the process of solving the mathematical model of H_∞-suboptimal robust controller is obtained. Its stripped-down strictly proper transfer function $K(p)$ (at a frequency of ω_c=46.6 rad/s of one of the weighting functions [9]) has the form

$$\frac{5.016\cdot10^5(p^2+148.963p+1.0612\cdot10^4)}{p^3+1.451\cdot10^4p^2+1.262\cdot10^7p+3.532\cdot10^7}. \quad (9)$$

Using the algorithm of the ancient Greek mathematician Euclid, we expand the transfer function (9) in the continued fraction [8]:

$$\cfrac{5.016\cdot10^5}{p+\cfrac{1}{\cfrac{0.6963}{10^4}+\cfrac{1}{-19.7p+\cfrac{1}{-\cfrac{0.5709}{10^4}+\cfrac{1}{1256p+\cfrac{1}{r}}}}}}, \quad (10)$$

where $r=0.2879\cdot10^{-3}$.

Structural circuit of the regulator corresponding fraction (10) is shown in Fig. 5. It consists of three integrating and four proportional units.

Fig. 6 shows curves (solid lines) obtained by simulating transient rotor flux linkage in the Robust Control Toolbox (Fig. 6,*a*) and the Simulink (Fig. 6,*b*) packages with a single step change reference variable, and the curve in Fig. 6,*b* is constructed with the assistance of the controller block diagram shown in Fig. 5. As expected, the two curves are identical at steady state. In transition mode, they are slightly different from each other in character and speed the flow of transients and overshoot are about 25%. This overshoot is easily eliminated by the aperiodic links with transfer function 1/(0.32*p*+1) on the right side of the setting unit setting signal (dashed line in Fig. 6,*b*).

Similar calculations were carried out with various combinations of increased or reduced in 2 times uncertain parameters. Here, transient deviations from nominal curves were not observed.

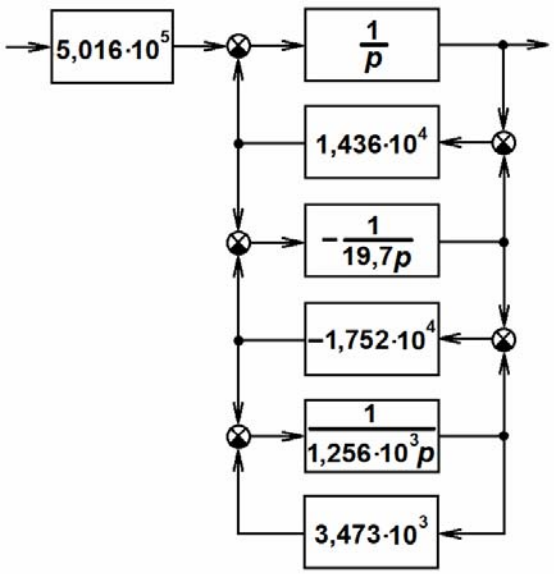

Fig. 5. Structural circuit of the H_∞-suboptimal stabilizing robust controller

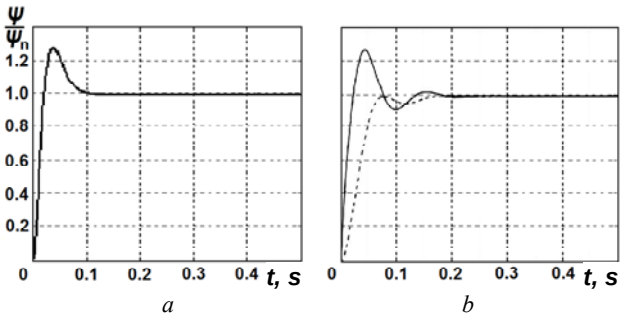

Fig. 6. Transients of the rotor flux linkage in packages Robust Control Toolbox (*a*) and Simulink (*b*): the dotted line – overshoot 0 %; solid line – 25 %

Conclusions.

The technique of structural synthesis of robust stabilizing control regulator of the rotor flux linkage is proposed, H_∞-suboptimal block diagram of which is presented in the form of connections of easily integrated and proportional parts of the same order as the regulator with a strictly proper transfer function, and takes into account the parametric uncertainty of the control object.

The results of the simulation of transient processes in a variety of packages MATLAB confirm the adequacy and small sensitivity of the system to parametric perturbations.

REFERENCES

1. Kuznetsov B.I., Nikitina T.B., Kolomiets V.V., Khomenko V.V. Investigation of the effect of nonlinearities and variations of the control object parameters on dynamic characteristics of the electromechanical servo systems. *Bulletin of NTU «KhPI»*, 2015, no.12(1121), pp. 68-71. (Rus).

2. Kuznetsov A.P., Markov A.V. Shmarlevsky A.S. Analysis of channel settings control the rotor flux vector control system. *Doklady BGUIR*, 2008, no.4(34), pp. 84-91. (Belarus).

3. Nesenchuk A.A., Opeiko O.F., Odnolko D.S. Dynamics simulation and calculation of robust parameters for the electric

drive control system on the basis of the root locus portraits. *Artificial Intelligence*, 2014, no.3, pp. 90-103. (Rus).
4. Peresada S.M., Kovbasa S.N., Bovkunovich V.S. Rough vector control torque and flux induction motor. *Tekhnichna elektrodynamika*, 2010, no.1. pp. 60-66. (Ukr).
5. Polilov E.V., Rudnev E.S., Skorik S.P. Synthesis of robust control algorithms for a synchronous electric motor means H_∞-theory. *Transactions of Kremenchuk Mykhaylo Ostrogradskiy State University*, 2010, iss.4/2010(63), part 3, pp. 15-20. (Ukr).
6. Shiyka A.A., Potapenko E.M. Robust control of asynchronous electric minimizing power loss in real time. *Bulletin of NTU «KhPI»*, 2013, no.36(1009), pp. 106-109. (Rus).
7. Egupov N.D. *Metody robastnogo, neiro-nechetkogo i adaptivnogo upravleniia* [Methods of robust, neuro-fuzzy and adaptive control]. Moscow, Publishing House of the MSTU named after N.E. Bauman, 2002. 744 p. (Rus).
8. Khinchin D.Y. *Tsepnye drobi* [Continued fractions]. Moscow, Nauka Publ., 1978. 112 p. (Rus).
9. Richard Y., Chiang R., Michael G., Safonov M. *MATLAB: Robust Control Toolbox. User's Guide. Version 2*, 1998. 230 p. Available at: http://www.mathworks.com (Accessed 12 May 2016).
10. Terekhov V.M., Osipov O.I. *Sistemy upravleniia elektroprivodov: uchebnik dlia studentov vysshikh uchebnykh zavedenii* [Control systems of electric drives: textbook for students of higher educational institutions]. Moscow, Akademiia Publ., 2006. 304 p. (Rus).

Received 21.10.2016

N.J. Khlopenko[1], *Doctor of Technical Science, Professor,*
I.N. Khlopenko[1], *Master of Science,*
[1] Admiral Makarov National University of Shipbuilding,
3, Central Ave., Nikolaev, 54021, Ukraine,
phone +38 0512 709100,
e-mail: ivan.hlopenko@yandex.ua

How to cite this article:
Khlopenko N.J., Khlopenko I.N. Structural synthesis of a stabilizing robust controller of the rotor flux linkage. *Electrical engineering & electromechanics*, 2017, no.1, pp. 21-25. **doi: 10.20998/2074-272X.2017.1.04.**

UDC 621.313 **doi: 10.20998/2074-272X.2017.1.05**

Yu.V. Shurub

STATISTICAL OPTIMIZATION OF FREQUENCY REGULATED INDUCTION ELECTRIC DRIVES WITH SCALAR CONTROL

Purpose. Working out of technique of synthesizing statistically optimal controllers of induction electric drives with frequency scalar control operating under stochastic loads. Methodology. It is shown, that one of the ways of increasing the energy efficiency of induction electric drives at random changes of loads is to create closed systems of electric drives with statistically optimal regulators that would take into account the stochastic nature of the disturbances and acted as filters of occasional high frequency fluctuations. The structure of such controls depends on the statistical characteristics of stochastic loads – correlation function and spectral density. In this mode, the minimum loss in dynamic mode with random intensive changed loads is provided by criterion of minimum mean square error of optimal parameter control. In the case of frequency controlled electric drive such a parameter is the optimum rotor flux. Results. The optimal structures of regulators of electric drives under stochastic loads according to type of random disturbances are identified. Originality. The technique of statistically optimal synthesis with feature of the expansion of a random process load on average, served as a useful signal, and high-frequency fluctuations around the average value, served as barrier, is developed. Practical value. On an example of simulation of work of the electric drive of a crusher of grain it is shown efficiency of a filtration by statically optimal regulator of the high-frequency components of random torques of load, reduction of dispersions of its outlet parameters, increase of cyclic indicators of energy efficiency of the electric drive, such as cyclic efficiency and power factor. References 4, tables 1, figures 3.
Key words: **induction electric drive, frequency scalar control, stochastic load, optimal regulator.**

Разработана методика синтеза статистически оптимальных регуляторов асинхронных электроприводов с частотным скалярным управлением, работающих при стохастических моментах нагрузки. Определены оптимальные структуры регуляторов электроприводов такого класса в зависимости от вида случайных возмущений. На примере моделирования работы электропривода дробилки зерна показана эффективность фильтрации статистически оптимальным регулятором высокочастотных составляющих моментов нагрузки и повышение циклических показателей энергоэффективности электропривода, таких как цикловые КПД и коэффициент мощности. Библ. 4, табл. 1, рис. 3.
Ключевые слова: **асинхронный электропривод, частотное скалярное управление, случайная нагрузка, оптимальный регулятор.**

Introduction. Wide class of induction electric drives including those used in agricultural mechanisms, in housing, in construction have load torque changing at random laws. They are drives of mechanisms as grain crushers, shredders, granulators, mixers, conveyors and more. At random changes since the current electric load, speed and electromagnetic torque of induction motor (IM) are also changed by random laws.

Stochastic character changes perturbation of electric greatly impairs their performance, requires overstatement installed capacity of motors, causing shocks in the mechanical parts of the drive makes the current surge in the motor and networks that worsens the quality of energy consumption and increases power loss, reduced quality regulation drives increases the likelihood of overload induction motor and its failure, makes it impossible for the realization of optimal modes of energy consumption in electric closed systems, such as «frequency converter – induction motor», «voltage converter – induction motor».

The goal of the work is to develop methods of statistically optimum synthesis of regulators of induction electric drives with frequency converters at random perturbations for mechanisms that do not require speed control.

Problem definition. One of the ways of increasing the energy efficiency of induction electric drives at random character of changes of loads is to create closed systems of electric statistically optimal regulators that would take into account the stochastic nature of the disturbances and acted as filters occasional high load fluctuations. The structure of such controls depends on the statistical characteristics of stochastic loads – correlation function and spectral density.

The problem of optimizing energy consumption in closed induction electric drive with frequency converters at a static moment load is sufficiently developed in Ukraine and abroad [1-3]. At the same time poorly investigated processes in such systems in dynamic mode at a variable for process cycle time of loading, including random law. In this mode, the minimum loss in dynamic mode with loads of intensive change at random by law, meets the criterion of minimum mean square error of optimal parameter adjustment. In the case of frequency controlled electric drive such parameter is the optimum rotor flux. This can be considered two types of frequency control of IM – scalar and vector.

When vector control possible direct regulation of the rotor flux through the separation process and flow control point. But high quality filtration components load depends on the quality of stabilization flux path that is difficult to implement frequency converters with voltage source properties because of the electromagnetic connection between circuits regulating moment and flux [4].

Based on these reasons, this work as an example of the synthesis of statistically optimal system is considered «frequency converter – induction motor» (FC – IM) with scalar control at a constant preset speed.

We know that in order to ensure minimum power losses in the induction motor by changing the static load should be regulated optimal flux linkage, which is defined by the formula

$$\Psi_{opt} = \Psi_n \frac{I_2}{I_{2n}} \sqrt{\frac{\Delta P_{\text{var}_n}}{I_{\mu n}^2 R_1 + \Delta P_{const_n} \left(\frac{f}{f_n} \right)^{\beta}}}, \qquad (1)$$

where ΔP_{const_n} are the nominal losses in motor steel; ΔP_{var_n} are the nominal losses in motor copper; Ψ_n is the nominal motor rotor flux linkage; $I_{\mu n}$ is the nominal magnetization current; I_{2n}, I_2 are the nominal and current value of the rotor currents; f_n, f are the nominal and current value of the frequency of power; β is the coefficient depending on the steel grade (here we accept 1.5); R_1 is the stator resistance.

For an optimal flux linkage (1) at a given speed of rotation, defined preset frequency, you must submit the optimum voltage U_{opt} that work in the area of slip can be determined approximately equivalent circuit IM by the formula

$$U_{opt} = \Psi_{opt} f + I_1 \sqrt{R_1^2 + (2\pi f L_1)^2}. \qquad (2)$$

This can be done using functional circuit closed system «frequency converter – induction motor», which is shown in Fig. 1. In this diagram marked: IM – asynchronous motor, CD – computing device in which the calculated value U_{opt}, FC – frequency converter, VS – voltage sensor, CS – current sensor, VR – voltage regulator, f_z – speed signal setting.

Incoming control action of the motor as part of a closed system «frequency converter – induction motor» mode optimizing the law is $\Psi = \Psi_{opt}$ stator voltage and frequency, which are connected to each other by (2). This frequency control circuit stabilizes the speed at a given level, and voltage regulation circuit stabilizes the optimum flux.

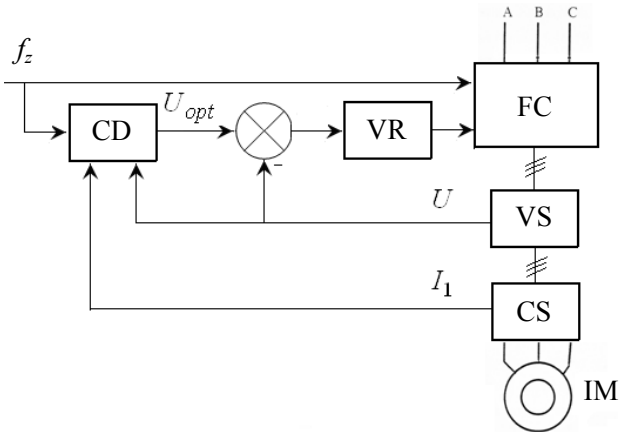

Fig. 1. Functional scheme of the closed system «frequency converter – induction motor» at scalar control

At static load torque the motor will run with minimal loss of power provided the relationships (1) and (2). In dynamic mode at a dramatically changing the law for random load electric current, electromagnetic torque and speed IM and replaced by random laws. Moreover, the stator and rotor currents at the given voltage and frequency and assuming the work of the linear section of the magnetization curve is uniquely determined slip. With the dynamic changes sliding computing device as a result of electromagnetic and electromechanical inertia will respond to the change of load inertia that will not receive optimal treatment in every time. So for implementation mode power optimization requires stabilization of sliding (rotor speed) at stochastic dynamic loads.

In scalar control only amplitude adjustable rotor flux vector using the ratio of *U/f* and its phase is unmanageable. Because of this electromagnetic torque is unmanaged components that do not allow to get high quality regulation in electric drives with variable control signals such as tracking, positional drives, but provides a fairly high quality of stabilization speed at variable loads, therefore, frequency regulated electric drives with scalar control can provide power optimization mode.

Results of investigations. Linearized block diagram of electric system «frequency converter – induction motor» of the scalar control is shown in Fig. 2.

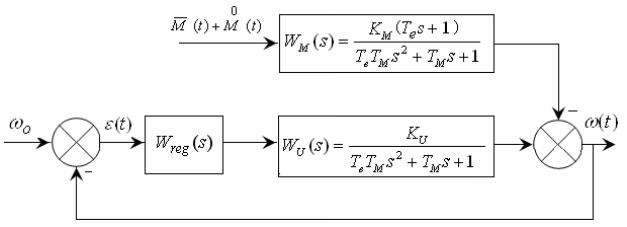

Fig. 2. Block diagram of the electric drive

In this diagram: ω_o is the setting task (cyclic load speed); $\omega(t)$ is the electric drive adjustable output value (cyclic speed); $M(t) = \overline{M}(t) + \overset{0}{M}(t)$ is the random perturbation signal that served as the sum of the mean

$\overline{M}(t)$ and centered random process $\overset{0}{M}(t)$, $W_{reg}(s)$ is the transfer function of the regulator, $W_U(s)$ is the transfer function motor control signal, $W_M(s)$ is the transfer function motor disturbance (torque of resistance).

In the transfer function in Fig. 2 marked: s is the Laplace operator, T_e is the electromagnetic time constant, T_M is the electromechanical time constant of the induction motor, K_U is the transfer coefficient for signal control; K_M is the transfer coefficient for the disturbance.

Input signal of the regulator

$$\varepsilon(t) = \omega_o - \omega(t) \tag{3}$$

we call accidental error system.

For optimality criterion we take the minimum criteria rms random error adjustment ε_{rms} which in the case of stationary and ergodicity process load can be calculated as the square root of the average error of regulation in time $\overline{\varepsilon}^2$ for a sufficiently long period of observation $T\to\infty$:

$$\varepsilon_{rms} = \sqrt{\overline{\varepsilon}^2} = \sqrt{\lim_{T\to\infty}\int_0^T \varepsilon^2(t)dt} \to \min. \tag{4}$$

This paper discusses the problem of statistically optimal synthesis for arbitrary structure regulator, which is previously unknown. This problem is formulated as follows. By according is the statistical characteristics of the signal disturbance – load $M(t)$ such as its spectral density $S_M(\omega)$, transfer function and object management – asynchronous electric drive. Need to find a transfer function regulator $W_{reg}(s)$ which provides the minimum mean square error of the system ε_{rms}.

For centered stationary random process with zero expectation root mean square error equal to the variance of the random error system

$$\varepsilon_{rms} = \sqrt{\overline{\varepsilon}^2} = \sqrt{D_\varepsilon}, \tag{5}$$

which can be found on the basis of the laws of conversion statistical characteristics of random process induction electric closed system of transfer function for the disturbance

$$W(s) = \frac{W_M(s)}{1 + W_{reg}(s)\cdot W_U(s)}. \tag{6}$$

In accordance with the Hinchyn-Wiener law

$$D_\varepsilon = \int_0^\infty \left|\frac{W_M(j\omega)}{1 + W_{reg}(j\omega)\cdot W_U(j\omega)}\right|^2 S_M(\omega)d\omega, \tag{7}$$

where $W_U(j\omega)$, $W_M(j\omega)$ are the frequency transfer function for the electric drive control and disturbance, respectively; $W_{reg}(j\omega)$ is the frequency transfer function of the regulator.

So, in order to minimize ε_{rms}, it is necessary that the condition $D_\varepsilon\to\min$ should be correct.

Because of the complexity of (7) directly used for synthesis of optimal statistical it can not. Therefore solution of this problem was the technique of statistically optimal synthesis feature is the expansion of a random process load on average $\overline{M}(t)$ served as a useful signal and high-frequency fluctuations around the average value $\overset{0}{M}(t)$ served as barrier – centered stationary random process.

After expansion signal load on the signal $\overline{M}(t)$ and signal of interference $\overset{0}{M}(t)$ dynamic random error system can be represented as the difference of two output signals (Fig. 3), one of which is designed with the terms of optimizing energy consumption at the moment of static frequency transfer function of a closed system disturbance

$$k_0(j\omega) = \frac{W_M(j\omega)}{1 + W_U(j\omega)}, \tag{8}$$

and the frequency transfer function of the second system

$$k(j\omega) = \frac{W_M(j\omega)}{1 + W_{reg}(j\omega)\cdot W_U(j\omega)} \tag{9}$$

is still unknown because the unknown frequency transfer function regulator $W_{reg}(j\omega)$ which sought to ensure the conditions of minimum mean square error by filtering high frequency fluctuations.

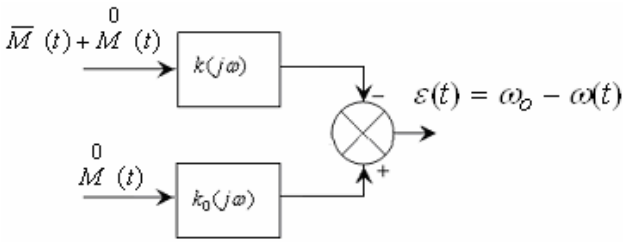

Fig. 3. Block diagram for optimal synthesis

Let $S_{\overline{M}}(\omega)$ is the spectral density of the useful signal and $S_{\overset{0}{M}}(\omega)$ is the noise signal spectral density.

Then the spectral density of random dynamic error adjustment according to Fig. 3

$$S_\varepsilon(\omega) = \left|k_0(j\omega) - k(j\omega)\right|^2 \cdot S_{\overline{M}}(\omega) + \left|k(j\omega)\right|^2 \cdot S_{\overset{0}{M}}(\omega). \tag{10}$$

The dispersion of accidental error of regulation

$$D_\varepsilon = \int_{-\infty}^{\infty} \left|k_0(j\omega)\right|^2 \cdot \{\left|1 - k'(j\omega)\right|^2 \cdot S_{\overline{M}}(\omega) + \left|k'(j\omega)\right|^2 \cdot S_{\overset{0}{M}}(\omega)\}d\omega, \tag{11}$$

where $k'(j\omega) = \dfrac{k(j\omega)}{k_0(j\omega)}$.

After some changes and minimize the expression (11) we obtain the frequency transfer function statistically optimal system would be:

$$k_{opt}(j\omega)=\frac{k_0(j\omega)\cdot S_{\overline{M}}(\omega)}{S_{\overline{M}}(\omega)+S_{\underset{M}{0}}(\omega)}. \qquad (12)$$

Analysis of the frequency transfer function (12) for loads with exponential and exponentially-cosine correlation functions shown that it has positive poles of the variable $j\omega$, therefore, such a system can not be physically realized. To correct solution of this problem should be made of the frequency transfer function that has negative poles, and the other part rejected.

For this it is necessary from $K_{opt}(j\omega)$ to separate the part $k_{opt}^{real}(j\omega)$ that is physically realized.

For this first we expand the denominator of (12) in the complex multipliers

$$S_{\overline{M}}(\omega)+S_{\underset{M}{0}}(\omega)=\psi(j\omega)\cdot\psi(-j\omega), \qquad (13)$$

where $\psi(j\omega)$ is the function which all poles by complex variable $j\omega$ are negative; $\psi(-j\omega)$ is the function which all poles by complex variable $j\omega$ are positive.

Now we divide the function $\frac{S_{\overline{M}}(\omega)}{\psi(-j\omega)}$ into two components:

$$\frac{S_{\overline{M}}(\omega)}{\psi(-j\omega)}=\left\{\frac{S_{\overline{M}}(\omega)}{\psi(-j\omega)}\right\}^{+}+\left\{\frac{S_{\overline{M}}(\omega)}{\psi(-j\omega)}\right\}^{-}, \qquad (14)$$

where $\left\{\frac{S_{\overline{M}}(\omega)}{\psi(-j\omega)}\right\}^{+}$ is the component which has negative poles of the complex variable $j\omega$ and can be realized physically, $\left\{\frac{S_{\overline{M}}(\omega)}{\psi(-j\omega)}\right\}^{-}$ is the component which has positive poles of the complex variable $j\omega$ and can not be realized physically.

Rejecting the part of the function $\frac{S_{\overline{M}}(\omega)}{\psi(-j\omega)}$ that can not be realized physically

We obtain closest to the optimum frequency transfer function of the closed electric drive that can be physically realized:

$$k_{opt}^{real}(j\omega)=\frac{k_0(j\omega)}{\psi(j\omega)}\cdot\left\{\frac{S_{\overline{M}_c}(\omega)}{\psi(-j\omega)}\right\}^{+}. \qquad (15)$$

For obtaining transfer function of statistically optimal system $k_{opt}^{real}(s)$ It is necessary to present (15) as a ratio of complex variable polynomials $j\omega$ with following substitution of the variable $j\omega$ by the operator s.

After determining the transfer function statistically optimal system $k_{opt}^{real}(s)$ we determine transfer function of the regulator with the following relationship which can be obtained from (9) solving this equation relatively $W_{reg}(s)$:

$$W_{reg}(s)=\frac{k_{opt}^{real}(s)-W_M(s)}{k_{opt}^{real}(s)\cdot W_U(s)}. \qquad (16)$$

Calculations showed that under load, which is exponential correlation function $R(\tau)=De^{-\alpha|\tau|}$ by statistically optimal transfer function of the regulator will be consistent connection aperiodic link and forcing a first-order link $W_{reg}(s)=\frac{a_0s+a_1}{b_0s+b_1}$, and for loading of exponentially-cosine correlation function $R(\tau)=De^{-\alpha|\tau|}\cos\beta\tau$ – serial aperiodic link and forcing a second-order link $W_{reg}(s)=\frac{a_0s+a_1}{b_0s^2+b_1s+b_2}$. Factors data gear functions are functions of the parameters of gear function electric $W_U(s)$ and $W_M(s)$ and parameters of correlation functions load $R(\tau)$.

Investigations of modes of induction electric drives with random character changes the load carried by the example of simulation of electric uniflow mills grain type of induction motor 4A80V2 load which has exponentially-cosine correlation function that corresponds to the statistical characteristics of the realizations obtained experimentally.

Simulation of the application of electric statistically optimal regulator showed reduction of variance electric output parameters (electromagnetic torque, current, speed) by 50-70 %.

Rate energy reserves through the use of statistically optimal regulator may cycle using indicators such as cycle efficiency and power factor. These figures for electric uniflow mills grain given in Table 1 in the case of non-regulated electric drive, the electric drive system «frequency converter – induction motor» with a typical speed control, designed with a static mode (with PI regulator) and with statistically optimal regulator.

Table 1

Power indicators of electric drives

Drive type	Cycle efficiency	$\cos\varphi$
Non-regulated	70 %	0.64
With PI regulator	71 %	0.68
With statically optimal regulator	76 %	0.81

From Table 1 it is shown that the use of default PI regulator does not allow to get significant energy efficiency through the use of optimal interlinkage law regulation in terms of action stochastic dynamic loads due to impacts of electromagnetic and electromechanical inertia. The use of statistically optimal regulator with stochastic disturbances enhanced the performance of electric energy. Moreover, the scalar driving these figures are close to the values obtained by statistical optimization

is electric vector control [4] under the same load conditions, but at simplest terms technical implementation.

Conclusions.

1. At actions of dynamic stochastic loads for optimal control law implementing it is appropriate to use statistically optimal regulators instead of or together with standard regulators.

2. Simulation of electric drive of the grain crusher showed statistically optimum filtration efficiency by the regulator of high-frequency components of random points in the load, improving cycle power performance of electric drive.

REFERENCES

1. E. Levi, M. Sokola, A. Boglietti, M. Pastorelli. Iron loss in rotor-flux oriented induction machines: identification, assessment of detuning, and compensation. *IEEE Transactions on Power Electronics*, 1996, vol.11, no.5, pp. 698-709. **doi: 10.1109/63.535402.**

2. Dymko S., Peresada S., Leidhold R. Torque control of saturated induction motors with torque per ampere ratio maximization. *Proceedings of 2014 IEEE International Conference on Intelligent Energy and Power Systems*, 2-6 June 2014, Kyiv, Ukraine, pp. 251-256.

3. Braslavskii I.Ya., Ishmatov Z.Sh., Plotnikov Yu.V. Energy- and resource-conserving technologies based on controllable asynchronous drives. *Russian Electrical Engineering*, 2004, vol.75, no.9, pp. 30-36.

4. Shurub Yu.V., Dudnyk A.O., Lavinskiy D.S. Optimization of regulators of frequency controlled induction electric drives under the stochastic loadings. *Tekhnichna elektrodynamika*, 2016, no.4, pp. 53-55. (Ukr).

Received 25.10.2016

Yu.V. Shurub, Candidate of Technical Science,
The Institute of Electrodynamics of the NAS of Ukraine,
56, prospekt Peremogy, Kiev-57, 03680, Ukraine,
phone +38 044 3662637, e-mail: shurub@bigmir.net

How to cite this article:
Shurub Yu.V. Statistical optimization of frequency regulated induction electric drives with scalar control. *Electrical engineering & electromechanics*, 2017, no.1, pp. 26-30. **doi: 10.20998/2074-272X.2017.1.05.**

UDC 621.3.022:537.311.8 **doi: 10.20998/2074-272X.2017.1.06**

M.I. Baranov, V.V. Kniaziev, S.V. Rudakov

CALCULATION AND EXPERIMENTAL ESTIMATION OF RESULTS OF ELECTRO-THERMAL ACTION OF RATIONED BY THE INTERNATIONAL STANDARD IEC 62305-1-2010 IMPULSE CURRENT OF SHORT BLOW OF ARTIFICIAL LIGHTNING ON THE THIN-WALLED COVERAGE FROM STAINLESS STEEL

Purpose. *Calculation and experimental researches of electro-thermal resistibility of the pre-production thin-walled sheet models of outward roof of height technical buildings from stainless steel are easily soiled 12X18H10T to direct action on them rationed by the International Standard IEC 62305-1-2010 aperiodic impulse of current of short bow of artificial lightning of temporal form 10/350 μs with the proper admittances on his peak-temporal parameters (PTP).* ***Methodology.*** *Electrophysics bases of technique of high voltage and large impulsive currents (LIC), and also scientific and technical bases of planning of high-voltage impulsive devices and measuring methods in them LIC with followings below extreme PTP: amplitude of impulse of current of I_{mL}=200 кА (with admittance ±10 %); integral of action of impulse of current of J_L=10·10^6 A^2·s (with admittance ±35 %); %); duration of wavefront current of T_1=10 μs (with admittance ±20 %); time, proper amplitude of impulse of current of I_{mL}, t_{mL}≤24 μs (with admittance ±20 %); duration of flowing of impulse of current of T_2=350 μs (with admittance ±10 %).* ***Results.*** *The results of evaluation calculation and experimental researches of electro-thermal resistibility of the indicated pre-production sheet models are resulted measuring in the plan of 0,5 x 0,5 m from stainless steel are easily soiled the 12X18H10T thickness of 1 mm to action on them of aperiodic impulse of current of short blow of artificial lightning with rationed PTP on the requirements of the International Standard IEC 62305-1-2010. In high current experiments amplitude of I_{mL} of the aperiodic rationed impulse of current of artificial lightning of temporal form of T_1/T_2=15 μs/315 μs changed in the range of (100-184) кА. The integral of action of J_L of impulse of current for I-IV of levels of protection of lightning of technical objects (TO) numeral made from 2,32·10^6 A^2·s to 7,88·10^6 A^2·s, and the flowing through the probed pre-production steel models electric charge of q_L numeral changed from 44,2 Kl to 81,3 Kl. It is shown that direct influence rationed by the International Standard IEC 62305-1-2010 impulse of current of short blow of artificial lightning with in-use PTP on the indicated pre-production steel models causes in them the rounded small hole of melting of surface of coverage a depth no more than 50 μm and diameter no more than 60 mm. The results of calculation and experiment coincide within the limits of 5 %.* ***Originality.*** *First in world practice on the unique generator of LIC of short blow of artificial lightning of type of GITM-10/350 experimental researches of electro-thermal resistibility of pre-production sheet models of outward roof are conducted TO of stainless steel 12X18H10T is easily soiled to direct action on them of impulses of current of an artificial storm air spark digit with extreme parameters.* ***Practical value.*** *Drawing on the got results in practice of protection height TO from linear lightning will allow substantially to promote their functional and fire-prevention safety in the conditions of direct action on them of the plasma ductings of high current storm air spark discharge.* References 20, tables 1, figures 4.

Key words: **artificial lightning impulse current of temporary shape 10/350 μs, thin-walled coverage made of stainless steel, electro-thermal effect of lightning current to the steel cover, radius and depth of penetration of the steel wall coverage, calculation and experimental estimation of damage zone of coverage.**

Приведены результаты расчетной и опытной оценки электротермической стойкости тонкостенного покрытия наружной кровли высотного технического сооружения из нержавеющей стали марки 12Х18Н10Т к прямому воздействию на него нормированного по международному стандарту IEC 62305-1-2010 апериодического импульса тока искусственной молнии временной формы 10/350 мкс с амплитудой от 100 до 200 кА и заданными допусками на его амплитудно-временные параметры. Показано, что указанный импульсный ток молнии вызывает лишь локальное поверхностное термическое повреждение исследуемого стального покрытия при радиусе данной зоны повреждения не более 30 мм и глубине проплавления его стенки не более 50 мкм. Библ. 20, табл. 1, рис. 4.

Ключевые слова: **импульс тока искусственной молнии временной формы 10/350 мкс, тонкостенное покрытие из нержавеющей стали, электротермическое действие тока молнии на стальное покрытие, радиус и глубина зоны проплавления стенки стального покрытия, расчетная и опытная оценка зоны повреждения покрытия.**

Introduction. In [1] the authors presented the results of computational and experimental studies electrothermal resistance experienced sheet of thin (1 mm thick and the size in terms of 500 x 500 mm) of the samples of the outer roof of stainless steel 12X18H10T tall technical installations to the direct impact on their valuation *A*- and *C*- pulse current component of artificial lightning, amplitude and timing parameters (ATP) which comply with current regulatory requirements of the United States SAE ARP 5412 and SAE ARP 5416 documents in relation to the aircraft [2, 3]. As is known, in this case, the impulse damped sinusoidal *A*- lightning current component characterized by the following normalized ATP [2, 3]: current amplitude I_{mA}=±200 kA (with tolerance of ± 10%); the integral action of the

current J_A=2·10^6 A^2·s with (with tolerance of ± 20%); time corresponding to the amplitude of the current I_{mA} constituting t_{mA}≤50 μs; the duration of the current flow τ_{pA}≤500 μs. Long aperiodic *C*- lightning current component in this case had the following normalized ATP [2, 3]: amplitude I_{mC}=±(200-800) A current; moved electric charge current q_C=±200 C (with tolerance of ± 20%); the duration of the current flow τ_{pC}=(0.25−1) s. Note that in [1], corresponding experiments were performed on designed and developed in 2007 at the experimental polygon at the Scientific-&-Research Planning-&-Design Institute «Molniya» of the NTU «KhPI» (at the Department No. 4 «Electromagnetic research and testing»), a powerful high-voltage generators of artificial lightning current УИТОМ-1 [4] is formed on the test technical object (TO) ATP current pulses from lightning described the *A*- and *C*- components on the requirements of the normative documents [2, 3]. According to the applicable requirements of the International Standard IEC 62305-1-2010 [5] in the assessment of protection from lightning strike short of buildings, technical installations and their parts, including those in which people and utilities, using a normalized aperiodic current pulse lightning temporary form T_1/T_2 = 10 μs/350 μs of positive polarity, where T_1, T_2 are, respectively, the rise time and duration of the halftime of the lightning current pulse. Other highlights of the ATP for the lightning current impulse I lightning certain level characterized by the following numerical values [5]: the current amplitude I_{mL} = 200 kA (with tolerance of ±10%); the integral action of the current (energy density) J_L=10·10^6 A^2·s with (with tolerance of ±35%); the amount of electric charge leaked q_L=100 C (with tolerance of ±20%). For level II lightning TO have the following numerical values [5] considered ATP lightning current: current amplitude I_{mL}=150 kA (with tolerance of ± 10%); current action integral (energy density) J_L=5.6·10^6 A^2·s (with tolerance of ±35%); the amount of electric charge leaked q_L=75 C (with a tolerance of ± 20%).

For most low III-IV levels of lightning then these ATP lightning current must meet the following specifications [5]: current amplitude I_{mL}=100 kA (with tolerance of ± 10%); the integral action of the current (energy density) J_L=2,5·10^6 A^2·s (with tolerance of ± 35%); the amount of electric charge leaked q_L=50 C (with tolerance of ±20%). In this context, an undoubted practical interest electrophysical task associated with the assessment of electro-thermal resistance of thin sheeting, stainless steel outer roof of high-rise buildings to direct technical impact on their aperiodic short strike lightning current pulse temporal shape 10/350 μs with ATP presented in [5].

The goal of the paper is the determination of the effects on the thin-walled sheeting made of stainless steel, mounted on the roof of high-rise buildings technical, short-current pulse of lightning strike with normalized according to the International Standard IEC 62305-1-2010 ATP.

1. Definition of the research problem of electrothermal resistance of thin-walled steel coating to the lightning current impulse 10/350 μs. In this applied research, consider a flat sheet thin-walled steel coating thickness h≤1 mm is tested in the air with a steady temperature θ_0 direct impact on it of a high plasma cylindrical channel short lightning with pulse aperiodic current $i_L(t)$, the relevant technical requirements [5]. Let the lightning channel in the area of its peg on the outer surface of the steel covering made of stainless steel 12X18H10T [1], has a maximum radius r_0 satisfying in the SI system at the location of the protected by the known Braginsky formula [6]: r_0≈0.093·$(I_{mL})^{1/3}$·$(t_{mL})^{1/2}$, where I_{mL} is the the amplitude of the temporal shape of the lightning current aperiodic pulse 10/350 μs and t_{mL} is the time corresponding to the amplitude of the current I_{mL}. Let us assume that the value of t_{mL} is approximated by the ratio of the form [7]: t_{mL}≈1.6·T_1. We believe that the pulse current density δ_L and heat flux in a cylindrical g_L lightning plasma channel substantially uniformly distributed over the cross section of its circular S_k=πr_0^2. One evidence of this is that virtually characterized by uniform distribution of its radius r_0 [8] in the high channel electric gas discharge electron and ion thermodynamic temperature of its low-temperature plasma in a first approximation. We believe that in the course of the impact of lightning channel considered thin-walled steel cover round the zone of its binding radius r_0 remains almost stationary relative to the covering wall. We accept the assumption that the volume V_0 of the molten aperiodic impulse lightning $i_L(t)$ the current metal coating determines ultimately the amount of damage zone under suitable conditions and the form of its area of penetration. The calculated evaluation of the results of said electrothermal action of a high cylindrical channel of lightning on the steel cover to do the assumption of immutability in the short strike lightning basic thermal characteristics of the material under consideration of the TO coating.

2. The calculation estimation of results of the electro-thermal effects on the thin-walled steel cover the lightning current impulse 10/350 μs. It is known that thermal damage to the metal and insulation (composite), then elements in the field of direct lightning strike in them due to the presence of intense heat flux in the plasma channel of a lightning discharge [9]. g_L density of heat flow in the channel of lightning, acting on the test steel cover TO determined δ_L current density in it (the channel) and the fall of the voltage U_{ac} in the electrode area of the plasma channel considered high-current discharge. We can use the following approximate relation [10, 11] to assess the magnitude of the heat flux density gL flowing in the steel cover (in one of the electrodes in the estimated two-electrode system air lightning) TO:

$$g_L = \delta_L \cdot U_{ac}, \quad (1)$$

where U_{ac} is the the value of the near-electrode voltage drop in steel coating, performing in a two-electrode system (TES) as a cathode at a predetermined positive polarity lightning current.

According to the experimental data presented in [10], the value for the basic U_{ac} conductive materials TES calculation used in aircraft (ground) and other apparatuses TO varies within a narrow range of from 5 to 10 V applied to the steel under consideration covering the value of the cathode U_{ac} numerically is about 6.1 V [10]. Then, taking into account (1) the amount of heat the Q entering the steel cover with a direct strike of lightning in it, we can write the calculated expression:

$$Q = \pi \int_0^\infty g_L r_0^2 dt = \pi U_{ac} \int_0^\infty \delta_L r_0^2 dt = U_{ac} q_L, \quad (2)$$

where $q_L = \int_0^\infty i_L(t)dt$ is the amount of electric charge of positive polarity of the plasma channel lightning flowing through the steel cover.

On the other hand, for the Q value of the amount of heat, to stand out in a steel coating material at his defeat by direct lightning strike, will have the following calculated relation [12]:

$$Q = m_0\left[C_0(\theta_m - \theta_0) + C_m\right], \quad (3)$$

where $m_0=d_0V_0$ is the mass of heated impulse lightning current to the melting temperature θ_m coating material having the density d_0 and volume V_0; C_0 is the heat capacity of the coating material; C_m is the specific heat of melting of the coating material.

2.1. The calculation estimation ov volume of the melting zone in the wall of a steel cover. From (2) and (3) for the magnitude of the volume V_0 of the molten coating material steel TO when exposed to short lightning obtain the estimated expression of the form:

$$V_0 = U_{ac} q_L d_0^{-1}\left[C_0(\theta_m - \theta_0) + C_m\right]^{-1}. \quad (4)$$

From (4) we see that we obtained above approximate electrophysical by design analytical expression for finding molten pulse aperiodic current of lightning $i_L(t)$ of the volume V_0 thin-walled steel that cover is fully consistent with the estimated ratio recommended in this case, according to [5] the International Standard IEC 62305-1-2010 (see in [5] Annex D, formula D.9). Below Table 1 shows the numerical data for the major electrical and thermal parameters we used steel grades for thin-wall coatings TO roof.

Then from (4) and the data of Table 1 it implies that the calculated estimate of the molten short lightning V_0 volume of the coating metal TO is necessary to know only the amount of electric charge q_L leaked through the test coverage. To find the charge on q_L (2) using the following analytical expression for aperiodic lightning current impulse $i_L(t)$ of temporary form of 10/350 μs flowing through the coating TO [14, 15]:

$$i_L(t) = k_L I_{mL}\left[\exp(-\alpha_1 t) - \exp(-\alpha_2 t)\right], \quad (5)$$

where $\alpha_1 \approx 0{,}76/T_2$, $\alpha_2 \approx 2{,}37/T_1$ are the coefficients of the lightning current with an aperiodic pulse given ATP; $k_L=[(\alpha_1/\alpha_2)^\beta - (\alpha_1/\alpha_2)^\gamma]^{-1}$ is the normalizing factor; $\beta=\alpha_1/(\alpha_2-\alpha_1)$; $\gamma=\alpha_2/(\alpha_2-\alpha_1)$.

As a result, taking into account (5) for the quantity of electric charge q_L, flowing at the time used the form of T_1/T_2=10/350 μs aperiodic current pulse through the susceptibility of short thunderbolt investigated steel cover TO, we find:

$$q_L = \int_0^\infty i_L(t)dt \approx k_L I_{mL}\left[1{,}315T_2 - 0{,}422T_1\right]. \quad (6)$$

Table 1

Main electric and thermal properties for steel 12X18H10T at room temperature (θ_0=20 °C) of air media [1, 10, 13]

Parameter	Dimensionality	Value
U_{ac}	V	6.1
d_0	kg/m^3	7900
C_0	J/(kg·°C)	462
θ_m	°C	1455
C_m	J/kg	$84\cdot10^3$

Estimated numerical estimate of the charge q_L on the proposed equation (6) shows that, at a given time form T_1/T_2=10/350 μs lightning current impulse $i_L(t)$ to (5) with the contact found normalizing factor $k_L \approx 1.054$ and normalized according to the specifications requirements [5] The amplitude of this pulse current I_{mL}=100 kA and I_{mL}=200 kA it (the quantity q_L charge) accepts numerical values, respectively 48.1 and 96.2 C. These estimates for (6) the values q_L charge for the above two cases, only normalized to no more than 4% different from his (charge) corresponding to normalized values by taking requirements [5] numerical indicators 50 and 100 C. Taking into account the last relation (6) can be used in the field of lightning protection TO estimates the value of the electric charge q_L flowing through the metal coating then the direct impact it short lightning.

In determining the effects of electro-thermal effects of a lightning strike on a short metal or insulation (composite) cover TO something important parameter of this action is normalized in [5] the integral action J_L lightning surge current $i_L(t)$ (the specific energy with the dimension J/Ω). Using (5), for the current integral action J_L aperiodic pulse lightning $i_L(t)$ of temporary form of T_1/T_2=10/350 μs to our approximation we obtain the following estimated ratio:

$$J_L = \int_0^{\infty} i_L^2(t)dt \approx k_L^2 I_{mL}^2 \left[0{,}658T_2 - 0{,}633T_1\right]. \quad (7)$$

From (7) at T_1/T_2=10/350 μs (k_L≈1.054) in regulated by the requirements of [5] when I_{mL}=100 kA or I_{mL}=200 kA it follows that the value of the integral action J_L received aperiodic lightning current pulse $i_L(t)$ takes respectively calculated numerical values of $2.49 \cdot 10^6$ and $9.96 \cdot 10^6$ $A^2 \cdot s$. These estimates we obtained the value of the integral action J_L considered lightning impulse current of not more than 1% different from the normalized with [5] numerical values J_L constituting respectively $2.5 \cdot 10^6$ и $10 \cdot 10^6$ $A^2 \cdot s$. Therefore, the relation (7) can be used in the field of lightning protection then the estimates of the value of a temporary form of a lightning current integral action J_L aperiodic pulse T_1/T_2=10/350 μs acting on metallic or insulating (composite) coating protected TO.

2.2. The calculation estimation of the depth of penetration of the hole wall of the steel cover. From (4) and cylindrical form specified radius r_0 wells of thermal damage to the outside of the surface of the flat metal coating TO that is because of the action of a high lightning channel to a depth of penetration wells h_m we obtain:

$$h_m = 36{,}8 \cdot U_{ac} q_L d_0^{-1} I_{mL}^{-2/3} t_{mL}^{-1} \left[C_0(\theta_m - \theta_0) + C_m\right]^{-1}. \quad (8)$$

From (8) at the normalized amplitude I_{mL}≈184 kA short stroke current pulse form of artificial lightning time T_1/T_2=15/315 μs (t_{mL}≈24 μs; k_L≈1.083; q_L≈81.3 C) we simulated in the laboratory (see. section 4 below), and the source of electricity and thermal parameters for stainless steel thin-walled 12X18H10T considered (h≤1 mm) covering TO in Table 1, for the depth of penetration h_m wells should be that it is numerically approximately 39.8 μm. The maximum radius $r_0 \approx 0.093 \cdot (I_{mL})^{1/3} \cdot (t_{mL})^{1/2}$ cylindrical penetration holes for the steel cover is numerically equal to about 25.9 mm.

2.3. The calculation estimation of the radius of penetration holes through the wall of the steel cover. On the basis of (4), for thin-walled steel cover when taking into account (8) the condition of penetration through aperiodic pulse lightning current $i_L(t)$ of temporary form T_1/T_2=10/350 μs its wall $h_m \geq h$, the estimated ratio for the radius r_m penetration hole through the wall of the test coverage takes the following approximate form:

$$r_m = \left\{U_{ac} q_L (\pi\pi h_0)^{-1} \left[C_0(\theta_m - \theta_0) + C_m\right]^{-1}\right\}^{1/2}. \quad (9)$$

Quantitative evaluation on (9) of the radius r_m round hole through the wall penetration of the steel under consideration cover the thickness of the micrometers h≈hm≈40 short lightning with these normalized to [5] values ATP pulse current (I_{mL}≈184 кА; T_1≈15 μs; T_2≈315 μs; k_L≈1.083; q_L≈81.3 C) shows that in this case, it takes a numerical value equal to approximately 25.9 mm. It is evident that in this approximation the numerical value of the radius r_m of the hole of the keyhole cover walls practically corresponds to the calculated value of the maximum radius r_0 lightning channel defined by the Braginsky formula above [6]. This result indicates the validity of the calculation of (9).

3. The calculation estimation of the temperature of the plasma channel high-current lightning spark discharge air. With an integrated approach to the problem before us electrophysical professionals is important to orient in the numerical temperature levels, resulting in high air spark discharges of lightning and a direct impact on the external elements of protected TO. In this case, we assume that the condition of its non-isothermal in which it (plasma) the maximum temperature T_{me} electronic charge carriers exceeds the maximum temperature T_{mi} carriers ion current ($T_{me} > T_{mi}$) for the low-temperature plasma of a high air spark lightning at times $t \leq t_{mL}$ [12]. Using the results of applied research, presented in [11, 15], to the maximum of the electron temperature of the plasma channel T_{me} short lightning in the air under normal conditions (air pressure is $1.013 \cdot 10^5$ Pa and at a temperature equal to θ_0=0 °C [12]) we can write the following approximate ratio calculated:

$$T_{me} \approx 3{,}28 \cdot \sqrt[4]{I_{mL}^{1/3} U_{ac} / (\sigma_c t_{mL})}, \quad (10)$$

where σ_c=$5.67 \cdot 10^{-8}$ $W \cdot (m^2 \cdot K^4)^{-1}$ is the Stefan-Boltzmann constant.

Substituting in (10) at σ_c=$5.67 \cdot 10^{-8}$ $W \cdot (m^2 \cdot K^4)^{-1}$ and U_{ac}=6.1 V the corresponding numerical data source for standardized requirements for [5] aperiodic pulse temporal shape of the lightning current T_1/T_2=10/350 μs ($I_{mL} \approx 2 \cdot 10^5$ A; $t_{mL} \approx 16 \cdot 10^{-6}$ s) we find that in the test case, the maximum electron temperature plasma T_{me} channel high-current lightning discharge air is numerically $T_{me} \approx 14.6 \cdot 10^3$ K . it should be noted that the obtained by (10) the numerical value for the electron T_{me} temperature is in good agreement with those given in [16, 17] known experimental results for the considered temperature plasma high-channel air spark discharges are widely used in electrotechnology, based on the basis of a high-voltage pulse technology [18].

4. Experimental evaluation of the influence on the electro-walled steel cover the lightning current impulse 10/350 μs. The experimental verification of its operation some given us the calculated relations (in particular, (4), (6), (8) and the Braginsky formula for r_0) will perform at the designed and developed at the Scientific-&-Research Planning-&-Design Institute «Molniya» of the NTU «KhPI» in 2014, a unique powerful high-voltage generator type ГИТМ-10/350 [19, 20], modeling on low-resistance and low-inductance electrical load aperiodic pulses temporary form T_1/T_2=10/350 μs of artificial lightning current in accordance with the requirements of the International

Standard IEC 62305-1-2010 [5] . To this end, the air discharge circuit TES of high ГИТМ-10/350 placed on the desktop of the high voltage generator, at $\theta_0 \approx 20$ °C experienced sheet samples were placed in stainless steel 12X18H10T having a size in terms of 500 x 500 mm and thickness h=1 mm. Note that TES used in experiments with the top electrode of cylindrical shape 25 mm in diameter, made of Steel 3, the length of the air gap between its rounded along the radius about 12.5 mm and experienced edge sheet sample of stainless steel 12X18H10T was approximately 14 mm. To initiate a steel model of an experienced high-current spark discharge plasma channel short artificial lightning strike in the air gap TES placed a thin copper wire 0.2 mm in diameter and about 37 mm in length, anchored at its upper steel electrode and a suitable normal to the top of the prototype steel roof plane TO with an air gap of approximately 3 mm.

Measurement of ATP of aperiodic artificial lightning current pulse is generated in the high-current discharge circuit ГИТМ-10/350 and acting on the prototype sample sheet steel roofing TO carried out with the help of agents of the state metrological service measuring coaxial shunt type ШК-300 [4] having a conversion factor $K_{mL} \approx 10417$ A/V, and digital storage oscilloscope Tektronix TDS 1012. Fig. 1 shows the waveform obtained in this case with the help of the ГИТМ-10/350 aperiodic pulse current $i_L(t)$ of positive polarity artificial lightning during a thunderstorm short air discharge.

We point out that in the preparation shown in Fig. 1 waveform deadbeat artificial lightning current pulse in the high-voltage high-current discharge circuit ГИТМ-10/350 three of his pulse current generator (PCG) contained in the total amount of 171 pieces parallel and charged to a constant voltage $U_{c1\text{-}3} \approx 17$ kV high-voltage pulse capacitors type ИК-50-3 and the fourth PCG was built on the basis of 288 pieces serial-to-parallel and parallel-charged to a constant voltage $U_{c4} \approx 4.5$ kV high-voltage pulse ИМ 2-5-140 type capacitors (on their way out) [19, 20]. From the data in Fig. 1 implies that the impact in this case on a sample of experienced sheet steel roofing impulse short stroke artificial lightning current is generally consistent with the stringent requirements of the International Standard IEC 62305-1-2010 [5] for the III-IV levels of lightning TO. Proof of this is that the main ATP flowing through an experienced steel sample the thickness h=1 mm normalized simulated lightning current pulse at the same time have the following numerical values: $I_{mL} \approx 100$ kA; $T_1 \approx 15$ μs; $T_2 \approx 315$ μs; $q_L \approx 44.2$ C; $J_L \approx 2.32 \cdot 10^6$ A^2·s.

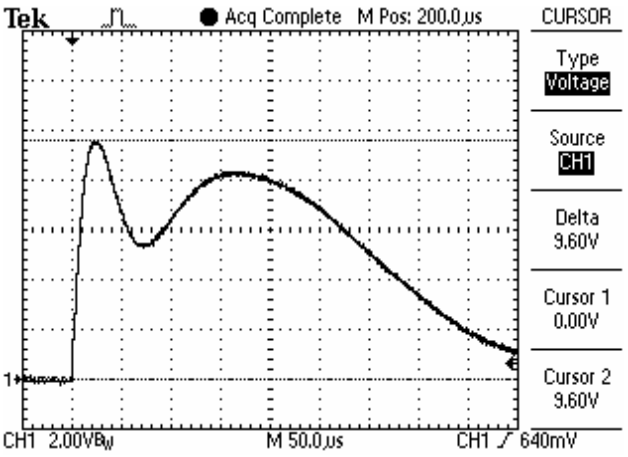

Fig. 1. Waveform current normalized aperiodic pulse temporal shape of artificial lightning 15/315 μs with an amplitude $I_{mL} \approx 100$ kA ($q_L \approx 44.2$ C; $J_L \approx 2.32 \cdot 10^6$ A^2·s) acting in circuit of ГИТМ-10/350 experienced a thin-walled (h=1 mm) sheet sample TO roof outer stainless steel 12X18H10T

Fig. 2 shows the waveform of the normalized technical requirements [5] of an aperiodic pulse of temporary form of artificial lightning current T_1/T_2=15/315 μs acting in high-current discharge circuit ГИТМ-10/350 prototype TO steel roof and corresponding practical level I lightning ($I_{mL} \approx 184$ kA; $T_1 \approx 15$ μs; $T_2 \approx 315$ μs; $q_L \approx 81.3$ C; $J_L \approx 7.88 \cdot 10^6$ A^2·s).

From local hopping «progress» in Fig. 2 short pulse hitting the artificial lightning current curve (its decline) in the discharge circuit powerful electrical ГИТМ-10/350 ($U_{c1\text{-}3} \approx 31$ kV; $U_{c4} \approx 9.4$ kV) placed on experimental research test range at the Scientific-&-Research Planning-&-Design Institute «Molniya» of the NTU «KhPI» (at the Department No. 4 «Electromagnetic research and testing») flowing through the sample experienced sheet metal roofing and TO measuring coaxial shunt type ШК-300, it follows that the lightning impulse current $i_L(t)$ with said normalized by [5] $J_L \approx 7.88 \cdot 10^6$ A^2·s action integral value leads to a large electrothermal and electrodynamic effects not only on the steel sample analyzed (Fig. 3), but also on the conductive structural elements used coaxial shunt. We point out that the resistance of high-current circuit bifilar shunt type ШК-300 was $R_i \approx 0.2$ mΩ [1, 4]. Numerical evaluation of W_i thermal energy released during high-conducted experiments on high-resistance nichrome thin-walled disk used measuring shunt type ШК-300 [4], can be performed by the following approximate formula:

$$W_i \approx R_i J_L . \qquad (11)$$

From (11) at the indicated initial data ($R_i \approx 0.2$ mΩ; $J_L \approx 7.88 \cdot 10^6$ A^2·s) it follows that in this experiment ($I_{mL} \approx 184$ kA; $T_1 \approx 15$ μs; $T_2 \approx 315$ μs; $q_L \approx 81.3$ C) at the measuring shunt type ШК-300 (mainly on its high-resistance nichrome thin-walled disk) energy is released about $W_i \approx 1.6$ kJ.

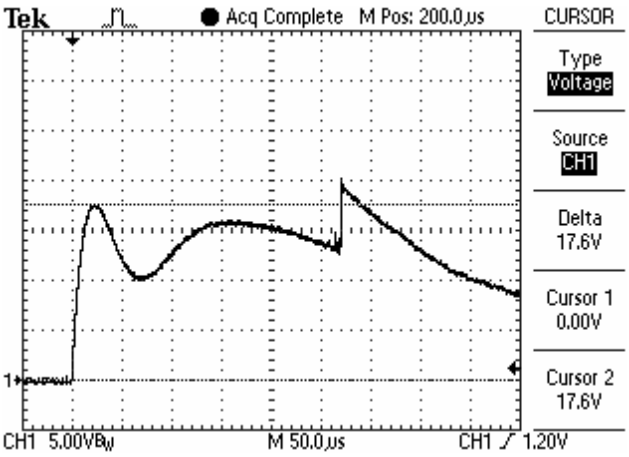

Fig. 2. Waveform of normalized aperiodic current of artificial lightning pulse temporal shape 15/315 µs with amplitude I_{mL} ≈184 kA (q_L ≈81.3 C; J_L≈7.88·10^6 A^2·s) acting in a chain ГИТМ-10/350 experienced a thin-walled (h=1 mm) sheet sample TO roof outer stainless steel 12X18H10T

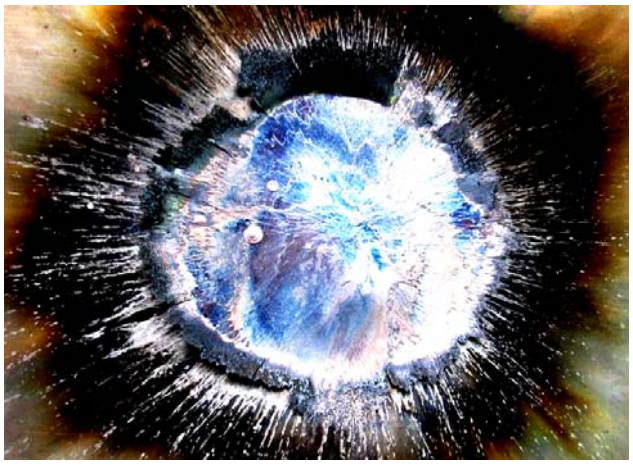

Fig. 3. Results of electrothermal effect of current normalized aperiodic pulse temporal shape of artificial lightning 15/315 microseconds with an amplitude I_{mL} ≈184 kA at experienced walled (h =1 mm) of a sample of the roof that of stainless steel 12X18H10T

Performed at a high-voltage high-current installation ГИТМ-10/350 experiments have shown that the measuring coaxial shunt type ШК-300 [4] the development of the Scientific-&-Research Planning-&-Design Institute «Molniya» NTU «KhPI» (Department No. 3 «High-voltage impulse technology») is almost the explosive release it by effects electric explosion (EE) of its metal thin-walled nichrome disc [15] of the amount of thermal energy can not withstand W_i. Conducted extreme experiments have shown that the quantity allocated for measuring coaxial shunt ШК-300 [4] W_i thermal energy from flowing through it of an aperiodic pulse of temporary form of artificial lightning current T_1/T_2=15/315 µs must not exceed the numerical value equal to 0.5 kJ. This value corresponds to the thermal power W_i III-IV levels of lightning protection, when I_{mL} ≈100 kA [5, 19]. In this case, a common indicator of dissipation high resistance nichrome thin-disk meter coaxial shunt ШК-300 thermal energy is the maximum allowable energy density of W_i/R_i equal to the maximum allowable integral action of the lightning current pulse J_{Li} and number about 2.5·10^6 J/Ω.

Fig. 4 shows the external view of the measuring coaxial shunt type ШК-300 [4], both before and after flowing through it in high-current discharge circuit ГИТМ-10/350 current normalized aperiodic pulse temporal shape of artificial lightning 15/315 µs with amplitude I_{mL}≈184 kA (q_L≈81.3 C; J_L≈7.88·10^6 A^2·s). It is evident that this momentum short simulated lightning strike current results due to a certain part of the EE nichrome thin-walled metal disc measuring coaxial shunt type ШК-300 [4], accompanied by a sharp rise in pressure inside the coaxial design of the shunt, to its destruction and damage.

Fig. 4. General view of the measuring coaxial shunt type ШК-300 before (left) and after (right) flow through it in high-current discharge circuit of the ГИТМ-10/350 normalized artificial lightning current aperiodic pulse temporal shape 15/315 µs with amplitude I_{mL}≈184 kA (q_L≈81.3 C; J_L≈7.88·10^6 A^2·s)

From the data in Fig. 3 shows that the direct impact on the prototype sheet sample TO roof stainless steel 12X18H10T thickness h=1 mm current normalized aperiodic pulse temporal shape of artificial lightning 15/315 µs with amplitude I_{mL}≈184 kA (q_L≈81.3 C; J_L≈7.88·10^6 A^2·s) formed in the discharge circuit ГИТМ-10/350, leads to substantial thermal damage only it (samples) in the outer surface of the rounded area on its cylindrical peg of a high air channel simulated lightning spark discharge at the stage of short shot. The radius of thermal damage to the area under consideration corresponds to the radius of the steel coating r_0≈0,093·$(I_{mL})^{1/3}$·$(t_{mL})^{1/2}$ according to the Braginsky formula for heavy air plasma channel artificial lightning [6, 7], is about 27 mm. One feature of the damaged area is education for its rounded perimeter sticking out in isolation from the outside of the surface of the steel sheeting spiked «beard» of up to 15 mm with a thickness of about 40 microns. The formation of such a «beard» under the direct influence of the air at the material steel cover short stroke artificial lightning current pulse temporal form T_1/T_2=15/315 µs due to surface melting steel coating round anchor zone on its channel of

lightning, followed by a radial discharge to the outside the molten metal due to acting on it electrodynamic Lorentz force [12]. Examination epicenter zone of thermal damage to the test-discharge circuit ГИТМ-10/350 ТО steel coating shows that in this case (I_{mL}≈184 kA; q_L≈81.3 C; J_L≈7.88·10^6 A^2·s) the depth of the well h_m penetration wall stainless steel coating 12Х18Н10Т (h=1 mm) of not more than 42 microns. This empirically derived numerical value of the depth h_m practically corresponds to its estimated value determined previously by (8).

Conclusions.

1. The results of estimates calculated and experimental studies at the Scientific-&-Research Planning-&-Design Institute «Molniya» NTU «KPI» electrothermal resistance experienced leaf samples outer roof to protect what in terms of size 500 x 500 mm stainless steel 12Х18Н10Т thickness h=1 mm to the direct impact on them air standardized by the International Standard IEC 62305-1-2010 artificial lightning aperiodic current pulse of temporal shape 10/350 μs with corresponding tolerances at its ATP indicate that the tested thin-walled steel TO samples are only local surface thermal damage. At said step of pulse current short pin artificial air lightning satisfying the requirements of I-IV levels lightning TO depth h_m wells subsurface penetration wall (h=1 mm) of the test steel coating is less than 50 μm, and its maximum radius r_0 - 30 mm.

2. It was found that the maximum permissible level of thermal W_i energy dissipated measuring coaxial shunt ШК-300 with high resistance nichrome thin-disk in high-current discharge circuit of high-voltage electrical ГИТМ-10/350 normalized by the International Standard IEC 62305-1-2010 current aperiodic pulse of artificial lightning of temporary form 15/315 μs, its numerical value is not greater than 0.5 kJ and meets the requirements of III-IV levels of lightning TO. This limit value specified shunt dissipation of thermal energy corresponds W_i for it such a generalized indicator of how specific they dissipated heat energy is defined as W_i/R_i and numerically equal to the maximum allowable for its circuit with resistance R_i integral action artificial lightning current pulse J_{Li}≈2.5·10^6 J/Ω.

REFERENCES

1. Baranov M.I., Kniaziev V.V., Kravchenko V.I., Rudakov S.V. Results of calculation-experimental investigations of electro-thermal resistibility of sheet steel samples to action of rationed components of pulsed current of artificial lightning. *Electrical engineering & electromechanics*, 2016, no.3, pp. 40-49. (Rus). **doi: 10.20998/2074-272X.2016.3.07.**

2. SAE ARP 5412: 2013. Aircraft Lightning Environment and Ralated Test Waveforms. SAE Aerospace. USA, 2013. – pp. 1-56.

3. SAE ARP 5416: 2013. Aircraft Lightning Test Methods. SAE Aerospace. USA, 2013. − pp. 1-145.

4. Baranov M.I., Koliushko G.M., Kravchenko V.I., Nedzel'skii O.S., Dnyshchenko V.N. A Current Generator of the Artificial Lightning for Full-Scale Tests of Engineering Objects. *Instruments and Experimental Technique*, 2008, no.3, pp. 401-405. **doi: 10.1134/s0020441208030123**.

5. IEC 62305-1: 2010 «Protection against lightning. Part 1: General principles». Geneva, IEC Publ., 2010.

6. Lozanskiy E.D., Firsov O.B. *Teorija iskry* [Theory of spark]. Moscow, Atomizdat Publ., 1975. 272 p. (Rus).

7. Baranov M.I. *Izbrannye voprosy elektrofiziki. Tom 2, Kn. 2: Teoriia elektrofizicheskikh effektov i zadach* [Selected topics of Electrophysics. Vol.2, Book 2. A theory of electrophysical effects and tasks]. Kharkiv, NTU «KhPI» Publ., 2010. 407 p. (Rus).

8. Rayzer Yu.P. *Fizika gazovogo razrjada* [Physics of gas charge]. Moscow, Nauka Publ., 1987. 592 p. (Rus).

9. Kuzhekin I.P., Larionov V.P., Prohorov E.N. *Molnija i molniezashchita* [Lightning and protection from lightning]. Moscow, Znak Publ., 2003. 330 p. (Rus).

10. Abramov N.R., Kuzhekin I.P., Larionov V.P. Characteristics of penetration of the walls of metal objects when exposed to lightning. *Electricity*, 1986, no.11, pp. 22-27. (Rus).

11. Baranov M.I. An approximate calculation of the maximum temperature of the plasma in high-current high-voltage spark discharge channel switch air atmospheric pressure. *Tekhnichna Elektrodynamika*, 2010, no.5, pp. 18-21. (Rus).

12. Kuz'michev V.E. *Zakony i formuly fiziki* [Laws and formulas of physics]. Kiev, Naukova Dumka Publ., 1989. 864 p. (Rus).

13. Available at: http://www.sgkarkas.ru/spravochnik/marochnik_stalej/12h18n10t (Accessed 11 July 2015).

14. Baranov M.I. *Izbrannye voprosy elektrofiziki. Tom 3: Teorija i praktika elektrofizicheskih zadach* [Selected topics of Electrophysics. Vol. 3: Theory and practice of electrophysics tasks]. Kharkiv, Tochka Publ., 2014. 400 p. (Rus).

15. Baranov M.I. *Izbrannye voprosy elektrofiziki: Monografija v 2-h tomah. Tom 2, Kn. 1: Teorija elektrofizicheskih effektov i zadach* [Selected topics of Electrophysics: Monograph in 2 vols. Vol. 2, book. 1: Theory of electrophysics effects and tasks]. Kharkov, NTU «KhPI» Publ., 2009. 384 p. (Rus).

16. Dashuk P.N., Zayents S.L., Komel'kov V.S., Kuchinskiy G.S., Nikolaevskaya N.N., Shkuropat P.I., Shneerson G.A. *Tehnika bol'shih impul'snyh tokov i magnitnyh polej* [Technique large pulsed currents and magnetic fields]. Moscow, Atomizdat Publ., 1970. 472 p. (Rus).

17. Gulyi G.A. *Nauchnye osnovy razriadno-impul'snykh tekhnologii* [Scientific basis of the discharge-pulse technology]. Kiev, Naukova Dumka Publ., 1990. 208 p. (Rus).

18. Mesiats G.A. *Impul'snaja energetika i elektronika* [Pulsed power and electronics]. Moscow, Nauka Publ., 2004. 704 p. (Rus).

19. Baranov M.I., Koliushko G.M., Kravchenko V.I., Rudakov S.V. A powerful high-voltage generator of aperiodic impulses of current of artificial lightning with the peak-temporal parameters rated on an International Standard IEC 62305-1-2010. *Electrical engineering & electromechanics*, 2015, no.1, pp. 51-56. (Rus). **doi: 10.20998/2074-272X.2015.1.10.**

20. Baranov M.I., Koliushko G.M., Kravchenko V.I., Rudakov S.V. A generator of aperiodic current pulses of

artificial lightning with a rationed temporal form of 10 μs/350 μs with an amplitude of ±(100–200) kA. *Instruments and Experimental Techniques*, 2015, vol.58, no.6, pp. 745-750. **doi: 10.1134/s0020441215060032.**

Received 29.08.2016

M.I. Baranov[1], *Doctor of Technical Science, Chief Researcher,*
V.V. Kniaziev[1], *Candidate of Technical Science, Senior Research Scientist,*
S.V. Rudakov[2], *Candidate of Technical Science, Associate Professor,*

[1] Scientific-&-Research Planning-&-Design Institute «Molniya», National Technical University «Kharkiv Polytechnic Institute», 47, Shevchenko Str., Kharkiv, 61013, Ukraine, phone +38 057 7076841, e-mail: eft@kpi.kharkov.ua
[2] National University of Civil Protection of Ukraine, 94, Chernyshevska Str., Kharkiv, 61023, Ukraine, phone +38 057 7073438, e-mail: serg_73@i.ua

How to cite this article:
Baranov M.I., Kniaziev V.V., Rudakov S.V. Calculation and experimental estimation of results of electro-thermal action of rationed by the international standard IEC 62305-1-2010 impulse current of short blow of artificial lightning on the thin-walled coverage from stainless steel. *Electrical engineering & electromechanics*, 2017, no.1, pp. 31-38. **doi: 10.20998/2074-272X.2017.1.06.**

UDC 621.317: 537.528 **doi: 10.20998/2074-272X.2017.1.07**

D.V. Vinnikov, K.V. Korytchenko, V.I. Tkachov, V.V. Egorenkov, D.V. Kudin, T.Y. Mirnaya

INVESTIGATION OF CHANGES OF PHYSICAL AND CHEMICAL PROPERTIES OF TAP WATER UNDER INFLUENCE OF POWERFUL UNDERWATER SPARK DISCHARGES

Purpose. ***The purpose of this investigation is to study the changes in the redox potential and pH-value of the tap water as a function of underwater spark discharges, storage device capacitance and the charging voltage. Methodology. To define the electric parameters of discharge circuit we used the Rogowski loop and the compensated capacitance-ohm potential divider. To determine water properties before and after the treatment we used the following devices: the water analyzer Anion -7051 with the limit of absolute error of the EMF measurement ± 2 mV, the BANTE 902 device with the absolute error of ± 0.002 pH. Results. We managed to establish the time of the origination of changes in the properties of treated water. A change in the positive redox potential to a negative one occurred already after the third pulse at a total energy input of ≥ 1 kJ. The pH value increased in the range of 0.2 – 0.45 pH units. We obtained the relationship of a change in the redox potential as a function of total energy of the pulse train that actually exhibits the linear relation to the mass of erosion products. We established that the electrodes made of stainless steel and the electrodes made of graphite provide similar changes in water properties. An increase in pH is indicative of the progress of reactions that result in the formation of*** OH^-***. Originality. The obtained experimental data prove a rapid and reliable change in the redox potential from positive to negative changes in the redox potential exponent can persist during ten days and even longer. The erosion products of electrodes can be removed from the treated water using the method of magnetic separation. Practical value. The «HYDRA» plant can be used as the electrochemical ideal mixing reactor of a discrete action with the removal of erosion products of the electrode using the method of magnetic separation.*** References 10, tables 5, figures 13.
Key words: **underwater spark discharge, electrodes material, water properties, redox potential, pH – value.**

Представлены результаты экспериментального исследования изменения физико-химических свойств водопроводной воды под воздействием мощных подводных искровых разрядов атмосферного давления. Выявлена зависимость изменения окислительно-восстановительного потенциала и pH обрабатываемой воды от параметров импульсов, задаваемых параметрами электрической разрядной цепи, и их количеством. Исследования проведены на разрядных электродах, изготовленных из материалов двух типов: нержавеющая сталь и графит. Библ. 10, табл. 5, рис. 13.
Ключевые слова: **подводный искровой разряд, материал электродов, свойства воды, окислительно-восстановительный потенциал, водородный показатель pH.**

Introduction. Powerful underwater spark discharges (PSD) are widely used for different branches of industry and science, in particular for the material destruction and deformation, the treatment of working holes, and also to change physical and chemical properties of liquid media and/or for the liquid media decontamination [1-3].

The underwater discharge is characterized by many physical factors that affect the medium treated both at the breakdown phase and at other phases of the discharge progress. These factors include the influence of strong electric field on the medium at the pre –breakdown phase of the discharge, the shock compression of environment, intensive pulse radiation of it in a wide wavelength range, thermal effect in the region of current conducting channel, the discharge of high-temperature fine particles of electrode materials into the vapor-&-gas medium due to the electroerrosion and cavitation processes. Such multifactor action allows us to change physical and chemical properties of the treated medium and to implement electrochemical ideal-mixing reactors of a discrete action due to the development of intense hydraulic gas dynamic flows in large volumes. Hence, the action discreetness and the ideal mixing are considered to be the main distinctive features of electrochemical PSD-based reactors.

One of the main indicators that characterizes the action of discharge on the chemical composition of water is the pH and the redox potential. A change in these exponents results in the water activation. It has been established [4] that the normal behavior of biochemical processes in the human body requires the correspondence of the redox potential of drinking water and that of intercellular liquid and it must be in the range of +100 to –200 mV. The redox potential of treated drinking water actually always exceeds 0 and it is in the range of +100 to +400 mV [4]. The water with the redox exponent below –200 mV exhibits high biological activity and the consumption of it must be limited.

Due to an ample amount of influencing PSD factors it is not easy to determine the individual influence of each factor on a change in the properties of treated liquid. At the same time, in order to control a change in the physical and chemical properties of water it is necessary to get a quantitative estimation of a change in the required properties of liquid in the specified chemical reactor as a function of the parameters of discharge pulses and their number.

The objective of this study was to investigate the relationship of a change in the redox exponent and pH of the water treated by the «HYDRA» plant as a function of pulses and their parameters specified by such parameters of electric discharge circuit as the storage capacitance and the charging voltage.

Experimental procedure. The HYDRA plant system and possible areas of its application are described in the papers [4-6]. A general view of the «HYDRA» plant and electric circuit are given in Fig. 1, 2.

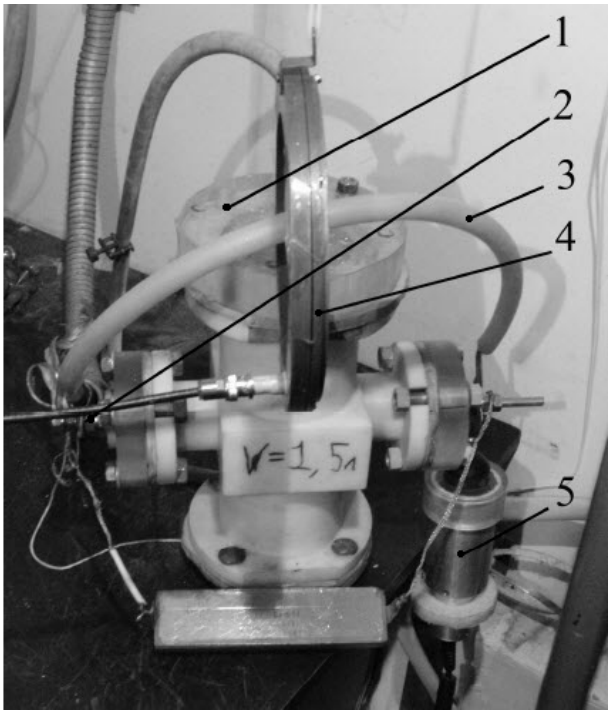

Fig. 1. General view of the electrochemical reactor 1 is the reactor vessel; 2 and 3 are current distributors that supply current to discharge electrodes; 4 is the Rogowski loop; 5 is the potential divider

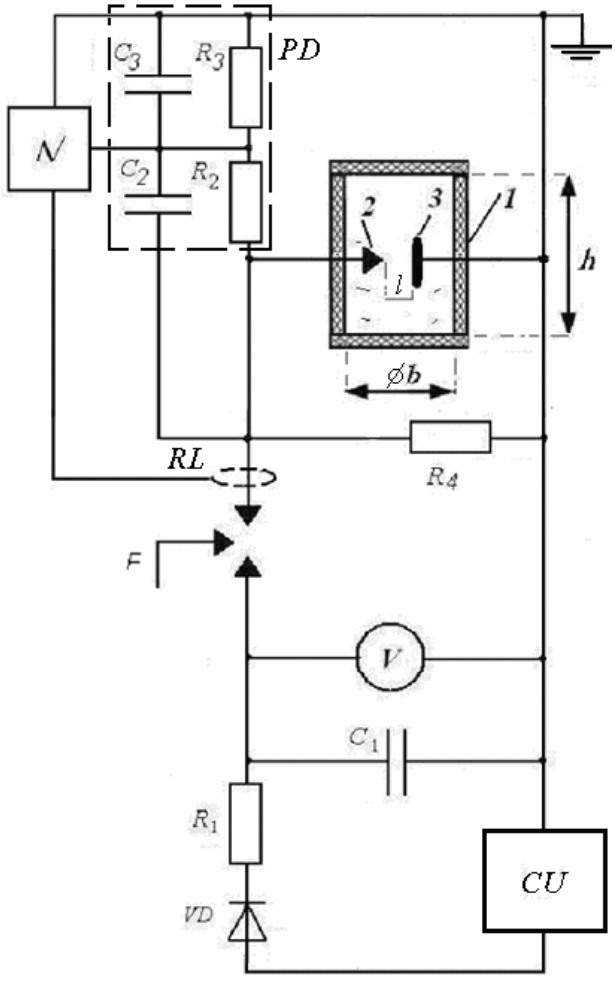

Fig. 2. Electric circuit of the «HYDRA» plant 1 – electric discharge chemical reactor; 2 and 3 are discharge electrodes

The capacitor bank C_1 is discharged via the controlled three-electrode air discharger F onto the chemical reactor 1 whose electrodes 2 and 3 form the discharge gap 1 and the damping resistance R_d connected to it in parallel. The pulse capacitors IK-100/0.4 and IK-100/0.25 were used for the capacitor bank.

The capacitor bank C_1 is charged by the DC voltage source formed by the following elements: charging unit *CU* in the form of step-up transformer UPC-70 and the autotransformer; the half-wave rectifier *VD* in the form of tandem diode assemblies of a KC-201E type; the charging resistance R_1 formed using the tandem resistance of TVO-60 type with the equivalent resistance of 270 kOhm.

The air discharger F was operating as a two-electrode discharger or three-electrode discharger. When the discharger F was working using no third electrode the charge voltage of the capacitor bank was controlled by the value of interelectrode gap of the discharger F. When the third control electrode of the discharger was used the charge voltage of the capacitor bank was controlled by the autotransformer. The charging voltage of the capacitor bank was equal to 10 kV, 15 kV and 20 kV.

Charging voltage of the capacitor bank C_1 was measured by the electrostatic kilovoltmeter of a C 196 type. The rated error was equal to ± 1 % of the maximum value of a measurement range.

The discharge current was measured using the Rogowski loop (RL) with the sensitivity of 3627A/V. The RL sensor sensitivity was measured at a frequency of 2.2 MHz using the categorized noninductive current sensor CSNM 191 of Honeywell company with the current value output that operates using the Hall Effect. The comparison data for the reference signal obtained from CSNM 191 sensor and the signal obtained from fabricated Rogowski loop are given in Fig. 3. A relative error of the reference signal was within ±0.5 % of the measured value.

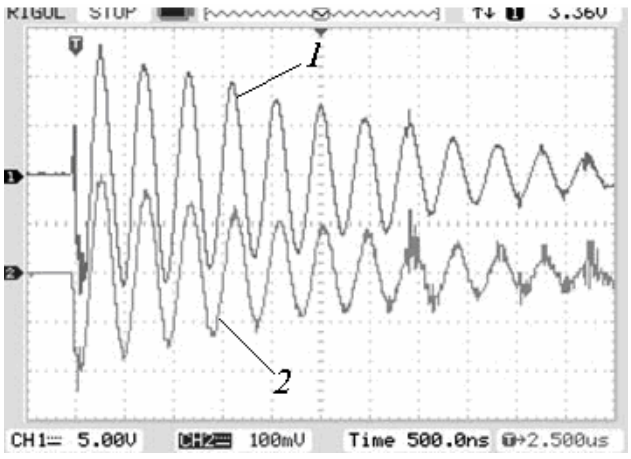

Fig. 3. Discharge Current Oscillographing Data. The current sensor CSNM 191 was used for first channel and the fabricated Rogowski loop was used for second channel

The discharge gap voltage was measured using the North Star High Voltage compensated capacitance-ohm potential divider (PD) of a *PVM-12* type with the dividing coefficient of 1:1000, bandwidth of 80 MHz and the maximum pulse voltage of 32 kV.

The damping of high frequency electric oscillations caused by the stray capacitances of the circuit was provided by the resistor *R4* connected in parallel to the discharge gap. The noninductive resistor of a TBO-60 type with the nominal of 47 kOhm was used as the resistance R_4.

The gap voltage and the discharge current were recorded using the ATTEN two-channel electronic oscillograph of an ADS 1102 CAL$^+$ type with the bandwidth of 100MHz and the digitizing rate of 1 GSa/s. The sweeping of signals registered by the potential divider was performed in a sleeping mode along the input signal front.

The electrochemical reactor corresponded to the dielectric chamber and its casing was made of caprolon (Fig. 2). The wall thickness of the casing was equal to 5 mm. The chamber height was h = 240 mm and its diameter was b = 90 mm. We used for studies the needle – semisphere system of electrodes (Fig. 4). To study the influence of electrode materials we manufactured two pairs of electrodes. One pair was made of stainless steel of a 12X18H10T grade and the other was made of graphite to produce electrocarbon products (GOST 10274-79). The steel grade was determined using the «SPRUT» plant and X-ray fluorescence method. The needle-semisphere electrode was shaped as a cone at an angle of 60°, the height of 25 mm and the base diameter of 30 mm. The semisphere radius of the second electrode was equal to 10 mm. Pin-like current leads to which the electrodes were connected were placed into the dielectric to prevent their oxidation and reduce pre-breakdown losses. The size of interelectrode gap l varied in the range of 1 to 5 mm.

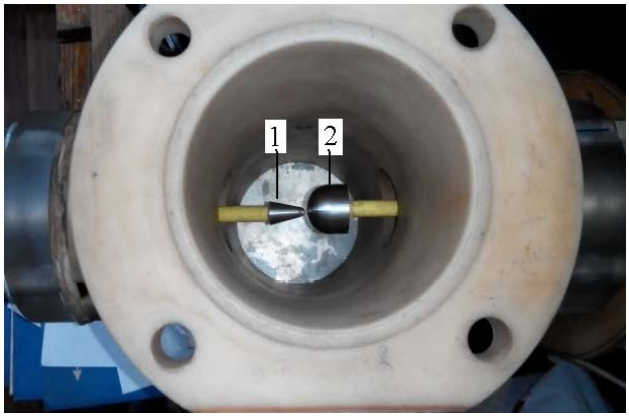

Fig. 4. General view of the discharge electrodes:
1 – needle; 2 – semisphere

Industrial capacitors of IK-100/0.4 and IK-100/0.25 types, have a high spread of nominal values (permissible deviation ±10 %), which prevents us from calculating the total discharge energy with sufficient accuracy. An absolute error of the capacitance measurement increased when the capacitors were connected to make up the capacitor bank. To obtain the specified values of the total capacitance two methods of its measurement were used, in particular the indirect method using the voltage measurements oscillographing data during the discharge of the capacitor bank, and the direct measurement method using measuring devices.

As for the indirect method the discharge circuit parameters were selected to meet the following condition:

$$R_c >> 2\sqrt{\frac{L}{C}}, \qquad (1)$$

where R_c is the charging resistance; C is the capacitor bank capacitance; L is the equivalent inductance of charging circuit.

The condition of the relationship of resistances expressed as

$$R_c >> R_{ir}, \qquad (2)$$

where R_{ir} is the internal resistance of DC source.

In this case the capacitor capacitance C was calculated proceeding from the time constant τ that was determined experimentally using the expression:

$$C = \tau/R_c. \qquad (3)$$

The capacities were charged by DC voltage source U_{const} = 4 V. The charging resistance was equal to R_c = 1±0.01 MOhm. Fig. 5 gives the measured capacitor voltage data. The voltage oscillogram shows that a drop in voltage from -4 V to U_{const}/e = –1.47 V occurs after τ = 390 ms. Hence, we have in this case C = 0.39 μF.

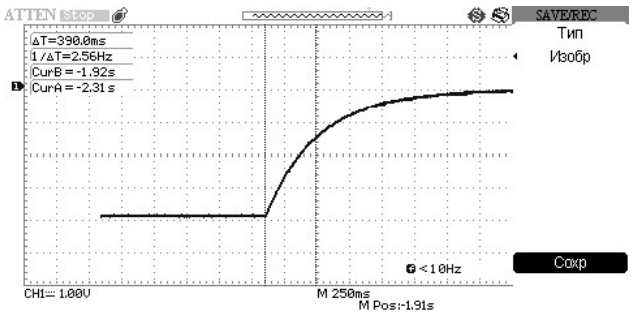

Fig. 5. Defining τ on the voltage curve of the capacitor during its discharge

We also measured the capacitance of capacitor banks using the digital measuring LCR device E 7-8 with the error in the measurement range of up to 10 μF within ±1.6 nF, and the measuring device DL-6243. Table 1 gives the measurement data.

Table 1

Measurement data of the capacitances of capacitor banks in μF

Bank number	Measuring method			
	Indirect	Device E 7-8	Device DL 6243	LSM
No 1	1,05	1,0495±0,0016	1,013	1,037
No 2	1,92	1,927±0,0016	1,925	1,924
No 3	2,95	2,947±0,0016	2,945	2,947

For the computations we took the capacitance value of a capacitor bank that was determined using the least-squares method (LSM) for the given measurement data: for the No 1 C = 1.037 μF, for the No 2 – C = 1.924 μF, and for the No 3 – C = 2.947 μF.

To calculate the discharge energy the bank capacitances were specified according to the data of five measurements that were processed using the least-squares method.

The PSD power was specified to a large degree by the discharge circuit inductance. The equivalent inductance of circuit was defined from the expression [7] using the analysis data of the curve of discharge current in the short-circuit mode:

$$L = \frac{T}{C\left[4 \cdot \pi^2 + \left(\ln \frac{I_1}{I_3}\right)^2\right]}, \quad (4)$$

where T is the discharge period; I_1 and I_2 is the current amplitude for first and third discharge half-periods.

Due to the strong influence of unwanted high-frequency oscillations onto the discharge current curve during the first discharge half-period the inductance for this paper was calculated using current amplitude values of second and forth discharge half-periods.

The equivalent circuit resistance that includes the active resistance of connecting wires and the internal resistance of capacitor bank was defined using the enumerative technique selected for the discharge current curve approximation. Fig. 6 gives the discharge current measurement data in the short-circuit mode and the appropriate approximating current curve for the selected resistance. The oscillogram was obtained for the capacitor bank discharge of C = 1.924 μF with the charging voltage of U_{charge} = 10 kV.

For the given data the discharge circuit inductance was equal to 2.398 μH, and the calculated active resistance of the discharge circuit was equal to R = 200 mOhm. Circuit parameters were measured in the same way, when different banks were used (Table 2).

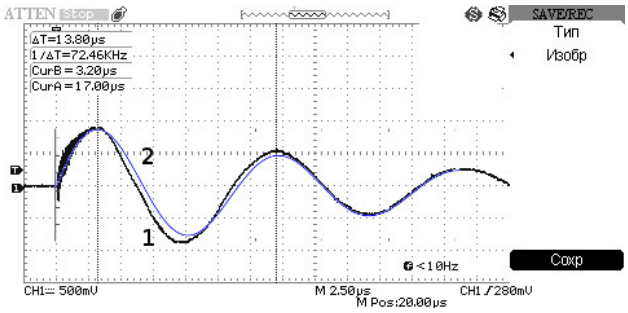

Fig. 6. Discharge current in the short-circuit mode 1 and the approximation curve 2

Table 2

Discharge circuit resistance and inductance measurement data

Bank number	Inductance, μH	Resistance, mOhm
No 1	2.40	200
No 2	2.54	225
No 3	2.62	240

A slight change in the inductance and resistance with a change in the capacitance of capacitor bank gives us all grounds to believe that it is necessary to establish the relationship of a change in the properties of water treated by the «HYDRA» plant as a function of the capacitance and charge voltage of the capacitor bank and the number of pulses.

The water properties were measured using the following devices. The water concentration of nitrates was measured using the nitrate meter IT – 1201 with the indication range of mass concentration of 0,001 to 9999 mg/l and the margin of error ±11 %. We also used the conductivity meter BANTE 902 with the range of 0~200 mS/cm, and the error of ±0.5 %. The redox potential was measured using the water analyzer Anion-7051 with the margin of absolute error of EMF measurement ±2 mV. The water pH was measured using BANTE 902 device with the measurement range of –2.000 ~ 20.000 pH and the absolute error of ±0.002 pH. A change in the ion concentration in the water solution was measured using the photometric method according to [8] that allowed us to measure Fe concentrations of ~10^{-6} mole/l.

The electrodes of diagnostic devices were washed properly in the distilled water before each measurement. The same sample (initial and treated water) was measured three times. The samples were subjected to a diagnosis during the first 15 minutes after the treatment and after 3 and 6 hours following the experiment.

The mass of discharge electrodes was measured using the scales of a VLR-200 type with the balance error of 0.5 mg for the weight up to 50 g and 1 mg for the weight range of 50 g to 200 g. The mass of electrodes made of stainless steel was compared after 280 pulses and that of graphite electrodes was compared after 30 pulses. Powerful underwater spark discharges were applied using the following parameters: U_{charge} = 10 kV, C = 2.947 μF, the single pulse energy was equal to W = 152.5 J/pulse.

The tap water with the conductivity of 758-766 μS/cm precipitated during 24 hours was selected as a test subject. To determine a change in the water properties in question the water was exposed to the train of pulses in amount of 1 to 200.

Test data. The water treated by powerful underwater spark discharges in the «HYDRA» plant contained the suspension of particles that precipitated with time. Fig 7 gives the data for the water treatment by steel electrodes at the following electric parameters of the circuit: U_{charge} = 20 kV, C = 2.947 μF.

The sediment is built up nonuniformly in time, which is indicative of the availability of the suspension of particles of a different size. The most intensive formation of the sediment was observed during first minutes after the treatment. And the sediment volume is increased with an increase in the number of pulses to which the tap water was exposed. The method of visual control showed that the precipitation of particles is stopped after 3 or 4 days upon the treatment completion.

The processed data of the research done using the «Hydra» plant were used for the establishment of the relationships of a change in the redox potential and pH of the treated water as a function of the number N of pulses at different parameters of electric discharge circuit (the capacitor charge voltage and the capacitance) given in Fig. 8-10. In Fig. 8-10 used the following symbols for the charge voltage of the capacitor bank: ■ – 10 kV, ▲ – 15 kV, ● – 20 kV. The data were obtained using steel electrodes.

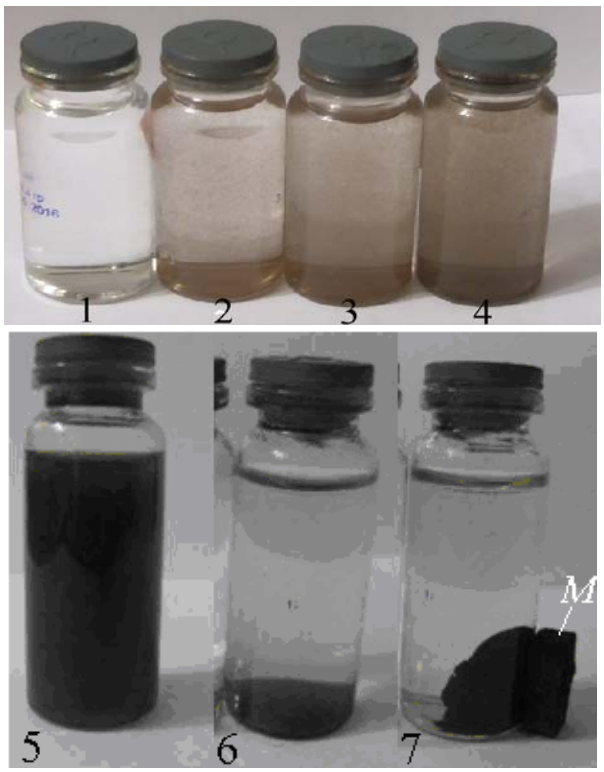

Fig. 7. The samples of tap water treated by underwater spark discharges:
1 – the initial sample; 2 – the sample after 5 pulses;
3 – the sample after 25 pulses; 4 – the sample after 50 pulses;
5 – the sample after 200 pulses; 6 – the sample No 5 precipitated during 4 days; 7 – the sample No 5 separated by the permanent magnet

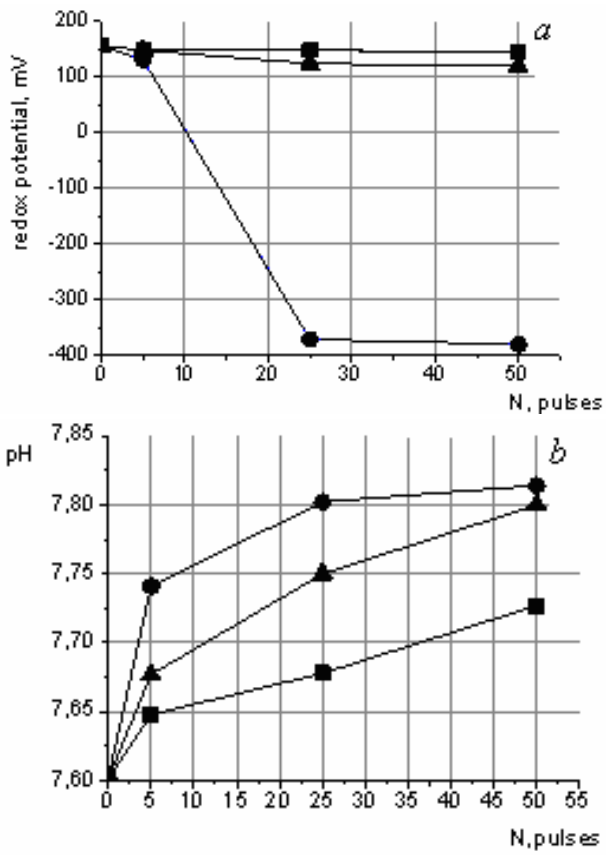

Fig. 8. Dependence of water properties on the number of pulses at C = 1.037 μF: *a* – the redox potential, *b* – pH

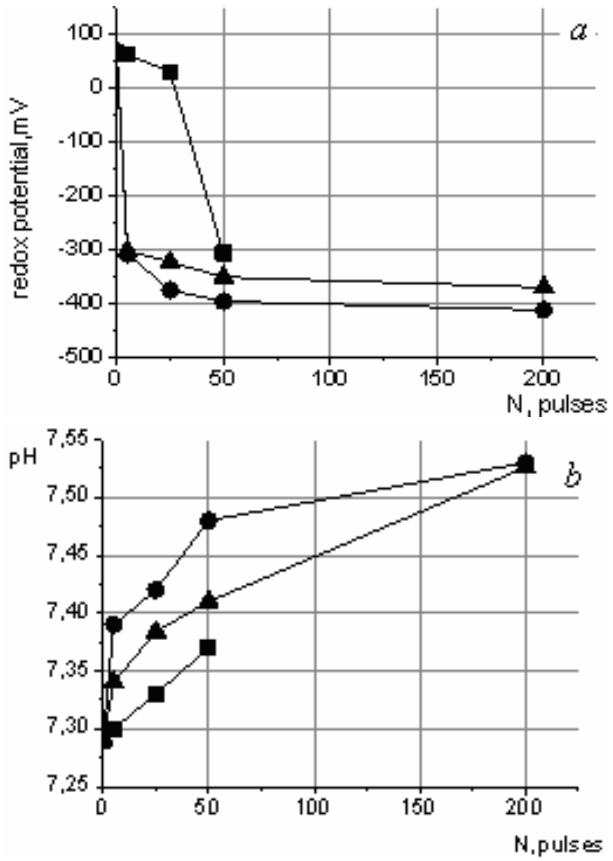

Fig. 9. Dependence of water properties on the number of pulses at C = 1.924 μF: *a* – ROP, *b* – pH

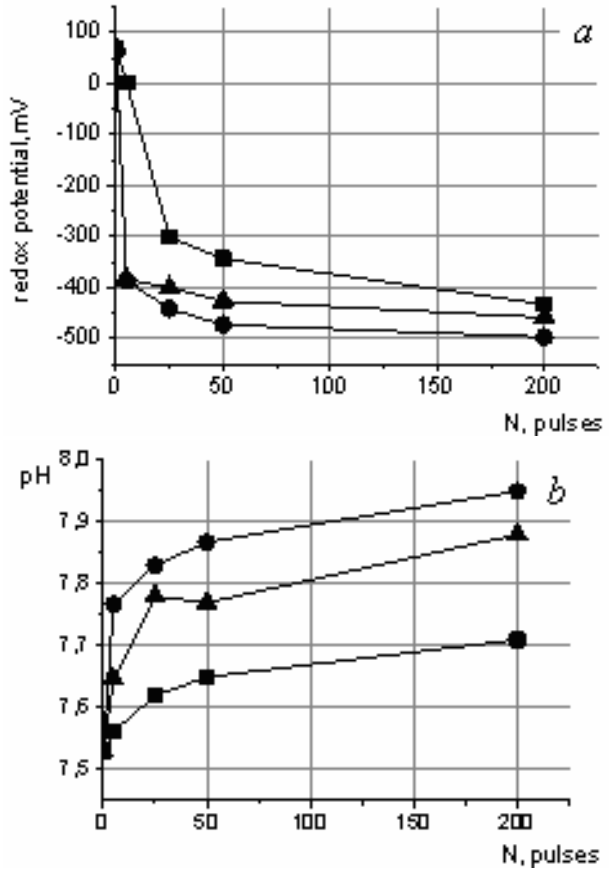

Fig. 10. Dependence of the water properties on the number of pulses at C = 2.947 μF: *a* – ROP, *b* – pH

With an increase in the number of pulses a decrease in the redox potential is observed and at a certain threshold of pulses the positive redox potential is changed to negative. The pH of treated water is increased with an increase in the number of pulses *N*.

To specify the ROP transition point the step discreteness with regard to the number of pulses was decreased. A one-pulse step was selected right up to 6 PPD, and then the additional train of pulses was generated with an increasing step. The data are given in Fig. 11.

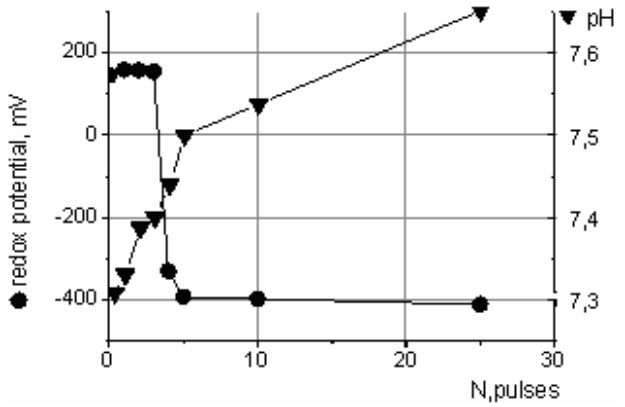

Fig. 11. Dependence of water indices on the number of pulses at U_{charge} = 20 kV, C = 1.924 μF

It has been established that the positive-to-negative change in the ROP occurs already after 3 to 5 pulses.

It is assumed that a change in the given water properties occurs due the effect of the erosion products of electrodes. It is known [9] that the mass of erosion products exhibits linear dependence on the discharge energy. Therefore, we had to establish the relationship of a change in the ROP as a function of total energy of the train of discharges (Fig. 12). The total energy is the sum of total energies of single pulses ($\Sigma[C\times U_{charge}^2/2]$).

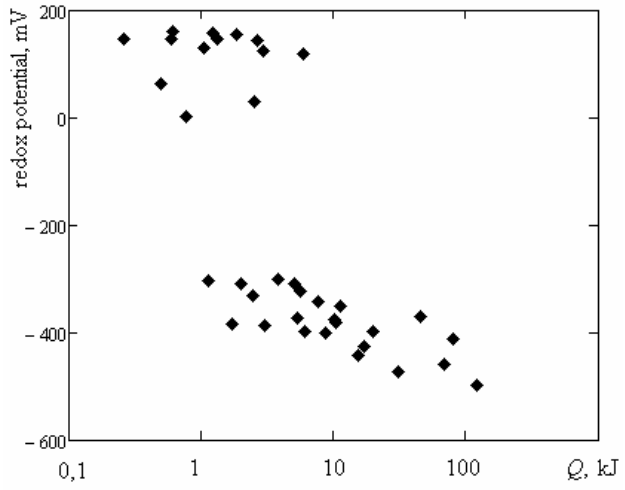

Fig. 12. Dependence of the water ROP on the total energy of the train of discharges

With regard to the «HYDRA» plant the positive-to-negative change in the water redox potential occurs in the range of total energy of 1 to 10 kJ. The availability of such a wide range can be related to a difference in the particle dispersion through which the surface area of the interaction of material particles with the water is specified. In other words, the difference is observed in the particle surface area at the same mass of erosion products.

A certain increase in the water conductivity is observed and the amount of nitrites is within the maximum permissible concentration it does not exceed 20 mg/l at EU norms of 50 mg/l.

To determine the influence of electrode material on the relationship of a change in the studied water properties we carried out the experiments using graphite electrodes. It should be noted that this material withstands lower shock loads due to its brittleness. Therefore, the number of pulses in the train was reduced 2-2.5 times. Fig. 13 gives the obtained research data.

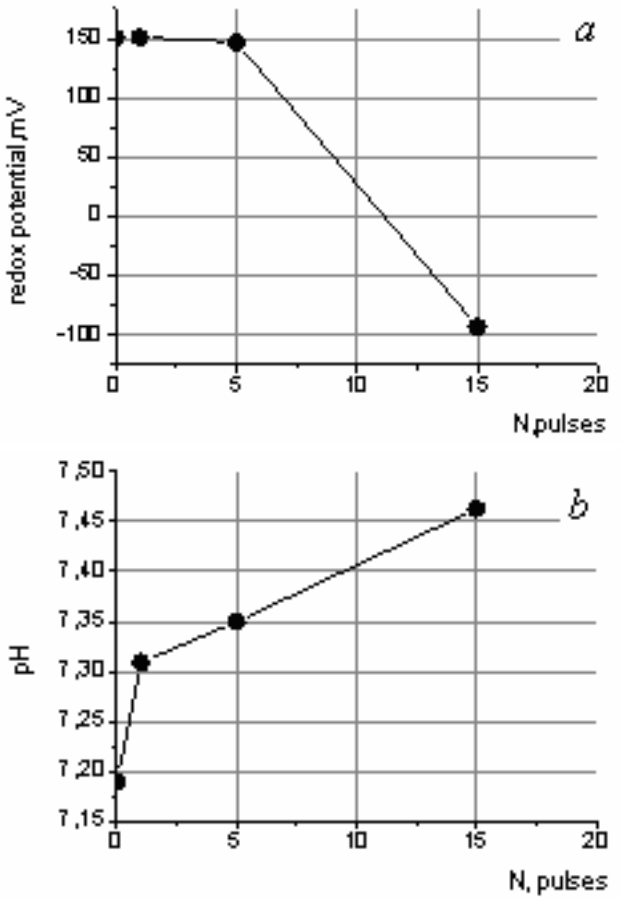

Fig. 13. Dependence of the water indices on the number of pulses at U_{charge} = 20 kV, C = 1.924μF, where *a* – ROP, *b* – pH

Graphite electrodes hold the tendency of the positive-to-negative change in the water ROP with an increase in the number of PPD. At the same parameters of discharge circuit the jump in ROP occurred already at third pulse. This can be related to a more intensive decrease in the electrode mass both due to the erosion and the mechanical destruction.

Table 3 shows the data of the change in the electrode mass. We can see that the graphite electrode erodes faster. We failed to measure a change in the mass of graphite cathode due to its mechanical failure. It is assumed

for the Table 3 that m_1, m_2 is the electrode mass before and after the experimental work, accordingly.

Table 3

A change in the mass of discharge electrodes

	m_1, g	m_2, g	Mass loss μg/J·pulse
Anode is the stainless needle	3.86520	3.79025	1.76
Cathode is the stainless half-sphere	62.31290	62.24010	1.7
Anode is the graphite needle	5.48075	5.47880	1.96

To determine the stability of changes in water properties the water treated at discharge circuit parameters of C = 2.947 μF, U_{charge} = 20 kV, N = 200 was subjected to the analysis after 24 hours.

Here, No 1 is the initial water sample; No 2 is the initial filtered sample; No 3 is the filtered water sample after the train of 200 pulses; No 4 is the water sample after the train of 200 pulses precipitated during 24 hours and then passed through the coal filter (Table 4).

Table 4

Comparison of the properties of water treated by the «HYDRA» plant

	No 1	No 2	No 3	No 4
ROP	+160	+158	–496	–330
pH	7.745	7.745	7.95	7.78

The water was filtered to eliminate the influence of admixtures on water properties, in particular the erosion of electrode material. The Table 4 shows that the samples No 1 and No 2 differ from each other within the device error, i.e. the coal filter introduces no changes into the indications. The sample No 3 has a highly negative ROP and an increased pH value. The properties of the sample No 4 give us all grounds to assume that the changes that occurred in the properties of water treated by the «HYDRA» plant are irreversible.

We also studied the changes in pH of the distilled water (DW) and the tap water (TW) after its exposure to the action of underwater spark discharges at the following electric circuit parameters: U_{charge}= 20 kV; C = 2.947 μF, and the number of pulses N = 100. The water pH was measured potentiometrically with the accuracy of up to 0.1 pH units. Table 5 gives the measurement data (lower index «0» corresponds to the measurements of water before the treatment with underwater pulse discharges; the index «1» is for the water after the treatment).

Table 5

Research data of a change in pH of the distilled water (DW) and tap water (TW)

Time / Water type	30 minutes after the treatment	24 hours	7 days	14 days
DW_0	6,65	6,66	6,67	6,65
DW_1	7,12	7,14	7,12	7,12
TW_0	7,70	7,72	7,71	7,71
TW_1	8,1	8,34	8,68	8,64

With the elapse of time (6 to 7 days) pH is increased insignificantly. It is assumed that this is the consequence of the removal of gaseous products from the water solution after the electrolysis and chlorination products.

It has been established that the electric discharge generated using steel electrodes may result in such processes:

$$2Fe + O_2 \xrightarrow{\text{discharge}} 2FeO\downarrow, \quad (5)$$

$$2FeO + 2H_2O \rightarrow 2FeO(OH)\downarrow + H_2\uparrow, \quad (6)$$

$$2H_2O + 2\bar{e} \rightarrow H_2\uparrow + 2OH^-, \quad (7)$$

$$FeO + OH^- - \bar{e} \rightarrow FeO(OH)\downarrow, \quad (8)$$

$$2FeO(OH) \xrightarrow{\text{discharge}} Fe_2O_3 + H_2O. \quad (9)$$

Hereat, a very small amount of Fe (III) can be formed in the solution. Therefore, we studied the changes in the concentration of Fe in the water treated with underwater pulse discharges. The measurements were taken for the untreated water (TW_0) and four samples treated by the discharges with the same electric circuit parameters U_{charge} = 20 kV, C = 2.947 μF. The number of pulses was equal to 100. We obtained the following iron concentrations: TW_0 = 0.48 mg/l; TW_{11} = 0.54 mg/l; TW_{12} = 0.56 mg/l; TW_{13} = 0.54 mg/l; TW_{14} = 0.56 mg/l. These data are indicative of a negligibly low change in the concentration of pure iron in the water that was treated with PPD. For the sake of comparison, the average statistic values of iron in the tap water correspond to 0.3 mg/l.

We also found out that it is quite possible to use the magnetic separation for suspended and precipitated water particles. It is known that the iron oxide (II, III) called the magnetic iron $FeO{\cdot}Fe_2O_3$ also possesses magnetic properties. The formation of iron oxide (III) in the reaction (9) is possible due to the thermal action of the discharge on iron oxide (II) particles that were formed earlier. Therefore, the «HYDRA» plant with the magnetic separation can be used for the controlled change in the water redox potential and pH values.

The properties of water treated by the «HYDRA» plant also changed when the graphite electrodes were used. We can thus assume that the reaction (7) progresses during the PPD. It should be noted that the paper [10] describes theoretical study of the influence of gas discharge processes on water properties.

Conclusions.

The «HYDRA» plant was used for the investigation of the relationship of a change in the redox potential and pH of the treated water as a function of the number of pulses and pulse parameters specified by the parameters of electric discharge circuit (the capacitance and the charging voltage). A decrease in the redox potential was observed with an increase in the charge voltage of the capacitor bank, the capacitance of it and an exact total energy of the discharges. The water pH is increased. A change in the water redox potential and pH is retained for a long time after the sediment removal. Specified discharge parameters have the pulse threshold and if it is exceeded a positive-to-negative change in the redox potential occurs. The «HYDRA» plant with the magnetic separation can be used as an ideal mixing

electrochemical reactor of a discrete action with the removal of aftereffect products.

Special respect for the data discussion we express to Prof. Vladimir Yuferov.

REFERENCES

1. Ushakov V.Ya. *Impul'snyj elektricheskij proboj zhidkostej* [Pulsed liquid breakdown]. Tomsk, Tomsk State University Publ., 1975. 258 p. (Rus).

2. Yutkin L.A. *Elektrogidravlicheskij effect i ego primenenie v promyshlennosti* [Electrohydraulic effect and its application in industry]. Leningrad, Mashinostroenie Publ., 1986. 252 p. (Rus).

3. Baranov M.I. Breakthrough impulse material processing technologies: history, basic physics and technical feasibilities. *Electrical engineering & electromechanics*, 2009, no.1, pp 42-54. (Rus). **doi: 10.20998/2074-272X.2009.1.10.**

4. Vinnikov D.V., Ozerov A.N., Yuferov V.B., Sakun A.V., Korytchenko K.V., Mesenko A.P. Experimental investigation of electrical discharge in liquid initiated between cone channel electrodes. *Electrical engineering & electromechanics*, 2013, no.1, pp. 55-60. (Rus). **doi: 10.20998/2074-272X.2013.1.13.**

5. Yuferov V.B., Vinnikov D.V., Ponomaryov A.N., Buravilov I.V., Mufel' E.V. Comparative analysis of acoustic pulses generated by the sources of millisecond and microsecond ranges. *Bulletin of NTU «KhPI»*, 2009, no.11, pp 185-189. (Rus).

6. Yuferov V.B., Vinnikov D.V., Buravilov I.V., Mufel' E.V., Pahomov A.Yu., Garbuz V.V., Zhivankov K.I., Ponomaryov A.N. Electrohydraulic method of degassing of de-aerated liquids. *Bulletin of NTU «KhPI»*, 2011, no.16, pp. 211-217. (Rus).

7. Kondrikov B.N., Vovchenko A.I., Annikov V.E., Ivanov V.V. *Vzryvnye prevrashenija elektricheskoj i himicheskoj energii* [Explosive conversions of electric and chemical energies]. Kyiv, Naukova Dumka Publ., 1987. 128 p. (Rus).

8. Novopolzeva V.M., Korovina O.A., Osipov A.K., Nishev K.N. *Sposob photometricheskogo opredelenija zheleza (III) v rastvorah chistyh solej i iskusstvennyh smesej* [Fe (III) photometric definition process in the pure salt solutions and synthetic mixtures]. Patent Russian Federation, no. 2298171, 2006. (Rus).

9. Gorovenko G.G., Ivliev A.I., Malyushevskiy, Pastuhov V.N. *Elektrovzryvnye silovye impul'snye sistemy* [Electroexplosive power pulsed systems]. Kyiv, Naukova Dumka Publ., 1987. 220 p. (Rus).

10. Vinnikov D.V. Numerical investigation of the influence produced by electric circuit parameters on the formation of chemically active radicals in water vapors. *Problems of Atomic Science and Technology*, 2015, no.3(97), pp. 159-165.

Received 01.11.2016

D.V. Vinnikov[1]*, Research Scientist,*
K.V. Korytchenko[2]*, Doctor of Technical Science,*
V.I. Tkachov[1]*, Research Scientist,*
V.V. Egorenkov[1]*, Research Scientist,*
D.V. Kudin[1]*, Research Scientist,*
T.Y. Mirnaya[2]*, Candidate of Chemical Science,*
[1] National Science Center «Kharkov Institute of Physics and Technology»,
1, Akademicheskaya Str., Kharkov, 61108, Ukraine,
phone +38 057 3356326, e-mail: vinniden@mail.ru
[2] National Technical University «Kharkiv Polytechnic Institute»,
192, Poltavskyy Shliakh Str., Kharkiv, 61098, Ukraine,
phone +38 057 3726167, e-mail: korytchenko_kv@ukr.net

Investigation of changes of physical and chemical properties of tap water under influence of powerful underwater spark discharges.

Purpose. *The purpose of this investigation is to study the changes in the redox potential and pH-value of the tap water as a function of underwater spark discharges, storage device capacitance and the charging voltage.* ***Methodology****. To define the electric parameters of discharge circuit we used the Rogowski loop and the compensated capacitance-ohm potential divider. To determine water properties before and after the treatment we used the following devices: the water analyzer Anion-7051 with the limit of absolute error of the EMF measurement ± 2 mV, the BANTE 902 device with the absolute error of ± 0.002 pH.* ***Results.*** *We managed to establish the time of the origination of changes in the properties of treated water. A change in the positive redox potential to a negative one occurred already after the third pulse at a total energy input of ≥ 1 kJ. The pH value increased in the range of 0.2 – 0.45 pH units. We obtained the relationship of a change in the redox potential as a function of total energy of the pulse train that actually exhibits the linear relation to the mass of erosion products. We established that the electrodes made of stainless steel and the electrodes made of graphite provide similar changes in water properties. An increase in pH is indicative of the progress of reactions that result in the formation of* OH^-. ***Originality.*** *The obtained experimental data prove a rapid and reliable change in the redox potential from positive to negative changes in the redox potential exponent can persist during ten days and even longer. The erosion products of electrodes can be removed from the treated water using the method of magnetic separation.* ***Practical value.*** *The «HYDRA» plant can be used as the electrochemical ideal mixing reactor of a discrete action with the removal of erosion products of the electrode using the method of magnetic separation.* References 10, tables 5, figures 13.

Key words: **underwater spark discharge, electrodes material, water properties, redox potential, pH – value.**

How to cite this article:
Vinnikov D.V., Korytchenko K.V., Tkachov V.I., Egorenkov V.V., Kudin D.V., Mirnaya T.Y. Investigation of changes of physical and chemical properties of tap water under influence of powerful underwater spark discharges. *Electrical engineering & electromechanics*, 2017, no.1, pp. 39-46. **doi: 10.20998/2074-272X.2017.1.07.**

UDC 621.315.2 **doi: 10.20998/2074-272X.2017.1.08**

O.V. Golik, L.A. Shchebeniuk

STATISTIC METHODS OF POLYIMIDE ENAMEL ISOLATION DEFECTIVE NON-DESTRUCTIVE CONTROL AT THE CONDITIONS OF PRODUCTION

In this paper can be used to not-destructive technological testing of defects isolation enameled wire with polyimide polymer. The thesis is devoted to the statistical method for processing, comparison and analysis of results of measurements of parameters isolation it enameled wire because of mathematical model of trend for application in active technological monitoring is developed; to development used of the recommendations for parameters of such testing. Is theoretically justified and the possibility of a diminution of dependence of an error from a velocity of movement of a wire for want of quantifying of defects enameled isolation not destroying tests by high voltage. This work is devoted to the statistical method for processing, comparison and analysis of results of measurements of parameters of polyimide isolation. The method is operating not destroying technological monitoring an amount of enameled isolation defect. The dependence of average value of amount of defects for enameled wire ПЭЭИДХ2 – 200 with two–sheeted polyimide by isolation in a range of nominal diameter 0.56 mm is experimentally determined. The technological monitoring purpose is reducing of quantifying of enameled isolation defect. References 7, tables 1, figures 8.

Key words: **enameled wire, polyimide isolation, isolation defective, statistical model of the trend, non-destructive testing.**

Представлены результаты применения статистической модели тренда к анализу показателей дефектности изоляции при неразрушающем технологическом контроле эмаль провода на основе полиимидного полимера в условиях производства. Рассмотрено применение такого контроля для использования результатов в активном технологическом контроле. Предложены рекомендации для практического использования параметров функции тренда в технологическом контроле. Параметром тренда является скорость уменьшения (или увеличения) длины провода с заданной дефектностью в течение технологического цикла. Теоретически показана и измерениями подтверждена возможность количественной оценки тенденции изменения в течение технологического цикла дефектности эмальизоляции для провода ПЭЭИДХ2 – 200 с двухслойной полиимидной изоляцией номинальным диаметром 0,56 мм. Выделение тенденции изменения дефектности эмаль изоляции в течение непрерывного технологического цикла и количественная оценка этой тенденции позволяет количественно оценить случайную ошибку технологического контроля – суммарную ошибку результатов технологического контроля, которая является характеристикой случайной составляющей стабильности технологического контроля и обусловлена большим количеством причин, влиянием каждой из которых можно пренебречь по сравнению с суммой. Библ. 7, табл. 1, рис. 8.

Ключевые слова: **эмаль провод, полиимидная изоляция, дефектность изоляции, статистическая модель тренда, технологический неразрушающий контроль.**

Problem definition. In cable production introduction of relatively expensive product innovation makes use as the main criterion of liquidity price factor. Such innovative product for the domestic cable industry is based enamel wire polyimide synthetic copolymers with a temperature index of 200 °C. These enamel wires are the highest to date electrical and mechanical properties of insulation [1, 2]. For their production they use complex and expensive manufacturing equipment with high speed enamelling (up to 1000 m/min) and deep catalytic combustion of solvent enamel paints [2]. The introduction of such innovative types of cable products in production ensures the highest level of modern electrical, mechanical strength and thermal resistance of winding insulation of electrical machinery and apparatus. According ensure competitiveness electromechanical engineering.

The contradiction between the relatively high cost of innovative products, production of which is based on the use of advanced technologies and materials, on the one hand, and using as the main criterion of liquidity price factor, on the other hand, requires the manufacturer of such implementing innovative technical and organizational solutions to technological support the highest modern level of production while decreasing costs of its production.

The solution to this problem for manufacturers during the development of the known world, but for them innovative products require innovative solutions to process control in order to significantly reduce the number of products which have not passed the acceptance control. This clearly demonstrates the modern concept of «Six Sigma» («6σ») [1]. It criterion of quality products is its high uniformity, ensuring the minimization of the number of products that the characteristics does not meet user requirements. In fact, the concept of «Six Sigma» (defined statistical procedure normal distribution [2]) is a demonstration of achievements in the protection and marketing products of mass production. The development of innovative products specific manufacturer requires development and implementation of innovative technical and organizational solutions process control with the

obligatory reference to the technical parameters of the achieved level of technology. In this case presents a solution for the control parameters defects insulation in non-destructive testing process of wires from polyimide polymer in a production environment.

The feature of poliefirimid and poliamidimid enamel paints is that the full completion of the polymerization occurs only in thin layers (up to 2 ... 3 μm). Therefore, the modern enamel units used trails to the number of passes through the wire nail 24 at length a passage through the oven to 10 m. This necessitates:

1) use of high speed enameling (up to 1000 m/ min);
2) continuity of production cycle making the maximum number of coils of wire;
3) automatic monitoring the number of defects in the enamel insulation in non-destructive testing of high voltage to pass.

The problem is that the results of such monitoring, realized on modern enamel devices (e.g. EFHP system by the MAG-ECOTESTER Company [3]) is not normalized in the technical documentation to the wire in which one of the main criteria is the breakdown voltage and variance breakdown voltage [5]. In this case, nondestructive process control of statistical indicators of the number of defects enamel insulation, realized in modern enamel lines, which would ensure active component of the control system, practically are not used.

Analysis of the literature. The contradiction between the relatively high cost of production and use as the main criterion of liquidity price factor for wires with polyimide insulation in [1] proposed solved by setting lower breakdown voltage requirements for admission and the adjustments to the thickness of the insulation. For example, for low-voltage products lower level voltage breakdown of insulation is sufficient. That prompted the introduction of spectrum needs of different customers. Implementation of the range specifications to meet the needs of different customers greatly extends the range of the applicable technical requirements and that at least blurs the range of values of parameters of the same product and difficult relationship between producer and user of the products.

An example of modern process control, which criteria decision-making process sets manufacturer is the continuous use of statistical control specific number of defects (*er*) of isolation *online* [3]. Number of defects is the number of places in which current flows through the insulation exceeds the set. Discrete measurement of current through the insulation when exposed high voltage direct current (Fig. 1) provides the EFHP system by the MAG-ECOTESTER Company [3].

The need to estimate the number of defects of isolation wires is recognized. The concept of defect isolation wires enough conditional:

- from lack of insulation in the spot defects: defects in the place matches on adjacent coils winding breakdown voltage is zero [4];
- to set forward the increased current through the enamel insulation, indicating the presence in this place insulation defect [3].

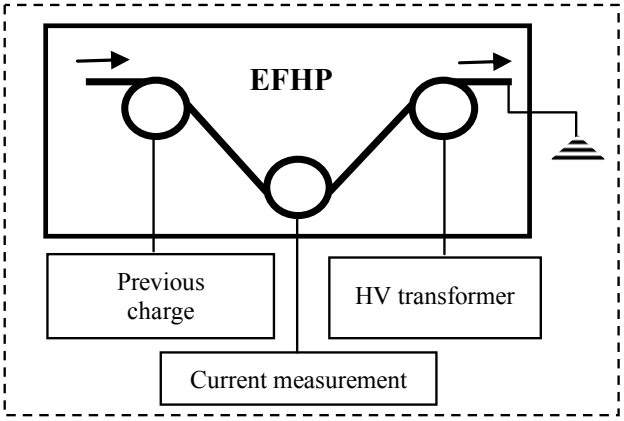

Fig. 1. Schematic diagram of monitoring the number of defects In enamel insulation at non-destructive testing by high voltage to pass

The current value which in [3] the detector circuit registers as a defect is regulated, for example, for a radial insulation thickness ≈30 μm is 10 μA at a test voltage of 1500 V.

So one of the key control parameters is normalized breakdown voltage [1, 3-5] and dispersion breakdown voltage is a parameter which indirectly corresponds to a specific number of local defects of isolation. Both characteristics (dispersion of breakdown voltage and specific defects) reflect the homogeneity of isolation.

Control of dispersion of main technical parameters of products serves the information base for the implementation of the principle of continuous improvement of quality according to ISO 9001:2000. However, such control is not provided normative technical documentation.

Using EFHP system [3] for statistical indicators to monitor the number of defects of isolation wires polyimide copolymers based on a real technological measure that provides the necessary information to implement the principle of continuous improvement of quality under ISO 9001.

To determine the statistical indicators of defects in the EFHP system unified statistical software modules are used. Each coil fixed number of monitoring sites wire (100 m) of four groups of defects: group 1 – 0 to 3 defects; group 2 – 4 to 9 defects; Group 3 – 10 to 18 defects; Group 4 – more than 18 defects (defects refer *er*). Also three major statistical indicators are recorded: the average number of defects in the control region, $M[er]$; defects in the control region with the most defects, er_m; the standard deviation of the number of defects in the control region, $\sigma[er]$.

Obviously, the recorded test results with the help of EFHP system depend on the dispersion of many parameters wire: mechanical properties and diameter of

the conductor d_p, process parameters of enameling and insulation thickness Δ, value the test voltage U and the minimum current through the isolation I in which the system records the defect .

Therefore, the analysis of the current process control defect isolation enameled wires is a complex multidimensional problem. The adoption of technological solutions based on the results of such monitoring depends on the experience of the responsible engineer and is not normalized. In the end, an arbitrator at the receiving control is the breakdown voltage and breakdown voltage variance [5]. In this case, control of statistical indicators of the number of defects enamel insulation, realized in modern enamel lines, hardly used. In our view, this is due to a fundamental difference between the tasks of receiving and process control.

A task of acceptance control in mass production is to match the basic parameters of the finished product technical regulatory requirements. The problem of process control is timely **warnings** of out the basic parameters of the product outside of the established process for admission to a particular production line.

The very task includes preventing the need to synchronize control engineering, process parameters and process time in one form or another. For example, for cables and wires in the tests «to pass» technology time is determined by the length of product that passes through the meter multiplied by the speed.

Evaluation changing trends in the technical and technological parameters for the process time is the main task of process control.

The goal of the work is to analyze the results of non-destructive testing by high voltage to pass of wires from polyimide-based synthetic copolymers with double insulation and with temperature index of 200 °C made at the domestic cable factory which lets you split:

- ***trend*** of the process – a significant change in the results of deterministic process control during the manufacturing process to establish technological factors that cause this change decision-making process of correction parameters; ***trend*** is deterministic quantitative characteristic of the stability of the process;
- ***random error*** of the technological process – total error of the process control which is a quantitative characteristic of the random component of the stability of the process and due to many factors influence each of which is negligible compared with the sum.

The purpose of this division is to develop deterministic and statistical criteria for the stability of high-speed automated manufacturing process of wires from polyimide-based synthetic copolymers with double insulation and a temperature index of 200 °C in the non-destructive testing of high voltage to pass.

The main results obtained. *er* number of defects in each unit length of 100 m for fifty reels of enamel wires (total of 180,000 meters of wire) in the chronological order in continuous production automatic technological process is experimentally determined.

Current control of diameter d_p of copper conductor in the enameling (Fig. 2) indicating the presence in the process as a trend of gradual changes in parameters (for route enameling is technological extract conductor – the trend of the technological process) and random component diameter d_p (after passing the calibers No. 4 and No. 10 increase the diameter d_p is the measurement error) which is part of the random component of the stability of the technological process.

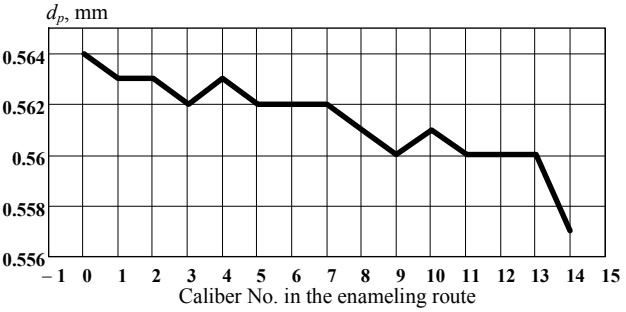

Fig. 2. The diameter of the copper conductor d_p after passing the appropriate caliber enameling route: the route is over the hood conductor technology which is more than one percent

For the analysis of a number of observations *er* per number of defects in each unit length of 100 m enamel wires we applied statistical trend model error (only error is a random variable) for a number of observations on the value x [6]:

$$x_i = f(t_i) + \delta_i, \quad (1)$$

where t_i is the deterministic variable that is a technological time, which in this case is proportional to the number of manufactured wire coil; $f(t_i)$ is the deterministic function (process trend); δ_i is the random variable (random component of the stability of the technological process).

The values of δ_i are independent and identically normally distributed. The function $f(t)$ is given by the formula or algorithm calculations and depends on a number of unknown parameters $c_1,\ldots, c_k$ whose values are determined by maximum likelihood.

In the case of the linear function for each t the value of x is normally distributed with a mean $x(t) = a + b\,(t - t_m)$ and mean-square σ. Estimations of unknown parameters a, b and σ:

$$a^* = x_m; \quad (2)$$

$$b^* = \Sigma(t_i - t_m)(x_i - x_m)/[\Sigma(t_i - t_m)^2]; \quad (3)$$

$$\sigma^* = \{n^{-1}\,\Sigma[x_i - a^* - b^*(t_i - t_m)]^2\}^{0,5}, \quad (4)$$

where t_m is the the average of the determined variable t; x_m is the the average number of observations on the value x.

Credible p-percent boundaries for $x(t)$ for given parameter t are determined by the γ_p Student distribution parameter with $n - 2$ degrees of freedom:

$$a^* + b^* (t - t_m) \pm \gamma_p \sigma^* (n-2)^{-0.5} [1 + (t - t_m)^2 n / \Sigma (t_i - t_m)^2]^{0.5}. \quad (5)$$

For enamel wire with double insulation based on polyimide copolymers in Fig. 3 shows the results of determination of the number of unit length (100 m) containing 18 or more defects. Conventionally, these individual lengths can be considered the most defective (hereinafter: «the worst 100 m»).

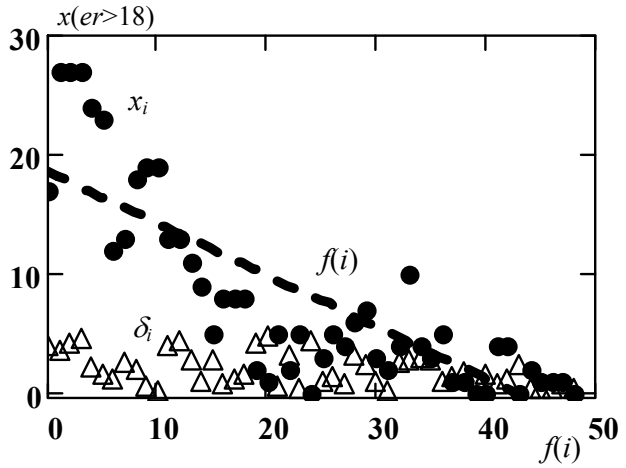

Fig. 3. The results determine the number of unit length (by 100 m) containing 18 or more defects for enamel wire with double insulation based on polyimide copolymers: x_i – the number of «worst 100 m» (18 defects and more) on the reel at the number i in continuous technological cycle of production; $f(i)$ – deterministic function (process trend) defined by (2), (3); δ_i – random part of the process, defined as $\delta_i = ([x_i - f(i)]^2)^{0.5}$

The trend of reducing the number of «worst 100 m» during the process quantifies the observation period is determined by the function $f(i)$. The random component of the stability of the process is represented as an array of values δ_i of absolute deviation number of «worst 100 m» x_i determined by the function $f(i)$:

$$\delta_i = ([x_i - f(i)]^2)^{0.5}. \quad (6)$$

In the presented example, the array δ_i has no pronounced trend and average value δ_m is a quantitative assessment of technological error during the process observation period, in particular – the error control method used.

The data in Fig. 3 indicate the theoretical possibility of separation and quantitative assessment of:

- first, the trend of the process, the causes of which appropriate technological measures should be established by technological service;
- second, the random component of the stability of the process, the average of which is a quantitative assessment of technological error, which is the subject of statistical process control.

Obviously, should be envisaged the possibility of a trend of stable random component of the process. In this case, should be applied a statistical model of the trend with an error to the random component δ_i (Fig. 4).

The sequence of statistical arrays and relevant statistical parameters specified by formulas recurrent procedures (2) – (6) is given in Table 1.

Settings trend identified statistically with the required accuracy (formula (5)), are parameters determined functions. In the example in Fig. 3 is the parameter b^* of the function $f(i)$ – the rate of reducing the number of «worst 100 m»: $b^* = -86.88 \pm 9.25$ (m/h), which is approximately one to reduce the «worst 100 m» for the manufacture of two coils (down 1.4 % relative to the length of the defective enamel wire on one coil).

Table 1

No.	Arrays	Trend parameters	Statistical parameters of random component	
			Average	Standard deviation
1	x_i, δ_i	a^*, b^*, σ^*	δ_m	$s\delta$
2	δ_i, $\delta 2_i$	$a2^*$, $b2^*$, $\sigma 2^*$	$\delta 2_m$	$s\delta 2$
3	$\delta 2_i$, $\delta 3_i$	$a3^*$, $b3^*$, $\sigma 3^*$	$\delta 3_m$	$s\delta 3$
…	…	…	…	…

Automation of control and statistical data, allocation deterministic trend and presenting the results in a quantitative parameter trend provides the possibility of the technological process current adjustment.

The simultaneous selection of the random component of the process δ_i ($\delta_i = ([x_i - f(i)]^2)^{0.5}$) allows to quantify the error process, the causes of which can be very much and reduce what by necessity requires a comprehensive approach that in the world practice called by Deming method [7].

The presented example (a linear trend, a random part of the process) is the easiest. Deterministic function $f(i)$ can not be linear (it can be periodic [6]). For example, an array x_i in Fig. 3 can be best described by a decreasing exponential function that change the coordinate system can be represented as a straight line. Completed relevant calculations are more complex, but technological findings remained unchanged.

Fig. 4 shows the results of the statistical analysis of the stability of the process of manufacturing the same enamel wire on the number of defect-free single lengths on the reel in a number x_i unit length (by 100 m), containing three or fewer defects: x_i is the number of «best 100 m» on the reel at the number i in continuous technological cycle of production.

The number of such recurrent procedures n can be limited by the presence of the random component of the trend, but it is insignificant because the variance of each subsequent random component $D[\delta n]$ rapidly approaching zero (Fig. 5).

The most effective is the procedure for the selection of the first trend, as this random component coefficient of variation $\delta 1_i$ close to unity, indicating the approximate equality $\delta 1_m$ average and standard deviation of the

random component $s\delta 1$ of the process (Fig. 6). Importantly, the dependences $V[\delta n] = f(n)$ (Fig. 5) are similar in character arrays (see Fig. 3, 4) which differ in shape of the visual pass (Fig. 3 – exponential decay, Fig. 4 – linear growth), and the direction of the trend (Fig. 3 – decrease; Fig. 4 – growth).

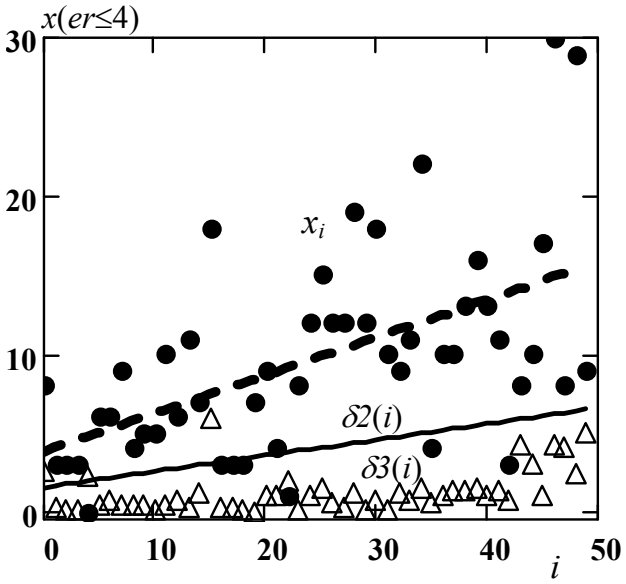

Fig. 4. Number of single lengths that contain three or fewer defects: x_i – the number of «best 100 m» on the reel at the number i in continuous technological cycle of production; $f(i)$ – deterministic function (process trend), defined by (2), (3); $\delta 2(i)$ – the second process trend (random component δ_i); $\delta 3_i$ – an array of random component

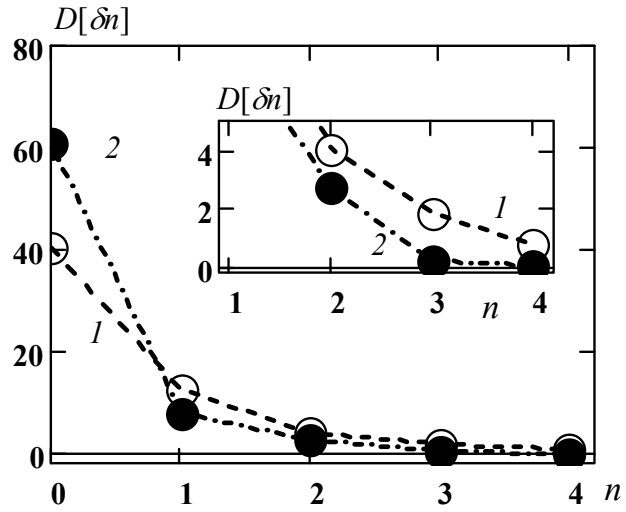

Fig. 5. The dependence of the variance of the random component $D[\delta n]$ on n number of recurrent statistical procedure: 1 – $D[\delta n(er \le 3)]$; 2 – $D[\delta n(er > 18)]$

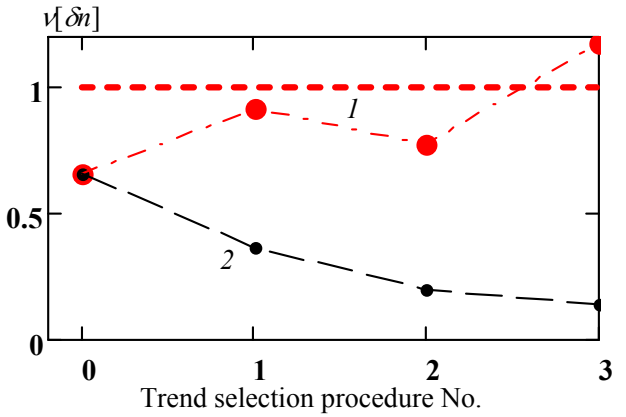

Fig. 6. The dependence of the coefficient of variation random component $v[\delta n]$ on n number of recurrent statistical procedure $v[\delta n] = f(n)$: 1 – v $[\delta n(er \le 3)]$: the coefficient of variation increases and is close to unity (1), and the relative standard deviation decreases exponentially (2)

It is advisable to use a coefficient of variation is random component $v[\delta]$ data set as a criterion for the number of recurrent procedures n which allows you to select a random part of the technological process δn_i ($\delta n_i = ([\delta(n-1)_i - \delta(n-1)(i)]^2)^{0.5}$) and thus estimate error process. Accuracy of process control is ± 1 «best 100 m».

Trends parameters that are deterministic functions technologically parameters may be analyzed, as they are not random.

The gap between the rate of increase in the number of «defect-free 100 m» (≈ 48 m/h) on the one hand, and the rate of decrease in the number of «worst 100 m» (≈ –86 m/h) on the other, clearly shows that the work cycle isolation on high-speed automatic enamel units in principle is not stable. It should be distinguished using technical terminology reliability, grinding in period (increased insulation defects), the normal isolation (insulation defects characterizes the level of technology) and the period of «fatigue» (defective insulation is growing faster than during normal isolation).

The duration of these periods, and hence logistics of enameling technology in a particular production is to be determined by separate and quantify the parameters of insulation defects, such as:

- insulation defect trends, causes and which appropriate technological measures should be established technological service;
- random component of the stability of the technological process, the average of which is a quantitative assessment of statistical process control error.

To quantify the relevant parameters trend superposition model and the random component of the database are necessary. Fig. 7 shows a model for the array data shown in Fig. 4.

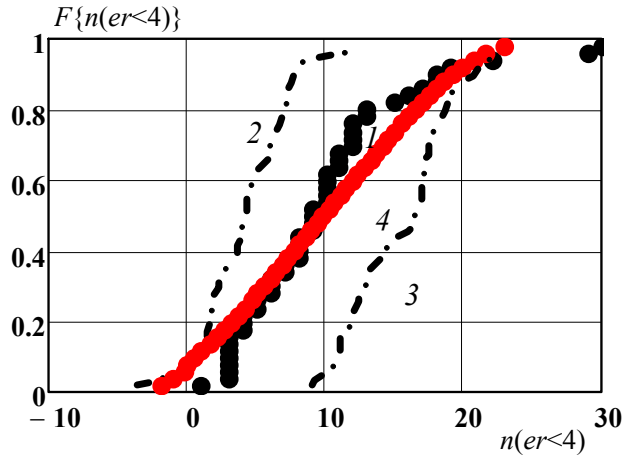

Fig. 7. Model of empirical distribution function of the number of defect-free reference lengths in a normal distribution function with the expectation that varies linearly over the manufacturing process and stable dispersion error control: 1 – empirical distribution function $F^*\{n(er<4)$; 2 – distribution function at the beginning of the observation period; 3 – distribution function at the end of the observation period; 4 – model distribution function

Because the value of the control parameter is positive and the procedure for normal distribution model involves the appearance of negative values for determining the random component used Weibull distribution (WD) (Fig. 8) that, first, rather than a normal distribution (ND) describes an array of data (for ND the Kolmogorov criterion is 0.71, for WD is 0.95).

Second, it permits to evaluate the random component of the array as a parameter exponential distribution, which degenerates WD at a value parameter form that is unity.

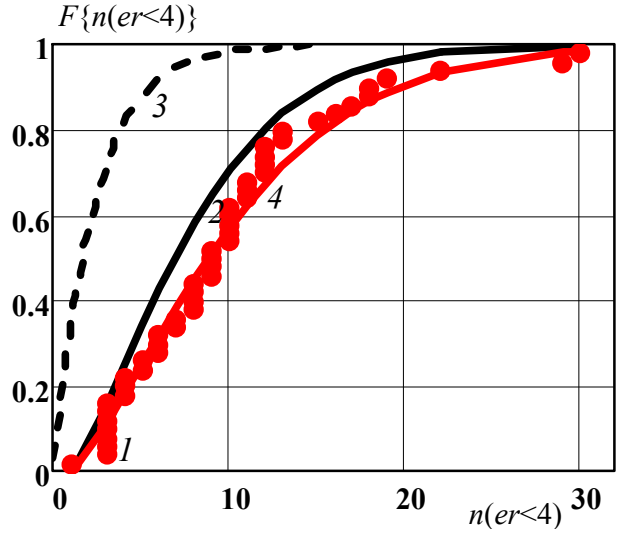

Fig. 8. Model of empirical distribution function of the number of defect-free control as a function of length of Weibull distribution: 1 – empirical distribution function $F^*\{n(er<4)$ (points); 2 – approximation of function $F^*\{n(er<4)$ by Weibull distribution function; 3 – distribution function of the random component of the array (dashed, forms parameter in the Weibull distribution $bv = 1.01$); 4 – model of distribution function $F\{n(er<4)$ as a superposition of trend and the random component array

Conclusions.

1. Results of control of defects of enamel insulation polyimide-based synthetic copolymers in the process of non-destructive testing technology for the passage of high voltage indicate the possibility and feasibility of the selection of technological process ***trend*** – determined quantitative characteristics of the stability of the technological process. Feasibility of the trend allocation is to establish technological factors that cause change deterministic control parameter to decide the process correction.

2. Selection of the technological process ***trend*** makes it possible to quantify the ***random error*** of the technological process which is a quantitative characteristic of the random component of the stability of the technological process and due to many factors influence each of which is negligible compared with the sum.

3. It is selected ***trend*** of the technological process of wire isolation with double insulation polyimide copolymers based on high-speed automatic enamel units as speed (trend parameter b^*) reduction of defects during the production cycle: $b^* = -86.88 \pm 9.25$ (m/ h) which is approximately 1.4 % decrease relative to the length of the defective enamel wire on a reel.

4. Comparison of speed reduction of defects in different periods of technological cycle shows that the work cycle of isolation on high-speed automatic enamel units in principle is not stable. It should be distinguished using technical terminology reliability, grinding in period (increased insulation defects), the normal isolation (defective insulation is stable and reflects the level of technology) and the period of «fatigue» (defective insulation is growing faster than during normal isolation). The duration of these periods, and hence logistics of enameling technology in a particular production is to be determined by limiting the duration of continuous work cycle of the normal period of isolation (defective insulation is stable and reflects the level of technology). The criterion for this limitation should change the sign for speed reduction defects elements of continuous production cycle, the duration of which is determined on the basis of the Mises principle [6].

REFERENCES

1. Zelenetsky Yu.A. About the improvement of technical documentation for enameled wires. *Cables and wires*, 2013, no.5, pp. 19-23. (Rus).

2. Shchebeniuk L.A., Antonets S.Yu. Statistical method purpose is the reduce of quantifying defects of enameled wire. *Bulletin of NTU «KhPI»*, 2012, no.23, pp. 166-169. (Ukr).

3. Golik O.V. Quantifying of defects for enameled wire with two-sheeted poliimid isolation by tests by high voltage. *Ukrainian metrological journal*, 2009, no.1, pp. 15-18. (Rus).

4. Andrianov A.V., Andrianov V.K., Bykov E.V. About the statistics of pin-hole damages of winding wires and

inter-turn short-circuits in windings. *Cables and wires*, 2013, no.5, pp. 28-31. (Rus).
5. Technical Report IVA Laboratories: Breakdown voltage. – classified: October 2007. − p. 18.
6. Tutubalin V.N. *Statisticheskaia obrabotka riadov nabliudenii* [Statistical analysis of observation series]. Moscow, Znanie Publ., 1973. 64 p. (Rus).
7. Mary Walton. *The Deming Management Method*. Foreword by W. Edward Deming. New York: NY 10016 Copyright, 1986. 262 p.

Received 05.11.2016

O.V. Golik[1]*, Candidate of Technical Science, Associate Professor,*
L.A. Shchebeniuk[1]*, Candidate of Technical Science, Professor,*
[1] National Technical University «Kharkiv Polytechnic Institute», 21, Kyrpychova Str., Kharkiv, 61002, Ukraine,
e-mail: unona.2013@mail.ru, agurin@kpi.kharkov.ua

How to cite this article:
Golik O.V., Shchebeniuk L.A. Statistic methods of polyimide enamel isolation defective non-destructive control at the conditions of production. *Electrical engineering & electromechanics*, 2017, no.1, pp. 47-53. **doi: 10.20998/2074-272X.2017.1.08.**

UDC 656.2.004.18 **doi: 10.20998/2074-272X.2017.1.09**

V.O. Bondarenko, I.V. Domanskyi, G.N. Kostin

ANALYSIS OF ENERGY EFFICIENCY OF OPERATING MODES OF ELECTRICAL SYSTEMS WITH THE TRACTION LOADS

Innovative scenarios of reliable energy supply of transportation process aimed at reducing the specific energy consumption and increase energy efficiency of the systems of electric traction. The paper suggests innovative energy saving directions in traction networks of railways and new circuit solutions accessing traction substations in energy systems networks, ensure energy security of the transportation process. To ensure the energy security of rail transport special schemes were developed to propose the concept of external power traction substations, which would increase the number of connections to the networks of 220 – 330 kV, as well as the creation of transport and energy corridors, development of its own supply of electric networks of 110 kV substations and mobile RP-110 kV of next generation. Therefore, the investment program of the structures owned by the Ukrainian Railways (Ukrzaliznytsia) need to be synchronized in their technological characteristics, as well as the criteria of reliability and quality of power supply with the same external energy investment programs. It is found that without any load on left or right supplying arm one of two less loaded phases of traction transformer begins generating specific modes in the supplying three-phase line. Thus, modes of mobile substation cause leakage in one of the phases of the supply line of traction transformers of active-capacitive current, and as a result generating energy in the main power line of 154 kV, which is fixed and calculated by electricity meters. For these three phase mode supply network is necessary to use 1st algorithm, i.e. taking into account the amount of electricity as the energy in all phases. For effective application of reactive power compensation devices in the AC traction power supply systems it is proposed to develop regulatory documentation on necessity of application and the order of choice of parameters and placement of compensation systems taking into account operation mode of power systems and the use of software systems with imitation of instantaneous interrelated schemes of transport loads. References 15, tables 3, figures 4.
Key words: **energy security; railway transport; the process of transportation; networks of power systems; efficiency of modes; mobile traction substations**.

В статье предложены инновационные направления энергосбережения в тяговых сетях железных дорог и новые схемотехнические решения присоединения тяговых подстанций к сетям энергосистем, обеспечивающие энергобезопасность перевозочного процесса. Дано обоснование необходимости расчета тяговых подстанций по векторному методу трехфазного потребления энергии от подстанций НЭК «Укрэнерго». Библ. 15, табл. 3, рис. 4.
Ключевые слова: **энергетическая безопасность, железнодорожный транспорт, процесс перевозок, сети энергосистем, энергоэффективность режимов, передвижные тяговые подстанции.**

Introduction and problem definition. Analysis of changes in the structure of the energy balance of railways shows a strong tendency of orientation of their energy mainly in the power consumption. For example, for the previous period (1997-2012) the share of electricity has increased from 51 % to 70.5 % in the total energy balance of the railways. To known positive properties of electric energy (easy accessibility, portability, willingness to consume, etc.) added another, extremely important in modern conditions – lower cost of works and services, which are performed with the use of electric energy compared to the other main types of fuel and energy resources [1-5].

In Ukraine since 1950-s on the AC system 25 kV, 50 Hz electrified 5.5 thousand km (53 % landfill) of railways. World experience confirmed the undeniable advantages of the AC system before electrification system DC 3 kV. Currently, the share of electrified portions of the total operational length of railways is 47.3 %, while the share of electric traction in the overall turnover equal to 91.2 %. However, the effects of the economic crisis significantly reduced the rate of electrification of railways in 2014-2016. As a result, the most important electrified line Kharkiv – Poltava – Kremenchug – Znamenka works internally powered modes of traction network from mobile substations [5-8].

One of the most urgent issues of energy transport process is the effective implementation of the traction electricity reserve capacity power supply of electrified railways AC roads. Ways of realization of reserve capacity are different. If the main focus of the railways of the advanced economies is placing on the traction substations stationary traction reserve units, the railways of Ukraine, this problem is solved by the mobile reserve of traction substations. Recently put into operation during the period of sustained growth in traffic. In the fall of traffic they may be involved in other areas which are expected to increase in traffic. Naturally, such a «flexible» reservation system must be linked in circuit and regime system with external power supply.

In order to reduce costs for the electricity industry all the railways of Ukraine carried out the supply of electricity to consumers at regulated tariffs, which saves hundreds of million UAH the procurement of electricity (in 2014 – 631 million UAH). Advantages of the wholesale electricity market, electricity purchases are obvious, but there are some features of payment for electricity in conditions of forced modes of electric traction networks with mobile traction substations [2-5].

The pace of aging power units at the existing funding gap continues to outpace reconstruction. The length of electrified lines of the landfill, which operated over the average period of time (40 years) increased to 6393 km or 62.3 % in 2012, and today this figure is closer to 6,820 km or 67 %. With a lifetime of over 30 years

232 stationary (78 % of the total) and 10 mobile traction substations are working. At the present time requires a complete reconstruction of more than 50 % of the expanded length of the catenary and traction substations. To stabilize the situation need to increase the pace of renovation of the traction power supply units in the period from 2016 to 2020 every year at least 600-670 km of catenary and traction substations 10-15, with an average financing needs for one substation about 50 million UAH [1, 7, 8].

Reasons of the low efficiency of power lie in the technical, economic, organizational processes: the degraded state of electrical networks due to wear and tear; unbalance load lines phases; unbalance modes of transmission lines; the impact of energy flows in the common elements of the network (the effect of the loss of non-linearity) uncompensated reactive power flows.

Therefore, the question of the substantial increase in the volume of works on modernization, improve the reliability and efficiency of the traction power supply, as well as the electrification of new railway lines belongs now to the most important priorities of development of the railway energy of Ukraine.

The goal of the paper is analysis and development of ways to improve the energy efficiency of modes of electrical systems with traction loads and the rationale for the calculation of traction substations for the vector method of three-phase energy consumption from substations of the National Energy Company «Ukrenergo».

1. Energy efficiency analysis of traction and external power supply for electrified line Poltava – Kremenchug – Alexandria. The general lack of circuit connections of traction substations (TS) of electrified areas for the period 1993-2011 lies in the fact that virtually all substation joined the network of 110 kV of regional power companies and a number of them to such networks 110 kV which connect different energy system.

The choice of external power supply scheme of TS (Fig. 1) is made in accordance with the «Standards for technological design of energy systems and electric networks of 35 kV and above» and new chart-technical solutions join the TS to the power system networks, which proved in [5, 9] used in railway electrification.

The source of external power supply of traction substation is a substation of 330 kV North and Dnieper power systems. 330/110 kV substations Poltava was introduced into operation in 1964 and 1997. Currently, the substation is equipped with 4 auto-transformer, two 125 MVA and two 200 MVA. Outdoor switchgear (OSG) 330 kV substations Poltava performed under the scheme 330-10 «transformer – bus lines with the connection by two switches». At this voltage are due to Zmiev thermal power plant, substations with 750/330 kV Severoukrainskaya and 330/154 kV Kremenchug.

110 kV OSG Poltava has four sections, two sectional and two co-located with the bypass section switch. The distribution of electrical power from the TS Poltava 110 kV voltage is carried to consumers of Poltava city and the Poltava region, and traction substations.

OSG 154 kV traction substation Alexandria has three sections 154 kV bus on which power is supplied from the substation «North» and the substation Znamenka. The distribution of electrical power from the TS Alexandria on voltage 154 kV, substation Konstantinovka made to consumers, the substation «Neftianik» and substation Morozivka.

At TS Alexandria in 2009 it was put into operation three continuously adjustable settings transverse capacitive compensation (CS) (manufacturer ČRD ELEKTROTEXNIKA), with total capacity of 18.4 Mvar. In the phase *A* and phase *B* included adjustable installation CTK with capacitors type CUEFS 23-8.7/600/ WF and compensating reactors and decompensating respectively KTL-182/155 and KTL-192/210 with 7609 of Q_A=7609 kvar and Q_B=7565 kvar. Unregulated installing KU with capacitors КЭК1-1,05-63-1У1 and reactor ФРОМ-3200/35У1, capacity Q=5699 kvar is included in the phase *A* or *B*. To ensure the compensation (decompensation) of reactive power and filtering of higher harmonic components of voltage and current general scheme applies dynamic compensation, in which the converter COMPACT system provides adjustment of the value of the phase current of decompensating reactors. The basis of this system is the semiconductor converter unit which includes optothyristors with protective resistor-capacitor elements and signaling unit.

Before installing CS average daily electricity consumption of traction substation in 2009 was S = = 250 – j80 MVA, tgφ = 0.32. For such a load, installed capacity capacitors (18.4 Mvar) exceed correctly calculated by the reactive power, voltage mode, unbalance, harmonics several times [10-15]. It is possible with such a huge power capacitors thyristors fully open permanently. It is interesting to know their real condition and mode of operation. Analyzing the state of the CS in the evaluation of energy losses in the first place should pay attention to the installation of the filter with oil-filled reactors ФРОМ-3200/35У1. In addition to the increased complexity of the maintenance of these reactors, they are characterized by higher energy losses. In particular, only the power loss in the steel reactor cores is 10.5 kW.

Technical and economic calculations show that in the current application smoothly regulated CS plants due to the large capital investment that determines the large payback period (10-15 years) for the traction network of national railways.

In general, the following measures can be applied to improve the efficiency of the heterogeneous network: division of low voltage network, the use of longitudinal capacitive compensation in high-voltage lines, inclusion of booster transformers in the branch networks of different nominal voltages. The most advantageous solution is determined by the feasibility study on the simulation models based on modes of supply of power systems [3-5]. Currently, the contact area network Kobelyaki – Kremenchug – Alexandria partitioned neutral accents and is a long cantilever sections with single feed.

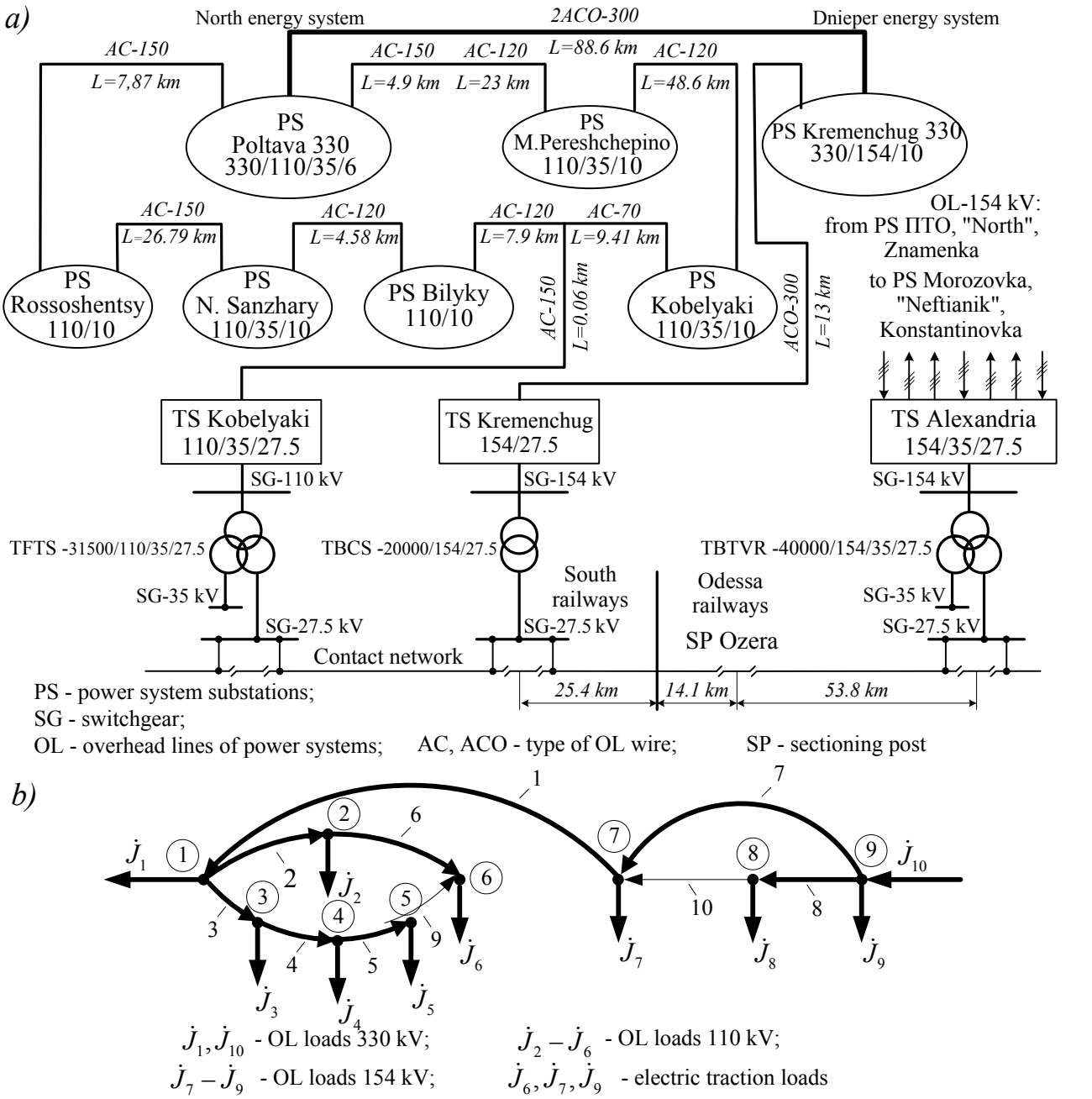

Fig. 1. The scheme of external power supply of traction substations at the junction of South and Odessa railways and its directed graph (here: TFTS – three-phase transformer with air-filters and three windings for mobile substations; TBCS – three-phase transformer, the oil cooling with blown and natural circulation of oil for mobile substations; TBTVR – three-phase transformer, cooling with blown and natural circulation of oil; three windings; with automatic load voltage regulation for rail, electrified with alternating current, rated power of 40,000 kVA, voltage class 154 kV)

Parallel running electrical traction networks 27.5 kV and the network 110, 154, 330 kV (Fig. 1) are heterogeneous and power transmission it happens when you increase the value of active power and energy losses, that is, at a reduced cost-network operation as a whole. Heterogeneity of traction power systems and supply chains leads to an increase in the equivalent resistance R_{eq} at the power transmission path. Thus, if for a homogeneous network, active equivalent resistance R_{eqo} will be equal $R_{eqo} = \frac{r_1 \cdot r_2}{r_1 + r_2} = \frac{r}{2}$, than for inhomogeneous one which graph is presented in Fig. 1,*b* $R_{eq} = Re\frac{\underline{Z}_1 \cdot \underline{Z}_2}{\underline{Z}_1 + \underline{Z}_2}$, and increase of the active resistance can be determined by the following expression

$$\frac{R_{eq} - R_{eqo}}{R_{eqo}} = \frac{(\xi_1 - \xi_2)^2}{2 + (\xi_1 + \xi_2)^2}, \qquad (1)$$

where ξ_1, ξ_2 are the ratios of reactance to active resistance of the corresponding graph branches.

Calculations with real values of resistance by the expression (1) lead to the conclusion that, in parallel to the network 110 and 27.5 kV, 154 kV and 27.5 kV have to expect an increase in the equivalent resistance

by 15-20 %. Consequently, at 15-20 % power loss will be large.

The main load of the network is the system load $\dot{J}_1$ and $\dot{J}_{10}$, loads of traction substations $\dot{J}_6$, $\dot{J}_7$, $\dot{J}_9$ have significantly less value. Count circuit branches, the reduced voltage to one have different ratios of reactance to active resistance $\xi = x/r$. For a given circuit condition heating low voltage network wires limit the capacity of the network. Part of the network of higher voltage (330 kV, 154 kV) underload, as part of a network with a lower voltage is overloaded. The flow of power is on the branches 6 and 10 of the graph circuit.

Heterogeneity of parallel networks 330, 154, 110, 27.5 kV, the specific modes of operation minimizes the benefits of closed networks, is the large power supply reliability, better quality of electricity and if you can not take into account for traction network power flow in fee, will inevitably use console power circuits.

Traction substation Kobelyaki and Kremenchug are powered by the North energy system and Alexandria – from the Dnieper energy system. The scheme of parallel operation and partitioning traction network is shown in Fig. 2. The inclusion of traction substations for parallel operation will inevitably lead to power flows on the network even when the traction according to the normalized values of primary voltage due to differences in their capacities.

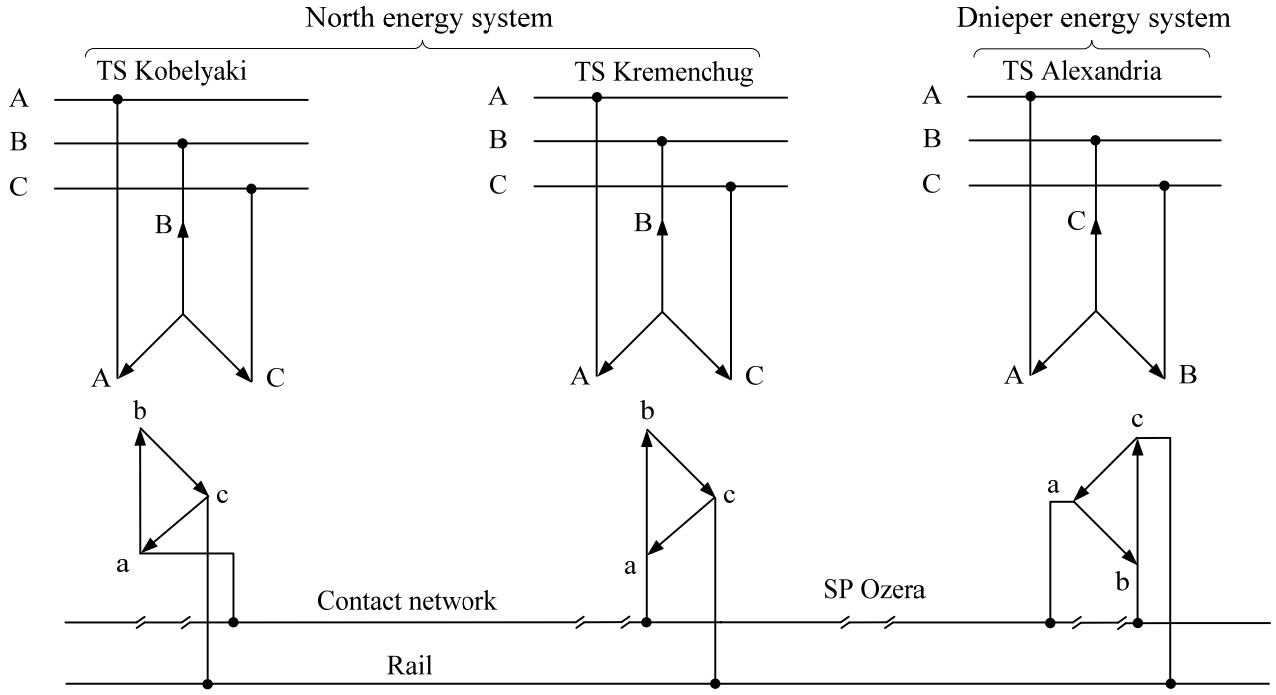

Fig. 2. The scheme of parallel operation of traction substations

Taking into account that the total power consumption of traction substation consists of the consumption of electricity for traction power, losses and power flows on the traction network, we can offer a formula for determining the flow

$$W_{over} = W - \Delta W - W_{ts} = \sum_{i=1}^{n} (\overset{*}{I}_{shi} \dot{U}_{ti} - \Delta \dot{S}_i) - W_{tsi},$$

where W is the comprehensive energy consumption of traction substation; W_{TS} is the electricity consumption for train traction; ΔW is the power loss in the traction networks; $\overset{*}{I}_{shi}$ is the conjugate complex of instant currents in shoulders of power traction substation; $\dot{U}_{ti}$ is the the instantaneous voltage on the tires traction substation; n is the number of solved instant schemes in simulations electrotraction networking modes.

A preliminary assessment of the scheme traction power network and the selection of the scheme, which allows to approach the power-saving mode of the traction power supply system is determined by modeling power flow and energy loss. At the same time the implementation of the automated system of commercial electric power accounting on all railways of Ukraine allows today to use these energy meters traction substations and implement the actual definition of the electricity costs for various power schemes. Last modification counters at traction substations (with appropriate software), and can measure power loss in the zone between substations. By analyzing this information, power dispatcher can select an energy-saving power supply circuit [5].

2. Forced modes of mobile traction substations and power system supply lines. Reality today is such that, almost without reserve, mobile substation for a long time working instead of fixed-to-congested areas, and some super-long cantilever sections loaded with only one arm power, which leads to a sharp current unbalance traction transformers phases (least loaded are two phases) and finally to increased energy losses [5, 6].

In May 2014 it was put into operation a mobile substation «Traction Kremenchug» which is attached directly to the main power grids of North grid, namely the PS-330 «Kremenchug». Modes of her work defined the technical specifications, including power and modes with long cantilever sections one shoulder power («lagging» or «advanced» phase). [8] It is necessary for the implementation of the transportation process on the condition of ensuring the minimum level of tension in the electric rolling limiting sections (U = 21 kV). As shown below, such mobile substation modes cause flow in a single phase traction supply line transformers active-capacitive current and as a result, the generation of energy in the mains power line 154 kV, which is fixed and the calculated electricity meters. According to the theory of electrical networks and the existing rules of electric power metering, for such modes of three-phase mains supply requires the use of a vector method, i.e., metering of electricity as the amount of energy in all phases, taking into account the sign.

It is known that on the roads of single-phase AC power traction network is usually carried out by a three-phase transmission line through transformers connected to this or that scheme [3]. Of all the possible connection scheme of the three-phase transformers, the most widely used on the railways of Ukraine got a scheme in which the traction winding is connected in a triangle. When connecting the traction windings delta loading, though not identical, but all three phases of high voltage lines. It is possible to power district load from a third transformer winding voltage of 10 or 35 kV. The primary winding of the three-phase transformer is always connected in a star. When connecting the traction winding triangle is no circuit for zero-sequence fundamental frequency currents. In this case, much less disturbing effect of high-voltage line on the communication line. These circumstances had a decisive influence on the fact that the traction winding three-phase transformer is connected in delta. A more uniform load three-phase transmission line phases is achieved when powered traction substations of all three phases of the transmission line. In this case, the traction network section of the left and right of the substation fed by various transmission line phase and consequently have a voltage out of phase with each other.

When considering schemes of traction substations for the positive direction of the currents ($\dot{I}_A$, $\dot{I}_B$, $\dot{I}_C$) to the transmission line, branches from the transmission line to the substation, and also in the feeders that feed a power train ($\dot{I}_L$, $\dot{I}_R$ and $\dot{I}_P$), will take direction from the feeding center to the consumer. For the positive direction of currents in electric locomotives will take direction from the conductor to the contact rail. For the power supply circuit (Fig. 3) combined vector diagram of voltages and currents in the particular case (the least loaded are two phases) shown in Fig. 4. When constructing diagrams accept transformation ratio equal to one and neglect the idling current and voltage losses in the windings. Then, the voltages $\dot{U}_A$, $\dot{U}_B$ and $\dot{U}_C$ and, accordingly, voltages $\dot{U}_{ac}$, $\dot{U}_{ba}$ and $\dot{U}_{cb}$ will be provided and the same vectors (Fig. 4). The current vector $\dot{I}_L$ (left side) received the voltage should be oriented with respect to the voltage vector $\dot{U}_{ac}$. In the vector diagram shows the current $\dot{I}_L$ shifted from «their» voltage at a certain angle φ_L. The current vector $\dot{I}_R$ (coming from the substation to the right) in the direction shown in Fig. 3, focused on the vector of «their» voltage $-\dot{U}_{cb}$ opposite to the voltage $\dot{U}_{cb}$ shown on the diagram (Fig. 4). Laying voltages on the chart $-\dot{U}_{cb}$ (shown in dotted line), it can relatively displaced by a certain angle φ_R applied $\dot{I}_R$ current vector. Knowing $\dot{I}_L$ and $\dot{I}_R$ it is easily find the current $\dot{I}_P$ in the wire attached to the rail as the magnitude of the counterbalance (as well $\dot{I}_L + \dot{I}_R + \dot{I}_P = 0$), and the phase current transformer [3]:

$$\dot{I}_a = ⅔\,\dot{I}_L + ⅓\,\dot{I}_R;\ \dot{I}_b = ⅓\,\dot{I}_R - ⅓\,\dot{I}_L;\ \dot{I}_c = -⅔\,\dot{I}_R - ⅓\,\dot{I}_L.$$

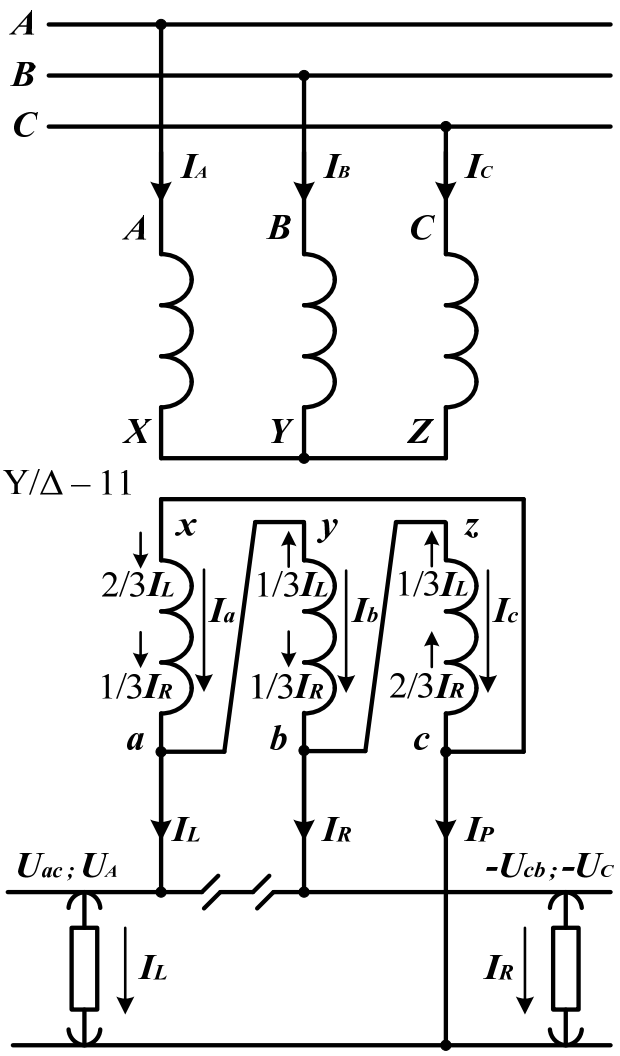

Fig. 3. Feeding diagram of the traction power supply of single-phase current using three-phase transformer connected according to the scheme Y/Δ–11

Left feeder zone to the current $\dot{I}_L$ powered by voltage $\dot{U}_{ac}$. This voltage is generated in the winding ah and windings *ybzc* (where it is obtained by adding the voltages of the two geometric windings *by* and *cz*). But *ax* winding resistance is half the resistance of the other two windings connected in series. Therefore, the current $\dot{I}_L$ is

divided between generating voltage $\dot{U}_{ac}$ windings in the ratio of 2:1. Similarly, current $\dot{I}_R$ is shared. It can be noted (Fig. 3) which is the least loaded phase is the phase of the triangle, which is not directly connected to the rails. In this case, when one of the loads, $\dot{I}_L$ or $\dot{I}_R$, equal zero, two phases are loaded least.

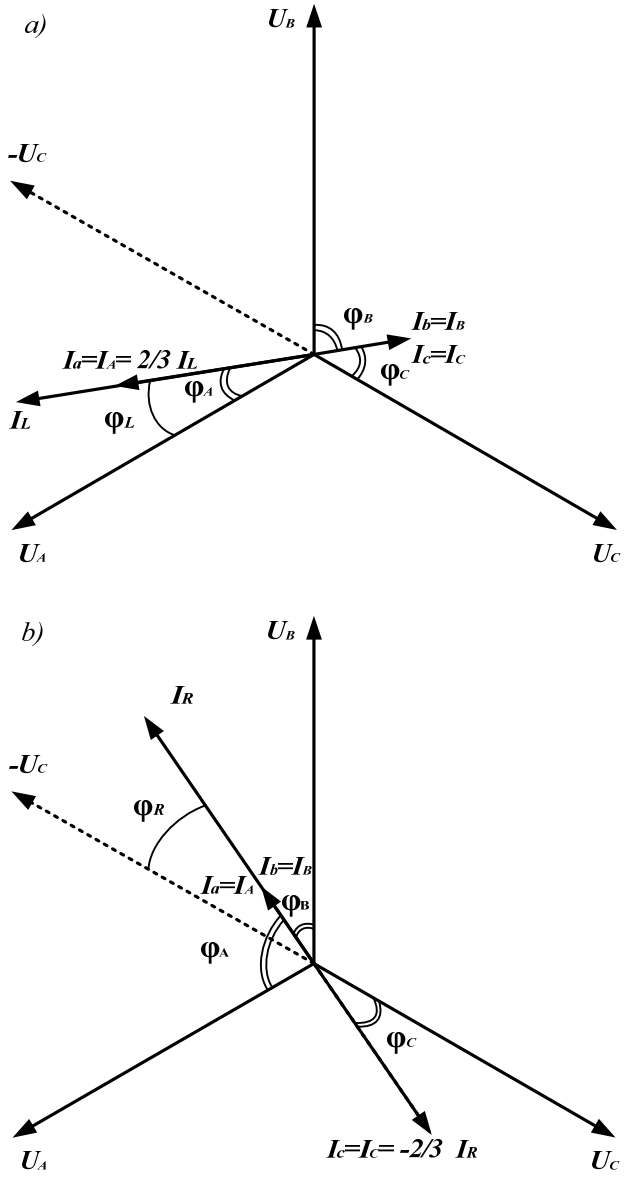

Fig. 4. Vector diagram to determine phase currents of the three-phase transformer for the particular case:
a – load $\dot{I}_R$ of the feeding right side equal zero;
b – load $\dot{I}_L$ of the feeding left side equal zero

Let us consider in more detail the special case where the least loaded are two phases, for example, when powered traction load only the left shoulder «lagging» phase (Fig. 4,*a*) or only the right shoulder «advanced» phase (Fig. 4,*b*). When powered load left shoulder $\dot{I}_L$ «lagging» phase (Fig. 4,*a*) the angles of phase shift between the currents $\dot{I}_A$, $\dot{I}_B$ and $\dot{I}_C$ and the voltages $\dot{U}_A$, $\dot{U}_B$, $\dot{U}_C$ is significantly increased. Note that $\varphi_A = \varphi_L$, current $\dot{I}_B$ lags the voltage $\dot{U}_B$ by an angle φ_B, and $\dot{I}_C$ leads the voltage $\dot{U}_C$ by an angle φ_C. Thus, one of the least-loaded traction of transformer phase begins to generate current in the supply network. When powered right shoulder load $\dot{I}_R$ «advanced» phase (Fig. 4,*b*) $\varphi_C = \varphi_R$, $\dot{I}_B$ current leads the voltage $\dot{U}_B$, and now this phase traction transformer generates a current in the supply network.

In the presence of the load on the district may not have the traction substations and low thrust loads this mode, but for mobile substations (10 kV for regional consumers are not always designed) are inevitable.

Experimental investigations were carried out for normal and forced modes of electric traction network. Forced (provisional) mode in a mobile operating conditions traction substation considered mode where plot Kremenchug – Ozera supply voltage of 27.5 kV phase *A* and phase *B* is in an idle mode. Normal mode will assume a mode in which the traction substation feeds Kremenchug – Ozera (phase *A*) and Kremenchuk – Kobelyaki (phase *B*). It was found that the power of the mobile traction substation «Traction Kremenchug» 20 MW does not allow transportation process on the console section of traction network length of 39.5 km Kremenchug – Ozera normally due to the need to ensure the minimum level of 21 kV voltage on the pantograph of electric rolling of limiting haul.

The presented results confirm that in the reverse direction of energy in the least loaded phase *B* from the higher voltage is the result of bias currents in the winding of a traction transformer *yb* forced mode mobile substation «Traction Kremenchug».

Experimental investigations have confirmed the cause of the generation mode in phase *B* of the OL 154 kV and traction load requirements of GOST 13109-97 «Power quality limits in public electrical networks».

The absence of power generation by the traction load is confirmed by experimental measurements at the input of 27.5 kW traction transformer substation mobile «Traction Kremenchug» under different loads on the feeder zone Kremenchug – Ozera (Table 1). Thus, the experimental research results confirm the theoretical study on the use of the vector algorithm, taking into account the amount of electricity when powered mobile traction substations of backbone electric grids of the National Energy Company «Ukrenergo».

3. Evaluation of electric energy in the traction substations. It is known that at the traction substations of electrified railways of commercial electric power accounting devices should be installed at the boundary equipment accessories, i.e. at the level of the power supply traction transformers. However, the majority of traction substations of electric energy accounting is conducted at low and medium voltage. In this case the loss of electrical energy in traction and step-down transformers are determined by calculation.

The unit of electric energy at levels low and medium voltage due to the lack of measuring transformers of current and voltage at a high voltage transformer substations with the old type of stationary, mobile and on they do not provide even a project.

Table 1

Experimental investigations on the feeder 27.5 кV of the TS «Traction Kremenchug»

No.	Measur. No.	P_a, kW	P_b, kW	Q_a, kvar	Q_b, kvar	U_{ab}, V	U_{ca}, V	U_{bc}, V	I_a, A	I_b, A	φ_a	φ_b
1	32	2604.3	60.9	577.5	38.9	102.6	94.6	86.2	99.0	2.6	133.2	272.6
2	36	3313.8	64.7	498.6	24.3	102.4	95.3	84.7	122.4	2.5	128.9	260.8
3	37	4513.3	64.8	156.0	20.2	101.6	95.0	83.4	162.1	2.5	122.7	257.2
4	41	4868.1	63.5	–1004.9	24.9	101.3	95.7	83.6	179.3	2.6	108.3	261.5
5	40	6391.0	61.4	–1944.8	24.8	100.2	95.3	82.6	239.6	2.5	103.1	262.2
6	33	8250.0	62.4	–2558.6	17.8	99.3	95.6	82.3	306.6	2.5	102.9	255.3
7	34	8789.0	63.0	–2328.2	18.9	99.0	96.3	81.1	321.4	2.6	104.6	256.6
8	25	10142.0	62.9	–3898.4	27.6	98.3	97.2	81.7	383.8	2.8	98.9	263.1
9	21	13013.0	186.4	–5024.8	78.8	96.8	96.3	78.2	485.4	8.1	99.1	263.1
10	10	14855.5	203.7	–5802.5	70.0	95.6	97.1	78.0	555.0	8.8	98.0	258.4
11	11	16439.5	218.1	–6666.0	70.7	94.8	96.6	76.5	615.2	9.5	98.2	258.3
12	14	18155.5	227.0	–6886.0	78.8	94.0	96.9	74.3	673.6	10.2	99.3	259.2
13	19	21235.5	246.5	–7804.5	87.8	92.5	97.9	72.4	781.0	11.4	99.8	259.8

Note. 9-13 – short-term connections of the phase *B* to feed traction network of the feeder zone Kremenchug – Kobelyaki (current transformer coefficient – 1000/5, account ratio – 55000).

Payment points with wholesale electricity market for electricity placed in cell No. 2 of OSG-154 kV of substation PS-330 «Kremenchug». Current account for traction feeders mounted on the contact network and the technical account – on the feeder of 27.5 kV power transformer of the mobile substation «Traction Kremenchug». Comparative analysis of the volume purchased and released electric energy for the period May – November 2014 indicates the presence of imbalance which is more than 10 % (Table 2, 3). Analysis of the data (see Table 2, 3) shows that the calculation of flow of electrical energy at the point of calculation intentionally or erroneously on the following principle.

Table 2

Reported data of release and reception of power of the TS «Traction Kremenchug»

Month	Electrical energy volume at the OL 154 kV, thousand kW·h		Reception on buses 27.5 kV, kW·h	Calculated losses, thousand kW·h		Unbalance OL 154 kW	
	Release	Generation		in the transformer	OL 154	thousand kW·h	%
May	3 270.6	406.8	2 855.7	27.082	1.686	386.115	11.8
June	3 643.2	457.2	3 172.3	27.877	2.223	440.758	12.1
July	3 965.4	472.68	3 472.6	29.541	2.557	460.697	11.6
August	4 215.6	526.86	3 666.3	30.629	2.904	515.796	12.2
September	4 726.8	600.48	4 100.5	29.427	3.881	593.009	12.5
October	5 238.0	635.04	4 573.2	31.544	4.594	628.704	12.0
November	5 455.8	671.58	4 751.7	31.961	5.218	666.926	12.2

Table 3

The balance sheets of release and reception of power of the substation PS-330 Kremenchug

Month	Received on buses 154 kV, thousand kW·h			Received from bus 154 кВ, thousand kW·h	Buses 154 кV unbalance, thousand kW·h
	From autotransformer	From other sources	From traction substation		
May	169 862.4	4 908.6	406.8	175 132.4	–361.8
June	163 753.2	4 307.4	457.2	168 269.4	–208.8
July	185 108.4	8 172.0	473.4	193 366.8	–86.4
August	223 824.6	543.6	527.4	224 535.6	–167.4
September	206 530.2	1 656.0	599.4	208 222.2	–64.8
October	212 432.4	6 161.4	635.4	218 410.2	–421.2
November	200 809.8	7 444.8	671.4	208 215.0	39.6

Installed at the design point per phase electricity meters are set to account in both directions, and in determining the amount of flow of electricity accounted for the volume of electricity supplied by each phase separately. Thus, the presence of lasing at any given volume of phase calculation is excluded. As a result of this calculation railroad monthly, starting in May 2014 (after OL 154 kV commissioning and mobile traction substation «Traction Kremenchug»), purchases of electricity by nearly 500 thousand KW·h more than the consumer supplies. With a monthly volume flow on the OL 154 kV 4000-4500 thousand KW·h OL loss exceeds 10 % of normative losses at the rate of class 1 power purchase 3.66-3.86 %. As a result of the imbalance between the amount of electric energy that was allotted to the substation PS-330 «Kremenchug», and the actual amount received by railway on TS «Traction Kremenchug» for the period May-November 2014 amounted to 3771 thousand KW·h. However, it should be noted that in determining the amount of unbalance of tires 154 kV Substation PS-330 «Kremenchug» and substation as a whole calculation is carried out taking into account of the full phase mode electricity flow at all points in the account, including taking into account the phase *B* of generation in the OL 154 «Traction Kremenchug». Thus, the calculation algorithm in the balance of the substation PS-330 «Kremenchug» is different from the volume calculation algorithm for suppliers of electrical energy connected to this substation, which is contrary to the rules.

Conclusions.

1. Analysis of the electrical system with loads traction shows that to improve their energy efficiency needs a full-scale program of modernization. The investment program included in the structures of JSC «Ukrzaliznytsia» must be synchronized on the technological parameters, as well as the criteria of efficiency and quality of power supply with the same external energy investment programs.

2. In the analysis of risks and threats to energy supply process traffic of railways from the external power supply is suggested to use a system of rating assessments of energy security for all of the following indicators: the reliability of power supply system taking into account the high measure of depreciation of fixed production assets of the energy economy of the region; power ratio of the amount of power and bandwidth interconnections to the maximum electrical load of consumers in the region; power flow estimation in electric traction network and their account in fees for payments for electricity.

3. To improve power quality, reliability and security of power supply and reduce the cost and time of construction of traction substations new schemes and technical solutions of external power supply are proposed, which are based on joining to networks of the National Energy Company «Ukrenergo» (220-330 kV) and use of reactive power controlled compensation devices.

4. As a result of theoretical and experimental investigations of forced modes of mobile traction substation «Traction Kremenchug» it is found that in the absence of the left or right shoulder load power of traction network one of the two least-loaded traction transformer phases causes flowing in one phase of the supply line of active-capacitive reverse current that is fixed by calculated electric meters with phase segregated algorithm calculations as generating the least loaded phase. Such modes of power supply systems lines are inevitable due to the need to ensure the minimum level of the voltage of electric rolling on long cantilever sections of the traction network and for them it is necessary usage of the vector method of determining the amount of electricity.

REFERENCES

1. *Energetichna strategija Ukrzaliznici na period do 2015 r. i na perspektivu do 2020 r. Zatv. derzhavnoju administracieju zaliznichnogo transportu Ukrainu 26.11.2013 r.* [Energy Strategy Railways for the period up to 2015 and for the future by 2020. Approved by State Administration of Railway Transport of Ukraine 11.26.2013]. Kyiv, 2013. 104 p. (Ukr).

2. Kornienko V.V., Kotel'nikov A.V., Domanskyi V.T. *Elektrifikacija zheleznyh dorog. Mirovye tendencii i perspektivy (Analiticheskij obzor)* [Electrification of railways. Global trends and perspectives (Analytical review)]. Kyiv, Transport of Ukraine Publ., 2004. 196 p. (Rus).

3. Markvard K.G. *Elektrosnabzhenie elektrificirovannyh zheleznyh dorog* [Power supply of electrified railways]. Moscow, Transport Publ., 1982. 528 p. (Rus).

4. Rene Pelis'e. *Energeticheskie sistemy* [Energy Systems]. Moscow, Higher School Publ., 1982. 568 p. (Rus).

5. Domanskyi I.V. *Osnovi energoefektivnosti elektrichnih sistem z tjagovimi navantazhennjami: monografija* [Basics of energy efficiency of electrical systems with traction load: monograph]. Kharkiv, TOV «Tsentr informatsiyi transportu Ukrayiny» Publ., 2016. 224 p. (Ukr).

6. Domanskiy I.V. Modes in electrical systems with mobile AC traction substations. *Vestnik of Railway Research Institute*, 2016, vol.75, no.1. pp. 19-25. (Rus).

7. Domanskyi I.V. Electrification of railways – source of energy efficiency of process transportations. *Railway Transport of Ukraine*, 2014, no. 1, pp. 19-23, 31-33. (Ukr).

8. *Pravyla ulashtuvannia systemy tiahovoho elektropostachannia zaliznyts Ukrainy. № TsE-0009: Zatv. Nakaz Ukrzaliznytsi 24.12.2004 r., № 1010-TsZ. / Min-vo transp. ta zviazku Ukrainy* [Terms ordering system Traction Power railways of Ukraine. Number IS-0009: approved. Order Railways year 24.12.2004., № 1010-CH. Ministry of Transport and Communications of Ukraine]. Kyiv, 2005. 80 p. (Ukr).

9. Domansky I.V. System analysis of external power supply of railways traction substation. *Electrical Engineering & Electromechanics*, 2013, no.3, pp. 54-63. (Ukr). **doi: 10.20998/2074-272X.2013.3.10.**

10. Shidlovskij A.K., Kuznetsov V.G., Nikolaenko V.G. *Optimizacija nesimmetrichnyh rezhimov sistem elektrosnabzhenija* [Optimization of asymmetrical modes of power supply systems]. Kiev, Naukova Dumka Publ., 1987. 174 p. (Rus).

11. Zhelezko Yu.S. *Poteri elektrojenergii. Reaktivnaja moshhnost'. Kachestvo elektrojenergii* [Loss of electricity. Reactive power. Power quality]. Moscow, ENAS Publ., 2009. 456 p. (Rus).

12. Borodulin B.M., German L.A., Nikolaev G.A. *Kondensatornye ustanovki elektrificirovannyh zheleznyh dorog* [Condenser units for electrified railways]. Moscow, Transport Publ., 1983. 183 p. (Rus).

13. German L.A., Goncharenko V.P. Modern longitudinal capacitive compensation scheme in the traction power supply. *Bulletin of Rostov State Transport University*, 2013. no.2. pp. 12-17. (Rus).

14. Domanskyi I.V. Modes of operation of the system of traction power AC using reactive power compensation devices. *Electrical Engineering & Electromechanics*, 2015, no.3, pp. 59-66. (Rus). **doi: 10.20998/2074-272X.2015.3.09.**

15. German L.A., Serebryakov A.S., Maksimova A.A. Filter compensating installation in AC traction networks. *Vestnik of Railway Research Institute*, 2016. no.1. pp. 26-34. (Rus).

Received 29.11.2016

V.O. Bondarenko[1]*, Doctor of Technical Science, Professor,*
I.V. Domanskyi[1]*, Candidate of Technical Science,*
G.N. Kostin[2]*,*
[1] National Technical University «Kharkiv Polytechnic Institute»,
21, Kyrpychova Str., Kharkiv, 61002, Ukraine,
e-mail: dvt.nord@mail.ru
[2] Kharkiv regional department of the branch «Energosbyt»
of Public Joint Stock Company «Ukrainian Railway»,
7, Konareva Str., Kharkiv, 61052, Ukraine,
e-mail: ee_ugd_kh@ukr.net

How to cite this article:
Bondarenko V.O., Domanskyi I.V., Kostin G.N. Analysis of energy efficiency of operating modes of electrical systems with the traction loads. *Electrical engineering & electromechanics*, 2017, no.1, pp. 54-62. **doi: 10.20998/2074-272X.2017.1.09.**

UDC 621.311.014 **doi: 10.20998/2074-272X.2017.1.10**

Yu.N. Vepryk

WAYS TO IMPROVE THE EFFICIENCY OF COMPUTER SIMULATION OF ELECTRICAL SYSTEMS MODES BASED ON EQUATIONS IN PHASE COORDINATES

The development of electrical systems must be accompanied by the development of tools and their modeling. However, the possibility of development models, traditionally developed on the basis of the transition from the real to the single-phase three-phase circuits equivalents, represented exhausted. Therefore, along with the use of single-phase three-phase equivalents need to develop models in phase coordinates. Showing the need to move to the development of models based on equations in the phase coordinates and the possibility of increasing the effectiveness of development through the use of implicit methods of integration, the transition to a higher level of decomposition and unification models developed for the implementation of the structural approach to modeling complex systems. References 3.

Key words: **stationary modes, electric networks, mathematical models, phase coordinates, transients.**

Показаны необходимость перехода к разработке моделей на основе уравнений в фазных координатах и возможности повышения эффективности таких разработок за счет использования неявных методов интегрирования, перехода на более высокий уровень декомпозиции и унификации разрабатываемых моделей. Библ. 3.

Ключевые слова: **стационарные режимы работы, электрические сети, математические модели, фазные координаты, переходные процессы.**

Introduction. The current stage of development of electrical systems characterized by the fact that all the more significant becomes the influence of a number of factors affecting the quality of electrical energy. These factors are linked, firstly, with the advent of new processes and new equipment, and, secondly, with aging and wear of the main equipment of electrical systems. The introduction of new technological processes tend to be associated with an increased harmonic sources, distorting the shape of the voltage curve in electrical networks and equipment wear increases the asymmetry sources as individual network elements are forced to work part number of phases for a long time required for maintenance and repair works on the damaged phase.

To solve the problems of analysis of electrical systems in these new conditions and the need to develop new, more complete and accurate mathematical models and corresponding software to allow playback modes systems in the presence of harmonics and unbalance sources. In the traditional approach to modeling, based on the transition from the real three-phase circuit to the single-phase equivalents (in symmetrical components, d-q-0, α-β-0 coordinates, etc.) such models in principle can not be implemented, as the transition itself strictly justified and is possible only when there is symmetry and sinusoidal [1]. For this reason, attempts to develop models based on the transition to single-phase equivalents, in a direction to account unbalance and harmonics, are meaningless.

The goal of the paper is the rationale for the transition to the development of models in the phase coordinates and identification of ways to enhance the effectiveness of such developments.

Statement of the base material. The need for a transition from single-phase to three-phase equivalent model (in phase coordinates), in an environment where development opportunities based on the traditional approach models are exhausted, becomes apparent. However, the three-phase model, reproducing three-phase mode with all the major influencing factors, especially in transitional processes is much more difficult phase and, accordingly, their development and program implementation require greater time and cost [2]. Therefore, the amount of work in this area is still small.

At the Department «Electric Power Transmission» of the NTU «KhPI» the development of models of electrical systems based on the equations in the phase coordinates, in stationary and transient, symmetric and asymmetric modes is conducted for a sufficiently long time, and the existing experience shows that these difficulties are surmountable if:

Firstly, for the solution of systems of differential equations to use implicit numerical integration methods. When using implicit methods of numerical integration eliminates the need to bring the systems of differential equations to the normal form of Cauchy, which significantly reduces the complexity of this stage modeling and its software implementation, especially in the simulation of complex systems. Furthermore, implicit methods provide higher processing stability. And another factor in favor of the choice of implicit numerical integration methods for solving the problems is that while it is possible to complete structural modeling – i.e. we first need to develop a finite-difference (discrete) model of individual elements of a

complex system, and then perform the formation of a system model as a whole.

Second, the move to a higher level of decomposition – as elements of the settlement scheme is not considered bipolar *R*, *L*, *C* elements, but three-phase multipoles corresponding to the three-phase network elements. Equivalent circuit complex systems created even on a single phase, have a large number of bipolar *R*, *L*, *C* elements and complex configuration, the transition to three-phase circuits and taking into account along with the longitudinal parameters of transverse capacitive and inductive coupling power line number increases more than threefold which greatly complicates the process of formation of systems of equations in the stationary, and, especially in transient conditions. In the transition to the level of the three-phase switching circuits the number of elements is reduced, simplified circuit topology, all of the features of embodiment, the parameters of the phases and their mutual influence is reflected in the matrices of the third order of the parameters of the corresponding elements, and the process by which systems of equations at the level of the three-phase switching circuits becomes less complicated. It should also be noted that the transition to the level of three-phase multiport matrix coefficients in the general equations in stationary and transient regimes acquire a pronounced block structure, and opportunities to improve the simulation efficiency is provided through the use of new means of modern programming languages (sub-types, object-oriented programming, etc.).

And third, to present three-phase multipolar equation elements in phase coordinates in unified manner. When used for solving systems of differential equations implicit numerical integration methods, as has been said, it is possible the implementation of formalized procedures for the construction of a model system for the pre-formed models of individual elements. At the same time significantly simplify all stages of the simulation can be achieved if the discrete models of all elements of the system at the stage of their formation to present in the unified form.

At modeling elements useful to distinguish two groups of elements:

- static elements (air and cable lines (AL and CL), power transformers and auto-transformers, static elements of the load units, means of reactive power compensation);
- rotating electrical machines (synchronous generators, synchronous compensators, synchronous and asynchronous motors).

The equations of transients of any of the static elements (AL, CL, transformers, etc.) in the phase coordinates in the matrix form are:

$$[L]_{ij}^{F}\frac{d}{dt}[i]_{ij}^{F}+[R]_{ij}^{F}[i]_{ij}^{F}=[\Delta u]_{i}^{F}, \qquad (1)$$

and for different elements differ only in the order and structure of the matrices [*L*] and [*R*], where [*L*] is the matrix of self and mutual inductances of the phases (windings of the transformer, wires of AL or CL, and others), [*R*] is the matrix of resistances of the corresponding element phases.

For implicit methods of integration equations of the element (1) in phase coordinates must be presented in the normal form

$$\frac{d}{dt}[i]_{ij}^{F}=[L]_{ij}^{F-1}[\Delta u]_{ij}^{F}-[L]_{ij}^{F-1}[R]_{ij}^{F}[i]_{ij}^{F}, \qquad (2)$$

and at using equations discretization to be sampled, such as the Euler-Cauchy method

$$x_{k+1}=x_k+\frac{h}{2}\left(f_{k+1}+f_k\right)$$

to perform an approximation of the original differential equations using formulas:

$$[i]_{L}^{(K+1)}=[i]_{L}^{(K)}+\frac{h}{2}\left(\frac{d}{dt}[i]_{L}^{(K+1)}+\frac{d}{dt}[i]_{L}^{(K)}\right). \qquad (3)$$

Substituting in (3) expressions for the derivatives of (2), we obtain the expression:

$$[i]_{ij}^{(k+1)}=[i]_{ij}^{(k)}+\frac{h}{2}\left([L]_{ij}^{-1}[u]_{ij}^{(k+1)}-[L]_{ij}^{-1}[R]_{ij}[i]_{ij}^{(k+1)}\right)+$$
$$+\frac{h}{2}\left([L]_{ij}^{-1}[u]_{ij}^{(k)}-[L]_{ij}^{-1}[R]_{ij}[i]_{ij}^{(k)}\right),$$

which can be solved for the currents at the current step of integration:

$$[i]_{ij}^{(k+1)}=\frac{h}{2}[K]_{L}^{(-1)}[L]_{ij}^{(-1)}[u]_{ij}^{(k+1)}+\frac{h}{2}[K]_{L}^{(-1)}[L]_{ij}^{(-1)}[u]_{ij}^{(k)}+$$
$$+[K]_{L}^{(-1)}[i]_{ij}^{(k)}-\frac{h}{2}[K]_{L}^{(-1)}[L]_{ij}^{(-1)}[R]_{ij}[i]_{ij}^{(k)},$$

where $[K]_{L}=[E]+\frac{h}{2}[L]_{ij}^{-1}[R]_{ij}$, [*E*] is the unit matrix.

Obtained equations can be written as:

$$[i]_{ij}^{(k+1)}=[Y]_{ij}[u]_{ij}^{(k+1)}+[Y]_{ij}[u]_{ij}^{(k)}+[A]_{ij}[i]_{ij}^{(k)}, \qquad (4)$$

where $[Y]_{ij}$, $[A]_{ij}$ are the matrices defined respectively by longitudinal and transverse element parameters.

Equations couple voltage and phase currents at the current step of integration with the phase voltages and currents in the previous step.

They are useful for modeling the transients in the corresponding element and to be included in the system model. And the fact that the equations solved for the currents, allows the formation of a system of differential equations in general, to use the most effective method of node.

Using any other implicit methods of numerical integration, differential equations (1) any static element can be represented in the integration step in the form of (4).

System of differential equations of electrical machines (synchronous, induction) in phase coordinates in the matrix form comprises two groups of equations:

1) flux linkage equations

$$\begin{aligned}[\Psi]_S &= [L]_S[i]_S + [L_{SR}][i]_R;\\ [\Psi]_R &= [L]_{RS}[i]_S + [L]_R[i]_R,\end{aligned} \quad (5)$$

2) voltage equilibrium equations of all electrical circuits in the stator and rotor

$$\begin{aligned}[U]_S &= -\frac{d}{dt}[\Psi]_S - [R]_S[i]_S;\\ [U]_R &= \frac{d}{dt}[\Psi]_R - [R]_R[i]_R,\end{aligned} \quad (6)$$

where indexes *S* and *R* taken to refer to quantities relating to the windings of the stator and rotor, respectively.

Winding fluxes are functions of the rotor angle γ. Therefore derivatives of flux linkage with respect to time taking into account this dependence has the form

$$\frac{d}{dt}\begin{bmatrix}\psi_S\\ \psi_R\end{bmatrix} = \begin{bmatrix}\frac{dL(\gamma L)}{d\gamma}\frac{d\gamma}{dt}\end{bmatrix}\begin{bmatrix}i_S\\ i_R\end{bmatrix} + [L(\gamma)]\frac{d}{dt}\begin{bmatrix}i_S\\ i_R\end{bmatrix}.$$

Substituting derivatives of flux linkage in the equation (6), we obtain

$$\begin{bmatrix}L_S & L_{SR}\\ L_{RS} & L_R\end{bmatrix}\frac{d}{dt}\begin{bmatrix}i_S\\ i_R\end{bmatrix} + \left(\omega\begin{bmatrix}\frac{dL(\gamma L)}{d\gamma}\end{bmatrix} + \begin{bmatrix}r_S & \\ & r_R\end{bmatrix}\right)\begin{bmatrix}i_S\\ i_R\end{bmatrix} = \begin{bmatrix}U_S\\ U_R\end{bmatrix}. \quad (7)$$

Since when the rotor rotates the inductance of windings depends on the angular position γ of the rotor, voltage balance equation (7) comprise transformer EMF $L_{ij}\frac{di}{dt}$, due to changes in current in the *j*-th circuit, and also rotation EMF $\frac{dL_{ij}}{d\gamma}\omega_{ij}$ of a change in inductance when the rotor rotates.

However, considering that the rotational EMF, as the voltage drop dependent on the current in the windings, in the equations (7) for the expression in brackets may be taken designation

$$\left(\omega\begin{bmatrix}\frac{dL}{d\gamma}\end{bmatrix} + [R]\right) = [R_1],$$

and write them as

$$[L]\frac{d}{dt}[i] + [R_1][i] = \begin{bmatrix}u_S\\ u_R\end{bmatrix},$$

we can say that they are similar to the equations of static elements and are characterized in that the matrix elements of the phase inductances are periodic functions of time.

To move to the difference equations it is necessary to solve the resulting equations for the derivatives

$$\frac{d}{dt}\begin{bmatrix}i_S\\ i_R\end{bmatrix} = -[L(\gamma)]^{-1}\left(\omega\begin{bmatrix}\frac{dL(\gamma)}{d\gamma}\end{bmatrix} + \begin{bmatrix}r_S & \\ & r_R\end{bmatrix}\right)\begin{bmatrix}i_S\\ i_R\end{bmatrix} + [L(\gamma)]^{-1}\begin{bmatrix}U_S\\ U_R\end{bmatrix};$$

and go to the difference approximation in accordance with the Euler-Cauchy formula

$$\begin{bmatrix}i_S\\ i_R\end{bmatrix}^{(k+1)} = \begin{bmatrix}i_S\\ i_R\end{bmatrix}^{(k)} - h\left[L(\gamma)^{k+1}\right]^{-1} \times \left(\omega\begin{bmatrix}\frac{dL(\gamma L)^{k+1}}{d\gamma}\end{bmatrix} + \begin{bmatrix}r_S & \\ & r_R\end{bmatrix}\right)\begin{bmatrix}i_S\\ i_R\end{bmatrix}^{(k+1)} + h\left[L(\gamma)^{(k+1)}\right]^{-1}\begin{bmatrix}u_S\\ u_R\end{bmatrix}^{(k+1)}.$$

If the obtained equation is solved for the currents in the windings at the (*k*+1)-th step, equations will have a form:

$$\begin{bmatrix}i_S\\ i_R\end{bmatrix}^{(k+1)} = \left[Y(\gamma)^{(k+1)}\right]\begin{bmatrix}u_S\\ u_R\end{bmatrix}^{(k+1)} + \left[Y(\gamma)^{(k+1)}\right]\begin{bmatrix}u_S\\ u_R\end{bmatrix}^{(k)} + \left[A(\gamma)^{(k+1)}\right]^{-1}\begin{bmatrix}i_S\\ i_R\end{bmatrix}^{(k)}, \quad (8)$$

where $[Y(\gamma)]$, $[A(\gamma)]$ are the matrices whose elements are determined by the self and mutual inductances of the windings and are functions of the rotor angle γ.

In equations (8), as in the discrete equations of static electricity network elements, the currents in the windings of the current step numerical integration of the equations expressed transient voltage on the windings through the current step and the currents in the windings of the previous step integration. In contrast to the static elements of the discrete parameters are variable and must be calculated at each step in the process of computing the angular position of the rotor function. In such form the unified equations may be incorporated into the system of equations to be solved at the numerical integration step.

Positive effect obtained when presenting items of electrical systems in a unified form (4) – (8) lies in the fact that:

- transient simulation algorithms in the individual elements can be regarded as a modification of a single generic algorithm, the main elements of which are: the calculation of the matrix elements of the original *R*, *L*, the formation of discrete parameters matrices *Y*, *A*, the calculation of the transition process in step parameters;
- unification of models of elements allows you to unify and other stages of the modeling system as a whole – topological analysis of network circuit, the formation of a system of equations, the solution of the resulting system, which, in turn, facilitates the realization of models in the phase coordinates on the basis of a structured approach to the modeling of complex systems.

The realization of the proposed approach, made in the study of operating modes of electrical systems with the asymmetry [3], confirms its effectiveness and feasibility – on a single algorithmic and methodological basis of the performed development of software tools to simulate the stationary and transient modes in the presence of any number of asymmetrical elements and switching.

Conclusions.

Further development of methods and means of electrical systems modes simulation for solving actual problems of control is possible only on the basis of the equations in the phase coordinates.

Improving the efficiency of development of models in the phase coordinates is provided on the basis of implicit numerical integration methods, the transition to a higher level of decomposition, the unification of models of elements and the use of the new features of modern programming languages.

REFERENCES

1. Golov P.V., Sharov Yu.V., Stroyev V.A. System of mathematical models for the calculation of transients in complex power systems. *Electricity*, 2007, no.5, pp. 2-11. (Rus).

2. Misrikhanov M.Sh. Clarification of the definition of places of damage to overhead lines by using the phase components. *Electric stations*, 2001, no.3, pp. 36-40. (Rus).

3. Vepryk Yu.N. *Komp'iuternoe modelirovanie rezhimov raboty elektricheskikh sistem: monografiia* [Computer simulation of electrical systems modes: monograph]. Kharkiv, NTU «KhPI» Publ., 2015. 304 p. (Rus).

Received 20.11.2016

Yu.N. Vepryk, Doctor of Technical Science, Professor,
National Technical University «Kharkiv Polytechnic Institute»,
21, Kyrpychova Str., Kharkiv, 61002, Ukraine,
phone +38 057 7076246, e-mail: veprik@email.ua

How to cite this article:

Vepryk Yu.N. Ways to improve the efficiency of computer simulation of electrical systems modes based on equations in phase coordinates. *Electrical engineering & electromechanics*, 2017, no.1, pp. 63-66. **doi: 10.20998/2074-272X.2017.1.10.**

UDC 658.5.012.7 **doi: 10.20998/2074-272X.2017.1.11**

Ya.S. Bederak

ON SUBSTANTIATION OF SELECTION OF ECONOMIC AND MATHEMATICAL METHODS FOR THE ASSESSMENT OF ENERGY EFFICIENCY OF PRODUCTION FACILITIES

Research purpose is generalization and further development of economic- mathematical methods for ensuring energy-efficient operation mode of production facilities. The above methods can be used for selection of the most energy-efficient production lines, mechanisms; pumping, compression, ventilation installations or other electric receivers among several similar ones by using equal and unequal weight criteria. An example of comparing the efficiency of the production facilities of the chemical industry is showed by a priori ranking and morphological (geometric) methods. The method of control the correctness of the production facilities in the case when the electric load depends on two parameters in triangular coordinates in the presence of boundary restrictions is described. The identity of the current energy values calculated by Holt predicted value at a predetermined optimal smoothing constant determines the stability of the process. Expedience of application the autocorrelation coefficient for testing processes on the stability is proved. References 10, tables 3, figures 5.
Key words: **power consumption, criteria of equal and unequal weights, the autocorrelation coefficient, energy efficiency.**

Целью исследования является обоснование выбора наиболее целесообразных экономико-математических методов обеспечения энергоэффективного режима работы производственных объектов. Рассмотренные методы могут быть использованы для выбора наиболее энергоэффективных технологических линий, агрегатов, насосных, компрессорных, вентиляторных установок или других электроприемников с нескольких им подобных по равновесным и неравновесным критериям. Приведен пример сравнения эффективности работы производственных объектов химической промышленности методами априорного ранжирования и морфологическим (геометрическим). Описан способ контроля энергоэффективности работы производственных объектов в случае, когда электрическая нагрузка зависит от двух параметров при наличии предельных ограничений их, используя треугольные координаты. Сделан вывод о том, что тождество текущего значения энергопотребления с рассчитанным методом Хольта прогнозируемым значением при определенных заранее оптимальных постоянных сглаживания определяет стабильность работы технологического процесса. Доказана целесообразность применения коэффициента автокорреляции первого порядка выборок электропотребления для проверки технологических процессов на стабильность работы. Библ. 10, табл. 3, рис. 5.
Ключевые слова: **электропотребление, равновесные и неравновесные критерии, энергоэффективность, коэффициент автокорреляции.**

Introduction. In industry it is often necessary to compare the energy efficiency of similar structure and functionality of two or more manufacturing facilities, such as production lines, machinery, pump, compressor, fan or other installations on several criteria (parameters) to select the best working unit. To do this, use the criteria as equal and unequal weight. Similarly, in practice we must solve the problem of determining the point in time during the change of day, decade, month, etc., which worked effectively manufacturing facility (or vice versa). It is necessary to provide real-time energy production facilities. These tasks proposed to deal with the known economic-mathematical methods and parameters.

The goal of the paper is substantiation of the most appropriate choice of economic and mathematical methods for energy-efficient mode of production facilities.

Analysis of recent investigations and publications. Statistical analysis in electricity supply systems (ESS) industry introduced by M.A. Denisenko in [1]. This approach is useful for other energy resources [2].

Methods of making the criteria equal and unequal scales considered in [3]. In this paper the technical working optimally choose an item using the procedure of constructing the utility function. To ensure efficient energy use and control operating mode processes appropriate to apply the control cards by Shewhart [4].

Material and research results. Investigations have shown that to ensure energy-efficient mode of production facilities necessary to carry out the following activities:

1. Monitoring the efficiency of technological process in the case when the electric load depends on two parameters.

Among all methods of visualization and control of process in the case when the electric load depends on two parameters, the easiest method is to use triangular coordinates [5]. Fig. 1 shows an example of building a triangular coordinate system for piston air compressor, which load (built on the axis *p*) depends directly proportional to the pressure (axis *m*) in the system and the temperature in the compressor (axis *n*). At the intersection of three straight arbitrary built equilateral triangle ABC. He called triangular base coordinate system. Axis, and therefore the coordinates of points are indicated by the letters *m*, *n* and *p*.

Using triangular coordinates, it is convenient to control the process, such as mode of operation piston air compressor (Fig. 2). Its power consumption depends on the pressure in the compressed air and the temperature of the compressed air in the system.

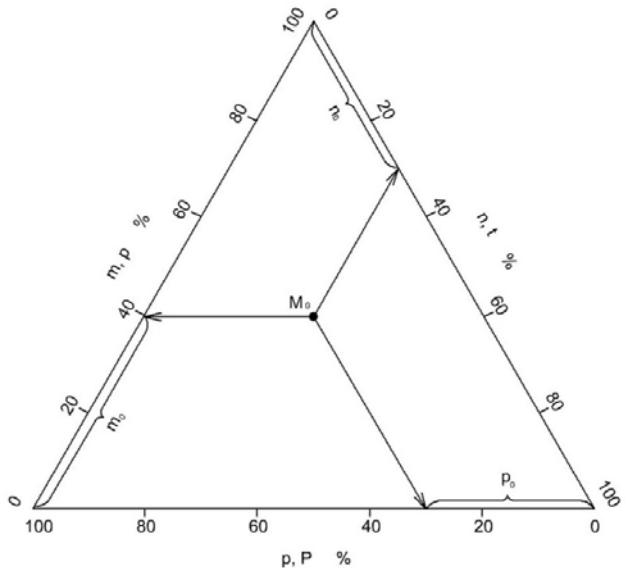

Fig. 1. Example of triangular frames for piston air compressor load which depends directly proportional to system pressure and air temperature in the compressor

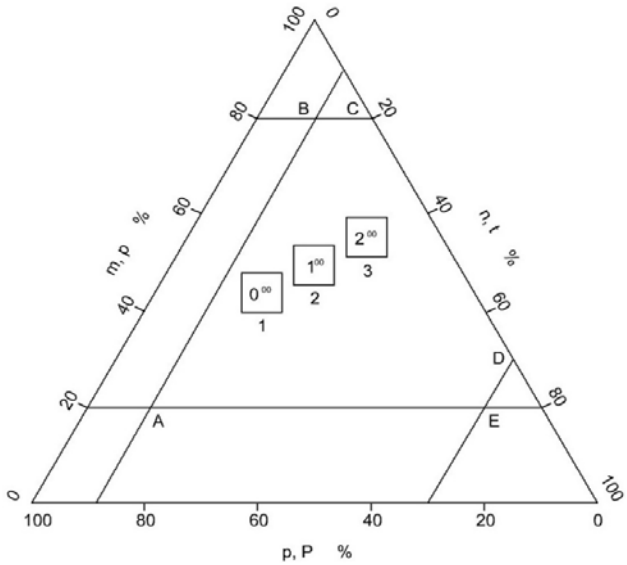

Fig. 2. Example of conducting the technological process by diagram n triangular coordinates

On the axis *m* delayed pressure in the compressed air in percentage, on the axis *n* – the temperature of the compressed air system in percent, on the axis *p* – capacity compressor at different time points percentage. When operating the compressor, there are several restrictions: maximum interval pressure on a percentage of 20-80 %, temperature 0-70 %, 0-90 % of capacity. Diagram of the process (Fig. 2) shows that the process should be conducted within the figure ABCDEA. The closer to the beginning of the axis is *p* (power percentage), the compressor works more effectively [5].

2. Comparison of energy production facilities whose consumption depends on many different factors of equal weight.

The power consumption of production facilities can be affected by many different factors equal weight. To compare the energy efficiency of objects by partial (only one characterizing feature of object) criteria of equal weight may be used either additive or multiplicative generalized criteria [3]. Under criteria imply controlled output parameter characterizing the degree of achievement. Partial criteria $F_i(X)$ in one way or another should be combined in a general criterion $f(X)=\Phi[F_1(X), F_2(X), \ldots, F_m(X)]$ which after that is optimized.

When all criteria are of equal value, the generalized additive criterion is written in the form of partial sums criteria in when they have the same weight. Multiplicative criterion is formed by simple multiplication of partial criteria in when they have the same weight. For when one object is better than generalized additive criterion and the other – for the multiplicative need to use to select the optimal geometric mathematical model (morphological) approach [6].

The morphological approach can be used not only for the comparison of the object at different times, but when using two identical units, production lines and so on. To use morphological approach requires the construction of radiation diagram. This chart is constructed as follows: from the center of the circle made by a number of factors straight lines (radii) that resemble rays diverge during radioactive decay. These tags are applied radii graduation in the fate of 100 % and lay them in the data value percentage. The points, which are marked pending value, combine segments. The values that are the rays that correspond to each factor, compared with the reference value (standard energy) or values for the previous billing period. Each of technological facilities necessary to determine the specific rate of electricity consumption per unit of production or calculate standard consumption by the algorithm specified in [7].

For example, ammonia plant based radiation diagram which compares energy plant for two days in a row for the equilibrium quality criteria. These criteria include energy consumption, heat consumption, the consumption of recycled water, natural gas consumption, consumption of demineralized water, ammonia output. Table 1 shows the ratio of energy consumption per unit of output normalized to a value (standard or specific energy consumption norms).

Table 1

The value of the ratio of energy consumption per unit of output normalized to a value two days in a row

Parameter	The value for the first day and marking points on the radiation diagram, %	The value for the second day and marking points on the radiation diagram, %
Electrical energy consumption	100 (A_1)	87 (A_2)
Heat energy consumption	110 (B_1)	90 (B_2)
Recycled water consumption	105 (C_1)	91 (C_2)
Demineralized water consumption	108 (D_1)	94 (D_2)
Natural gas consumption	115 (E_1)	95 (E_2)
Ammonia output	103 (F_1)	96 (F_2)

Example of the determination the best working object is shown in Fig. 3.

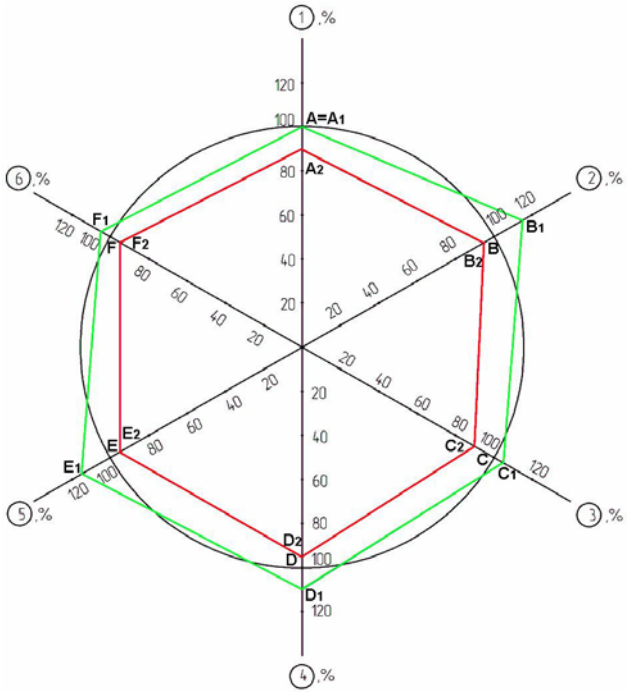

Fig. 3. Radiation diagram comparing the energy efficiency of ammonia production plant with two days in a row for the equilibrium quality criteria

Designations in Fig. 3: beam 1 – percentage of the «standard of consumption» in electricity (it are points A_1 and A_2), 2 – by heat energy (B_1 and B_2), 3 – by circulating water (C_1 and C_2), 4 – by demineralized water (D_1 and D_2), 5 – by consumption of natural gas (E_1 and E_2), 6 – percentage of the daily ammonia output norm (F_1 and F_2).

Polygon $A_1B_1C_1D_1E_1F_1A_1$ is an assessment of efficiency of the plant for production of ammonia for the first day, and polygon $A_2B_2C_2D_2E_2F_2A_2$ – for the second day. Circumference that passes through the points A, B, C, D, E, F is the standard power, or a mark that meets the specific rate of consumption of specific energy per unit of output. From Fig. 3 it is possible to conclude that effective personnel department worked on the second day than the first. Analyzing and controlling energy efficiency by radiation diagrams possible to assess the state of energy efficiency in the workplace. The smaller the area of polygons (polygons) $A_1B_1C_1D_1E_1F_1A_1$ and $A_2B_2C_2D_2E_2F_2A_2$ better working manufacturing facility.

Likewise it is possible to assess energy efficiency of the process unit, department, company.

3. Comparison of energy production facilities whose consumption depends on many different factors of unequal weight.

In practice must be performed comparing the effectiveness of several technological and energy facilities on the criteria of unequal weight. To carry out this comparison by constructing utility function is not always appropriate. The method requires knowledge of the person who decides mathematical statistics and methods of decision-making. It is therefore necessary to develop or use other methods of finding the best operating production facilities of several of these on several criteria. The simplest method is a priori ranking [3].

At the initial planning stages of the experiment based goals experimenter should select the independent variables (factors), which will later be used in the experiment. Generally, factors selected for analysis prior information that requires the use of different methods to systematize the knowledge gained. To solve the problems of this kind commonly used methods of peer review. These methods are based on receiving and processing data from a survey of experts. Regarding the evaluation and selection of the most significant factors was widespread priori ranking method that can be used to evaluate the energy efficiency of industrial facilities.

Thus, in the ammonia plant by a priori ranking weight ratios are calculated. Power consumption of the plant depends on such factors: heat consumption, recycled water, demineralized water, cost of natural gas output of ammonia. Weight coefficients K_w measured by factors present in ammonia plant following: for electric power consumption $K_w = 0.24$; for heat consumption $K_w = 0.21$; for consumption of recycled water $K_w = 0.16$; for demineralized water consumption $K_w = 0.13$; for the cost of natural gas consumption $K_w = 0.26$. It is necessary to multiply each value calculated weight ratio in percent (normalized) value criteria specified in Table 1.

Table 2 shows the ratio of energy consumption per unit of output normalized to a value (standard or specific energy consumption norms) subject to weight ratios.

Table 2

The value of the ratio of energy consumption per unit of output normalized taking into account the weight ratio to a value two days in a row

Parameter	The value for the first day and marking points on the radiation diagram, %	The value for the second day and marking points on the radiation diagram, %
Electrical energy consumption	100·0.24 = 24 (A_1)	87·0.24 = 21 (A_2)
Heat energy consumption	110·0.21 = 23 (B_1)	90·0.21 = 19 (B_2)
Recycled water consumption	105·0.16 = 17 (C_1)	91·0.16 = 15 (C_2)
Demineralized water consumption	108·0.13 = 14 (D_1)	94·0.13 = 12 (D_2)
Natural gas consumption	115·0.26 = 30 (E_1)	95·0.26 = 25 (E_2)
Ammonia output	103·1.0 = 103 (F_1)	96·1.0 = 96 (F_2)

Fig. 4 shows the radiation diagram comparing the energy efficiency of ammonia production on the criteria of unequal weight.

The areas of polygons $A_1B_1C_1D_1E_1F_1A_1$ and $A_2B_2C_2D_2E_2F_2A_2$ are calculated. From Fig. 4 it is possible to conclude that for the first day ammonia plant worked worse than for second.

4. Checking the stability of the technological process.

Condition of the technological process is characterized by the total error that occurs as a result of accidental and systematic.

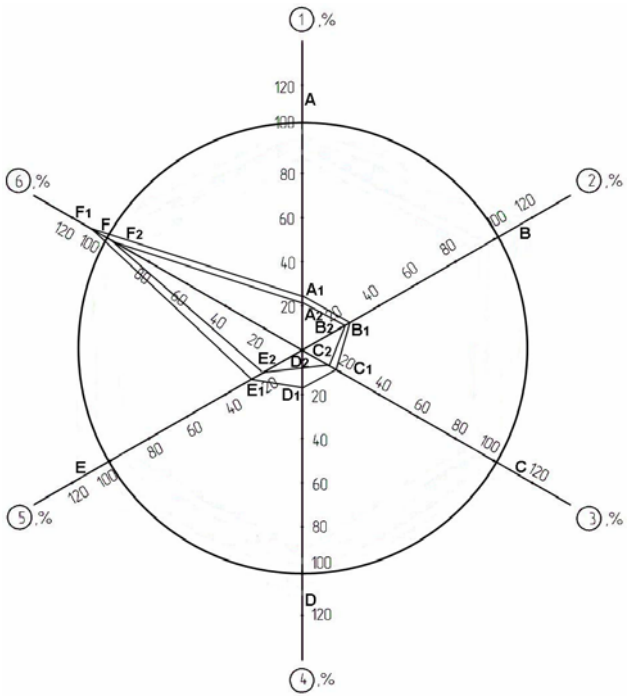

Fig. 4. Radiation diagram comparing the energy efficiency of ammonia production for two days in a row for the nonequilibrium quality criteria

Assessment of the stability process in general is as follows. First a set of experimental data is implemented by measurement parameters controlled sample of units with simultaneous detection of measurement results. Then a table of frequencies; calculated statistical characteristics; determined indicators of process; determined by the status of the level of defects; established distribution law and carried out statistical verification harmonization of the law of the normal law. However, this procedure takes a lot of time, it requires knowledge of mathematical statistics in operating personnel. It is therefore proposed to use to test the stability of the process simpler methods.

In 1957, Charles Holt exponential smoothing developed a method, called two-parameter method Holt [8]. This method takes into account local linear trend present in the time series. If the time series are a tendency to increase, in addition to assessing the current level of assessment it is required and inclination. In the method of Holt value and slope smoothed directly with them using various steel smoothing which to assess the current level and slope, specifying them whenever there are new observations. One advantage of the Holt technique is its flexibility which allows you to select the ratio, which tracks the level and slope.

The basis of the method consists of three Holt equations:

$$Y_t^{pr} = \alpha \cdot (Y_{t-1}^{pr} + T_{t-1}) + (1-\alpha) \cdot Y_t, \quad (1)$$

$$T_t = (1-\beta) \cdot (Y_t^{pr} - Y_{t-1}^{pr}) + \beta \cdot T_{t-1}, \quad (2)$$

$$Y_{t+p}^{pr} = Y_{t+1}^{pr} + p \cdot T_t, \quad (3)$$

where Y_t^{pr} and Y_{t-1}^{pr} are the projected (smoothed) value of the index in the next and previous times; Y_t is the table value of the index in time t; T_{t-1} is the trend value in time t–1, determined from (2); α and β are the constants of smoothing required to smooth the trend assessment.

Investigations in [8] showed that the value of constant α and β determine the stability of the process. The stability of the process is a property that determines the sustainability of its probability distribution parameters for some length of time without interference. The process is considered stable if the controlled parameters do not exceed the limits of control and there is no trend to release them over the limit. The coefficient of variation of power consumption data for the billing period should be minimal. For large chemical plants for the production of ammonia, weak nitric acid, a powerful pumping station supplying water first ascent found that for different processes optimal value smoothing constant α is 0.1, and the smoothing constant β is equal to 0.9 (for stable process).

Knowledge of smoothing constant values allows real-time power consumption compared with the current value calculated by Holt method predicted value. If the values of the smoothing constant α = 0.1 and β = 0.9 [8] actual value of power consumption coincides with the predictable, the technological process with the stable.

Reducing or increasing the last time the sample values of power consumption makes it impossible to make a proper conclusion about the proper conduct of the process. To test the stability of the process proposed to use the autocorrelation coefficient (AC) [9] of the first, second and further orders to check the stability and efficiency of process of energy consumption.

A number of studies on the efficiency of AC utilization for the evaluation process at several sites of the chemical industry are carried out. Data on hourly power consumption P of the large ammonia plant chemical enterprise for several days of the year 2016 are collected. Sample data consumption is shown in Table 3.

Table 3

The values of hourly electricity consumption of the large ammonia plant for one of the days in 2016

Interval No.	1	2	3	4	5	6	7	8
P, MW·year	37.264	37.275	37.290	37.189	37.058	37.088	37.131	37.124
Interval No.	9	10	11	12	13	14	15	16
P, MW·year	37.112	37.074	37.171	37.201	37.239	37.259	37.189	37.162
Interval No.	17	18	19	20	21	22	23	24
P, MW·year	37.450	37.465	37.527	37.510	37.472	37.267	37.074	37.133

*The coefficient of variation of the sample 0.24 %.

The last (the 24-th) the sample ranges from 0 to 100 % in increments of 25 % in the range from 0 to 75 % and 5 % in the range of 75 % to 100 % ($P_{24}^{'} = K \cdot P_{24}$), where K is the ratio changed recently the sample to its full value. Coefficient K = 0-1.0; it takes the values 0; 0.25; 0.5; 0.75; 0.8; 0.85; 0.9; 0.95; 1.0. Estimated spacecraft first, second, third order for each of the samples when changing the last sample.

Investigations have shown that there are three types depending on the size AC last modified the sample (Fig. 5).

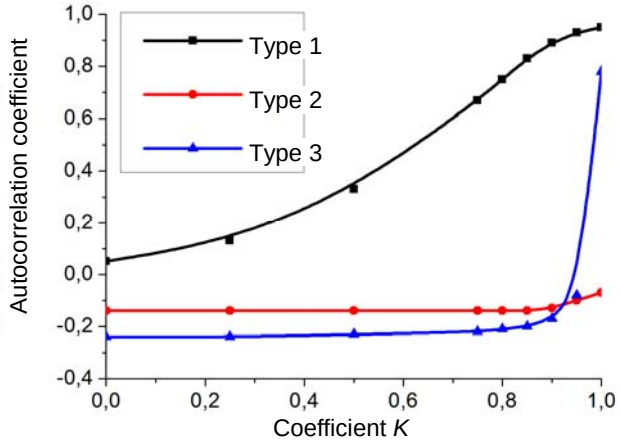

Fig. 5. Dependence of AC of the first order on changing the sample last

For the first and third type depending spacecraft first order proportional to the changing value of the last sample. Therefore, when there is such a relationship, the AC should be used to control power consumption mode. The calculation results proved that the AC swings of the first order for the first and third type depends 30-40 % more than the second or third order. Therefore, it is better to use to control power consumption mode.

For the first type is characterized by a strong sensitivity to the dramatic change in the value of the last sample and the zero power consumption. Thus, by changing the last value of the sample 25 % spacecraft first order reduced 2.5 times. AC describes the closeness linear relation only current and previous number of levels. Therefore, the autocorrelation coefficient can judge the presence of linear (or close to linear) trend [9].

For the third type of spacecraft observed a strong dependence of the first order from changes in the value of the last sample. AC of the second and third order for the third type of AC is resembling the first order for this type.

For some time series with strong non-linear trend (for example, take the form of a parabola of the second order, or exponential) autocorrelation coefficient series output levels may be close to zero. When sampling spacecraft dependence on changes in the value of the sample resembles the last second type (Fig. 5), then the AC is not suitable for the control of energy consumption.

To calculate AC of the second and third orders for all types depending on its value last modified the sample is also necessary in order to use the Ljung-Box for the autocorrelation [9].

All the above economic and mathematical methods may assist operational staff to quickly assess the situation at work, better monitor energy production facilities and in a short time to take measures to ensure the stability of the process, which corresponds to the concept of Smart Grid [10].

Conclusions.

1. We proved the feasibility of a number of economic and mathematical methods for monitoring the energy efficiency of production facilities and testing technological process stability.

2. The easiest way to control of the energy efficiency of technological processes when the electric load depends on two parameters, it is a way to use triangular coordinates which are useful for visualization and monitoring of the technological process.

3. The method of a priori ranking and morphological method are used for comparison of several similar energy production of the chemical industry, where energy consumption depends on many factors. These methods are recommended for use for the evaluation of energy efficiency in other industrial facilities.

4. An indication of the stability of the process is the identity of the current value of the power consumption calculated by the Holt method predicted value at predefined optimal smoothing constant.

5. For the first time autocorrelation coefficient is applied to evaluate the stability of technological processes. It is proved that at changing the range in a small power consumption value of the sample with a probability of 66 % is a significant change autocorrelation coefficient of the first or second order.

6. Considered in the paper economic and mathematical methods can be used to support the actions and decisions of operating personnel to conduct monitoring energy efficiency and stability of production facilities, to visualize current information, to support actions and feasibility of making human-operator's decisions that will promote Smart Grid concept in the industry.

REFERENCES

1. Denysenko M. A. *Spetsial'ni pytannya elektropostachannya: navch. posib. Ch.I.: Vybir elementiv elektropostachal'nykh system na osnovi stokhastychnoho modelyuvannya protsesiv, shcho vidbuvayut'sya v nykh* [Special issues of power supply. Part 1. Selecting items of electricity supply systems based on stochastic modeling of processes occurring in them]. Kyiv, NTUU «KPI» Publ., 2009. 288 p. (Ukr).

2. Zamulko A.I., Bederak Ya.S. Comprehensive statistical data analysis of active power consumption, energy expenditures and production volumes. *Power Engineering: Economics, Technique, Ecology*, 2014, no.2, pp. 79-83. (Ukr).

3. Gorbunov V.M. *Teoriia priniatiia reshenii* [Decision making theory]. Tomsk, NRTPU Publ., 2010. 67 p. (Rus).

4. Uiler D., Chambers D. *Statisticheskoe upravlenie protsessami. Optimizatsiia biznesa s ispol'zovaniem kontrol'nykh kart Shukharta* [Statistical control of process. Optimization of business using Shewhart control charts]. Moscow, Alpina Business Books Publ., 2008. 419 p. (Rus).

5. Bederak Ya.S. Visualization of reports and templates, which are formed in the monitoring systems of power consumption and energy management. *Bulletin of Kharkiv Petro Vasylenko National Technical University of Agriculture*, 2012, no.130, pp. 3-5. (Ukr).

6. Voloshko A.V., Bederak Ya.S., Lutchyn T.M. The problems of selection of optimal mathematical model of energy consumption at industrial enterprises. *Eastern-European Journal of Enterprise Technologies*, 2013, no.5/8(65), pp. 19-23. (Ukr). **doi: 10.15587/1729-4061.2013.18122.**

7. Nakhodov V.F., Borychenko O.V. Monitoring and analysis of implementation of established «standards» in the statistical

control systems of effective use of electric energy. *Informational collected papers «Promyslova electroenergetyka ta elektrotekhnyka» Promelektro*, 2011, no.2, pp. 16-23. (Ukr).
8. Stetsenko Y.V., Bederak Ya.S. Recovery and operational forecasting by Holt's method of electricity consumption at enterprises with a continuous work cycle. *Electronic modeling*, 2015, no.4, pp. 119-126. (Rus).
9. Luk'yanenko I.G., Krasnikova L.I. *Ekonometryka* [Econometrics]. Kyiv, Tovaristvo «Znannya» KOO Publ., 1998. 494 p. (Ukr).
10. Kobets B.B., Volkova I.O. *Innovatsionnoe razvitie elektroenergetiki na baze kontseptsii Smart Grid* [Innovative development of the electric power on the basis of Smart Grid concept]. Moscow, IAC Energiya Publ., 2010, 208 p. (Rus).

Received 11.10.2016

Ya.S. Bederak, Engineer,
PJSC «AZOT»,
72, Pervomayskaya Str., Cherkassy, 18014, Ukraine,
phone +380 47 2392979,
e-mail: ei@uch.net

How to cite this article:
Khlopenko N.J., Khlopenko I.N. Structural synthesis of a stabilizing robust controller of the rotor flux linkage. *Electrical engineering & electromechanics*, 2017, no.1, pp. 67-72. **doi: 10.20998/2074-272X.2017.1.11.**

Матеріали приймаються за адресою:
Кафедра "Електричні апарати", НТУ "ХПИ", вул. Кирпичова, 21, м. Харків, 61002, Україна
Електронні варіанти матеріалів по e-mail: a.m.grechko@gmail.com

Довідки за телефонами: +38 050 653 49 82 Клименко Борис Володимирович
+38 067 359 46 96 Гречко Олександр Михайлович